Multidisciplinary Optimization of Aircraft Design and Takeoff Operations for Low Noise

by

Anya Rachel Jones

B.S. Aeronautical Engineering and Mechanical Engineering,
Rensselaer Polytechnic Institute (2004)

Submitted to the Department of Aeronautics and Astronautics
in partial fulfillment of the requirements for the degree of

Master of Science in Aeronautics and Astronautics

at the

MASSACHUSETTS INSTITUTE OF TECHNOLOGY

June 2006

Author .....
Department of Aeronautics and Astronautics
May 26, 2006

Certified by .....
Karen Willcox
Associate Professor of Aeronautics and Astronautics
Thesis Supervisor

Accepted by .....
Jaime Peraire
Chairman, Committee on Graduate Students

Multidisciplinary Optimization of Aircraft Design and Takeoff Operations for Low Noise

by

Anya Rachel Jones

Submitted to the Department of Aeronautics and Astronautics
on May 26, 2006, in partial fulfillment of the
requirements for the degree of
Master of Science in Aeronautics and Astronautics

Abstract

Aircraft planform design, takeoff operations, and airfoil design are examined as a complete system in order to quantify tradeoffs that can result in a quiet aircraft. An aircraft design model was developed to generate blended-wing-body-type designs using simple-physics models and empirical scaling from a reference design. This model generates a scaled airframe and engine, an estimate of aircraft weights and center of gravity, a takeoff trajectory, outer wing airfoil profiles, and takeoff noise predictions.

Integrating the model with a single-level optimization framework, it was found that optimization for minimum noise can result in a significant noise reduction on takeoff, primarily due to changes in aircraft design and operations. There exists a design-operations coupling between the departure flight path angle and the engine size which must be exploited. Low-noise designs resulting from the single-level optimization require more fuel to complete the design mission. Modifications to the airfoil profiles do not significantly contribute to further reductions in takeoff noise, but do mitigate the fuel burn increase without adversely affecting noise levels.

A distributed optimization framework was constructed from a problem decomposition into three subspaces: aircraft planform and engine design, aircraft operations, and wing design. In this framework, a system level optimizer is responsible for minimizing the system noise while subspace optimizers control the disciplinary models individually. This setup allowed for the exploration of different areas of the design space. As a result, the distributed optimization converged to a fundamentally different design solution with the same minimum noise value as in the single-level optimization, but with a much lower fuel burn.

The key contributions of this thesis are the development and quantitative analysis of a weight and center of gravity model for an unconventional aircraft configuration, a distributed optimization framework, and a low noise aircraft design with competitive fuel burn.

Thesis Supervisor: Karen Willcox
Title: Associate Professor of Aeronautics and Astronautics

Acknowledgments

This research would not have been possible without the help and support of many people.

First and foremost, I would like to thank Professor Karen Willcox. Her consistent guidance and support was invaluable throughout my time at MIT. I could not have asked for a better advisor.

Many thanks to all of my colleagues here at MIT and across the ocean at Cambridge. Dr. James Hileman provided me with many ideas, tidbits of data, and headaches. Special thanks for all of his help in the airfoil design and noise prediction models. His knowledge and willingness to help with my research are greatly appreciated. Thanks to Dr. Cesare Hall at Cambridge for taking the time to help me with the engine design portion of this research and Steve Thomas for his help with the thrust vectoring model and for providing the SAX20 rendering. My officemates Angélique, Adrian, Ryan, and Parthiv provided some much needed distractions.

This work was funded by the National Defense Science and Engineering (NDSEG) Fellowship Program and the Cambridge-MIT Institute (CMI), Silent Aircraft Initiative (SAI). Many thanks to the NDSEG program for supporting me and CMI-SAI for providing all of the wonderful opportunities for travel to the United Kingdom.

Thanks to all of the crew back in New Orleans. My parents, Isidro and Kathy Magaña, have always encouraged me to do my best in school and have been a great help along the way. (Look Mom, I finished my thesis!) My siblings Katie and Bernie have sent me innumerable amusing cards and toys throughout my college days in the land of ice and snow. Mama2, my grandmother, has been a source of inspiration through her letters, phone calls, and anecdotes.

Finally, a special thanks to Dave, the best husband in the world. It is his programming knowledge that introduced me to the Matlab struct and his constant willingness to do the cooking and cleaning that allowed me to complete this research. He has supported me wholeheartedly every step of the way, even to the point of reading this entire thesis.

Contents

List of Figures

List of Tables

Nomenclature

Roman Symbols

a	speed of sound, m/s
A_f	fan area, m^2
b	wingspan, m
C_{D_0}	parasite drag coefficient
C_{D_i}	induced drag coefficient
C_m	pitching moment coefficient
D	wheel diameter, m
D_f	fan diameter, m
D'_f	reference fan diameter, m
D_R	ram drag, N
d_{GR}	distance covered during ground roll, m
d_{ROT}	distance covered during rotation, m
d_{rwy}	distance covered during ground roll and rotation, m
g	gravitational constant, m/s^2
$g(\mathbf{x})$	inequality constraints
h	altitude, m
$h(\mathbf{x})$	equality constraints
J	objective function
K_{ow}	outer wing chord scaling factor
M	Mach number
N_{core}	number of engine cores per engine

N_{cr}	number of crew members
n_{eng}	number of engines
N_{fan}	number of fans per engine
N_{pax}	number of passengers
R	range, nm or m
R	gas constant for air, J/kg-K
S	planform area, m^2
S	wheel separation, m
S_{ff}	area of cargo bay floor, ft^2
T_{max}	maximum wing twist, deg
T_N	net thrust, kN
T_V	vectored thrust, kN
U	airspeed, m/s
V_{pax}	volume of passenger cabin, ft^3
V_{tank}	fuel tank volume, m^3
W	wheel width, m
$\mathbf{x}$	vector of design variables
$\mathbf{z}$	vector of target variables

Greek Symbols

α	angle of attack, deg
β	thrust vectoring angle, deg
γ	flight path angle, deg
ρ	density of air, kg/m^3

Aircraft Weights

W_{api}	weight of air-conditioning, pressurization, and anti-/de-icing system, lbs
W_{apu}	weight of the auxiliary power unit, lbs
W_{aux}	weight of auxiliary gear, lbs
W_{bc}	weight of baggage and cargo handling equipment, lbs
W_{core}	weight of one core, lbs
W_{cs}	weight of crew seats, lbs
W_{els}	weight of the electrical system, lbs
W_{eng}	bare engine weight, lbs
W'_{eng}	bare reference engine weight, lbs
$W_{fairing}$	weight of the fairing for one bogey of the landing gear, lbs
W_{fan}	weight of one fan, lbs
W_{fc}	weight of the flight control system, lbs
W_{fds}	weight flight deck seats, lbs
$W_{fixed\ equipment}$	fixed equipment weight, lbs
W_{food}	weight of food, lbs
W_{fuel}	total fuel weight, lbs
W_{furOps}	weight of furnishings and operational items, lbs
$W_{galleys}$	weight of galleys, lbs
W_{hps}	weight of hydraulic and pneumatic system, lbs
W_{iae}	weight of instrumentation, avionics, and electronics, lbs
W_{ife}	weight of in-flight entertainment, lbs
$W_{landing\ gear}$	landing gear weight including fairing, lbs
W_{lavs}	weight of lavatories, lbs
$W_{missionfuel}$	weight of fuel required to complete the design mission, lbs
W_{misc}	weight of miscellaneous items, lbs
$W_{nacelle}$	weight of one nacelle, lbs
$W'_{nacelle}$	weight of one reference nacelle, lbs
W_{ox}	weight of oxygen system, lbs

$W_{payload}$	payload weight including passengers and luggage, lbs
$W_{payload}^{cabin}$	payload weight located in the passenger cabin, lbs
$W_{payload}^{cargo}$	payload weight located in the cargo bay, lbs
W_{paxs}	weight of passenger seats, lbs
$W_{propulsion}$	propulsion system weight, lbs
W_{pt}	weight of paint, lbs
$W_{structure}$	structural weight, lbs
$W_{trans\ sys}$	weight of engine transmission system, lbs
W_{water}	weight of water and related equipment onboard, lbs

Acronyms

CG	center of gravity
FPR	fan pressure ratio
L/D	lift to drag ratio
MTOW	maximum takeoff weight, lbs
OEW	operating empty weight, lbs
SFC	specific fuel consumption, kg/N-hr

Chapter 1

Introduction

Steady growth in commercial aviation and the resulting increase in air traffic has caused great concern over the impact of aircraft noise. Research suggests that living in high noise areas, such as those surrounding an airport, can have adverse effects on health and learning ability as well as property values [20, 27, 38, 41]. 62% of all airports face a noise problem and in the United States the 50 largest airports consider noise their biggest problem [44]. In an effort to address the noise problem, NASA announced a goal to lower aircraft noise 20 dB from 1997 technology by the year 2022 [21, 48].

1.1 Background and Related Work

Faced with increasingly strict regulations, airlines are forced to restrict operations and adhere to potentially costly noise abatement procedures. As a result, noise regulations are directly affecting the profitability of the airline industry and airlines are increasingly interested in lower noise aircraft. Modest noise reductions are possible using current technology, but it is becoming increasingly apparent that to achieve a step-change in noise, a radical re-design of the commercial aircraft configuration is necessary. Rather than considering noise a problem to be dealt with upon completion of a design for good performance, noise must become a primary concern from the early stages of the design process.

1.1.1 Aircraft operations

In the last twenty years, airframe noise has generally been considered negligible with respect to engine noise. There has been so much research invested in reducing engine noise that for a modern aircraft with high-bypass ratio engines, airframe noise is now comparable to engine noise on approach [21, 37]. Further reduction can only come with the simultaneous reduction of airframe and engine noise sources by a combination of lowering the acoustic power generated by all noise sources and developing approach and departure flight trajectories to minimize the noise impact on communities surrounding airports.

At many airports around the world, noise abatement procedures are in use to reduce noise in certain areas near the airport. Clarke and Hansman developed an aircraft operations tool which combines a flight simulator, noise model, and Geographic Information System (GIS). Population density and distribution data is considered along with the noise footprint of a flight path to evaluate the impact of the noise on the surrounding community [12]. Using a similar model, Visser and Wijnen have successfully demonstrated an algorithm which allows for the numerical optimization of departure trajectories for noise abatement purposes [49].

The obvious way to lower approach noise is to steepen the flight path and thus increase the distance between approaching aircraft and the communities surrounding the airport. Unfortunately, a slow and steep approach, while significantly reducing the impact of noise on the surrounding community, requires a much larger wing area and thus a heavier aircraft with higher operating costs [2, 3, 4, 7, 31, 36]. Even with modifications, conventional aircraft designs are not capable at maintaining a comfortable descent rate at angles steeper than about 4.5°. Increasing the approach path angle from the standard 3° to 4.5° can significantly reduce the impact of aircraft noise on communities near the airport, but even steeper approaches are more promising. Noise reductions, airport capacity, and safety margins all increase with steeper approach paths [8, 36].

With current technology, engine noise is still the dominant noise component on

takeoff. Further engine noise reductions are possible with modifications to bypass ratio, acoustic liners, and jet mixers, but current practice is to maintain a steep initial climb to gain altitude as quickly as possible [36]. Engine cutback is also used as a means to reduce engine noise by lowering the engine power once achieving a set altitude. Unfortunately, cutback is only marginally successful unless the pilot need not reapply engine power until away from inhabited land, as is the case at John Wayne (SNA) airport in Orange Country, California [3].

1.1.2 Design optimization

Multidisciplinary Design Optimization (MDO) is a process in which models are built to represent the assorted disciplines involved in a design process and integrated with an optimizer. Together, the models and optimizer are used to explore the design possibilities as defined by a set of variables. These "design variables" are typically a high level description of the system and, through a mathematical algorithm, are chosen by the optimizer to minimize an objective. In the case of aircraft design, typical disciplines represented include aerodynamics, structures, propulsion, and controls.

MDO is particularly useful in the preliminary design stage when critical design decisions are made which eventually impose constraints on the end result. With the use of MDO, more knowledge can be acquired in this early stage and trade-offs between disciplines can be explored without bias towards the historically well-established design decisions [28].

When designing an aircraft to perform well with respect to an unconventional metric such as noise, MDO can be used to add constraints to the design problem such that an aircraft that is too noisy is not a design possibility. Antoine and Kroo performed an optimization for low operating cost on conventional aircraft designs and operations with the constraint that the designs must meet certification noise requirements. In this study, it was found that the most important variable for noise reduction was engine bypass ratio rather than any planform or operations characteristics such as wing area, wing sweep, approach angle, or engine cutback points. An aircraft constrained to a noise reduction of 18 dB had a 6.3% higher operating cost

than one optimized for low cost with no noise constraint [3].

In another problem formulation, Antoine et al. optimized conventional aircraft with the objective of finding designs with minimum noise, fuel burn, cost, and NO_x emissions. It was found that optimizing for low noise resulted in a 15 EPNdB reduction in noise with respect to the minimum cost result, but the minimum noise design suffered from a 27% higher MTOW, a 17% higher fuel weight, and a cruise Mach number that dropped from 0.844 to 0.664 [4].

Leifsson et al. developed an optimization framework to design transport aircraft for low airframe noise on approach by targeting a noise reduction relative to a minimum maximum-takeoff-weight baseline. An aircraft is first optimized for minimum takeoff weight without considering noise. The resulting aircraft is considered the reference design and a noise analysis is performed to determine a reference noise level. The optimization for minimum weight is then performed again, this time with an added constraint that the noise must decrease by a set value. They conclude that a slow and steep approach is necessary to attain drastic noise reductions, but an aircraft design noise capable of this will incur a large weight penalty. Drastic design changes are needed to overcome the weight and performance penalties associated with designing for low noise, including a re-design of high lift devices and landing gear or possibly the entire aircraft configuration [31].

The general consensus is that with current technology it is possible to produce aircraft designs to meet strict environmental regulations, but only at a large cost. From an airline's perspective, the minimum noise aircraft is 26% more expensive to operate than the minimum cost aircraft [4]. From a passenger's perspective, a slower cruise speed translates to longer flights. Clearly, today's environmentally friendly aircraft would not be a practical solution unless mandated by extraordinarily strict regulations. One way to circumvent the adverse effects of a conventional low noise aircraft design is to reconfigure the aircraft.

1.1.3 The Blended-Wing-Body concept

The Blended-Wing-Body (BWB) concept is an attractive configuration when designing for noise because it is inherently quieter than a conventional aircraft design [11, 32, 34, 40]. High drag devices such as flaps and slats are the primary airframe noise sources on a conventional aircraft, but the BWB has a smooth trailing edge lacking slotted flaps and is thus an aerodynamically cleaner design [32, 37, 40]. Also, the top mounted engines allow the centerbody to shield forward radiated fan noise and prevent engine exhaust noise from reflecting off of the wing surface towards the ground [11, 32].

The BWB has long been known to offer significant aerodynamic performance advantages over the conventional "tube and wing" design [34]. Because the design closely integrates the wing, fuselage, propulsion, stability, and control, MDO is a promising way to investigate the tradeoffs amongst the traditional engineering disciplines. In particular, the Boeing Company's Wing Multidisciplinary Optimization Design (WingMOD) code has been applied to the BWB with great success [50, 51, 52]. It was originally applied to the design of a composite wing for a stretched MD-90 and later modified to be used in the optimization of a BWB [51, 52, 53]. Given a baseline BWB design, WingMOD juggles the closely coupled design requirements in aerodynamics, structures, and stability and control to produce a feasible BWB design with minimum takeoff weight [51].

1.2 Silent Aircraft Initiative

The Silent Aircraft Initiative (SAI) was formed by the Cambridge-MIT Institute as a collaborative effort between the Massachusetts Institute of Technology and the University of Cambridge. The goal of SAI is to produce a viable aircraft design representing a step-change in noise reduction technology. In a typical urban area the Silent Aircraft would be inaudible outside of the airport boundary. For this design to be competitive in the target year 2030, fuel burn and overall performance must meet or exceed standards set by modern conventional transport aircraft. Throughout the

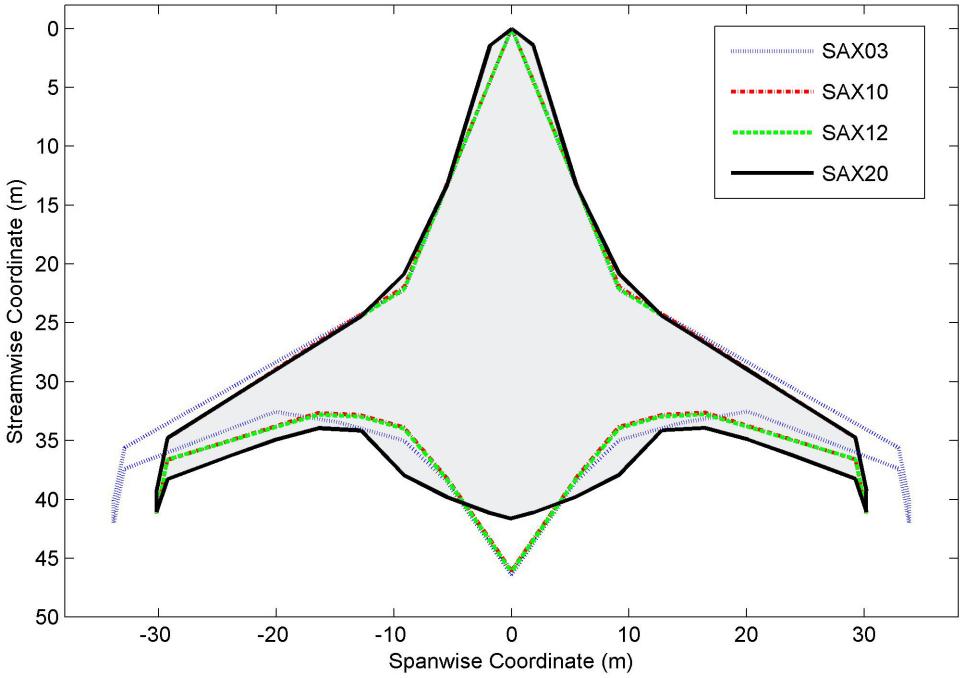

Figure 1-1: Evolution of the Silent Aircraft eXperimental (SAX) planform designs

design process, the airframe and engine designs, aircraft operations, and economic impact are being investigated simultaneously to bring these disciplines together and produce an integrated conceptual design of an aircraft radically quieter than those flying today–the Silent Aircraft eXperimental (SAX) passenger aircraft.

1.2.1 Evolution of the SAX and Granta designs

Under the assumption that for a constant technology level a lighter aircraft is always a quieter aircraft, WingMOD was used to optimize the BWB-like SAX designs for minimum takeoff weight [16]. Figure 1-1 and Table 1.1 show the evolution of the SAX planform designs and performance characteristics. The SAX10 design is described in detail by Diedrich [15].

Along with the SAX airframe designs, the SAI team has developed the Granta low noise engine. Figure 1-2 and Table 1.2 show the schematics and characteristics of the major engine designs, in the Granta series. For a typical propulsion system, the design is set by the top-of-climb (TOC) operating point. At top of climb, the engines

Table 1.1: Selected characteristics of the Silent Aircraft eXperimental (SAX) designs

	Range (nm)	Mach number	Cruise L/D	Span (ft)	Area (ft^2)	MTOW (lbs)	SFC (lbm/lbf-hr)
SAX03	4,000	0.85	18.2	216	8,506	357,549	0.58
SAX10	4,000	0.80	22.0	192	8,113	336,944	0.54
SAX12	5,000	0.80	21.9	192	8,114	340,151	0.50
SAX20	5,000	0.80	22.3	192	9,086	328,919	0.50
SAX31	5,000	0.80	22.6	185	9,096	326,606	0.50

Table 1.2: Characteristics of the Granta designs [22]

	Configuration	Fan Diameter (m)	Length (m)	Total Thrust (kN)	Fuel Flow (g/s)
Granta-151	4 engines	2.159	3.45	88.56	1050.0
Granta-252	4 engines	2.159	2.41	88.56	1043.0
Granta-3201	3 cores, 9 fans	1.292	1.98	61.00	845.7

must provide sufficient thrust to maintain a positive climb rate despite unfavorable atmospheric conditions. For the Granta engines, however, the takeoff operating point is also of great concern due to the noise generated by the engines operating at maximum power. To reduce noise, the Granta propulsion system incorporates ultra-high bypass ratio engines with an embedded, boundary layer ingesting inlet and a variable exhaust nozzle. A detailed analysis of the engine cycle and acoustics has been performed by Hall and Crichton [13, 23].

1.2.2 The SAX20 design with Granta-3201

Although a number of Silent Aircraft designs will be considered in this thesis, the primary baseline design is SAX20. SAX20 is a 215 passenger aircraft designed for a cruise mission of 5,000 nautical miles at Mach 0.8. The beginning cruise altitude is 40,000 feet climbing to 45,000 feet by the end of cruise. The propulsion system is made up of three embedded Granta-3201 engines, each with one core and three fans as shown in Figure 1-2(c). Each engine consists of one main fan and two auxiliary fans connected to the core by a transmission system of shafts and gear boxes. Further details on the Granta design are given in References [13] and [23]. To create a

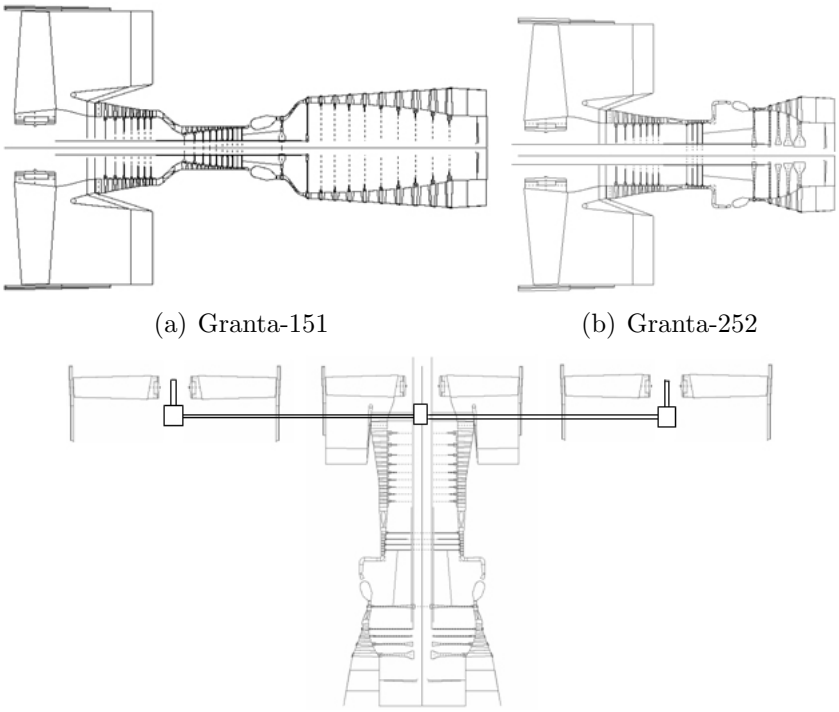

(a) Granta-151 (b) Granta-252

(c) Granta-3201

Figure 1-2: Evolution of the Granta engine designs [24]

Figure 1-3: Artist's rendition of SAX20

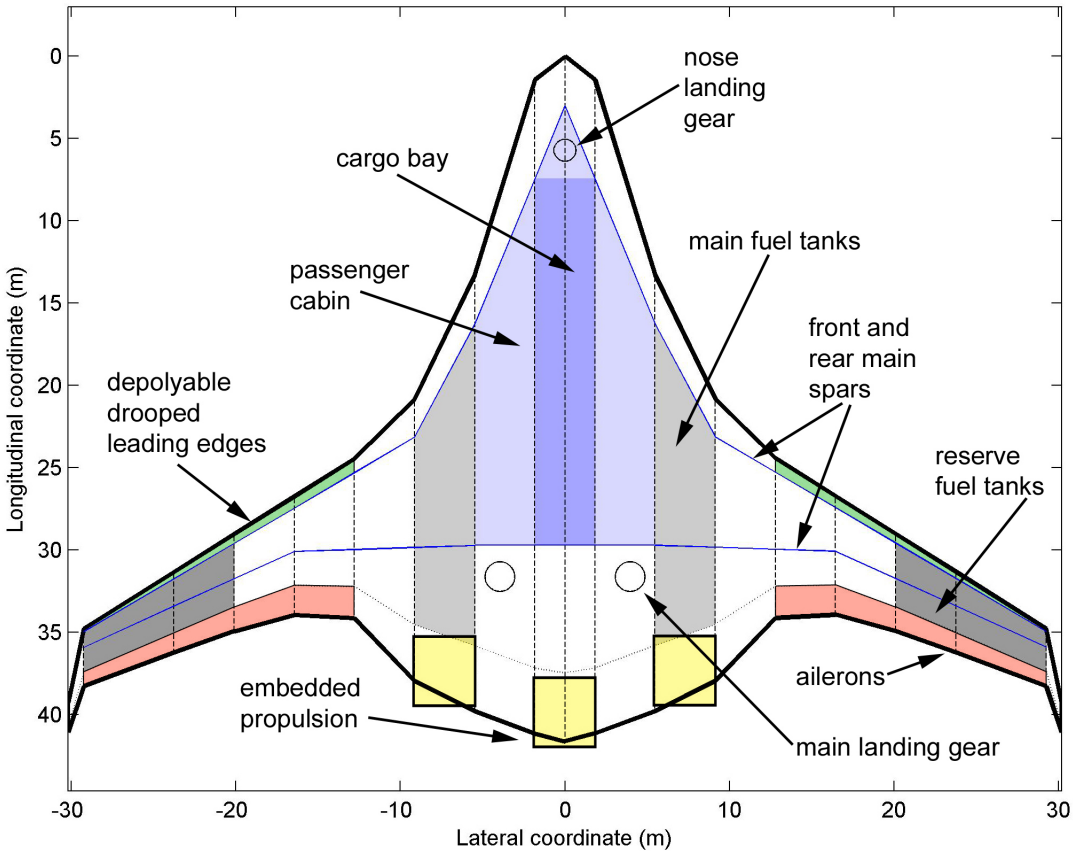

Figure 1-4: Planform layout for the SAX20 design

three-dimensional airframe, a quasi-inverse design methodology was developed. The airframe design process, cruise performance analysis, and approach performance analysis was integrated into an overall design framework in order to achieve a low-noise aircraft with performance comparable to modern conventional aircraft [26].

The SAX20 planform layout is shown in Figure 1-4. The airframe ribs are shown as dashed lines. Also shown are the front and rear spars and the control surface hinge line. Regions intended for use as high lift devices and ailerons are shaded, along with the cabin, cargo bay, and fuel tanks. The SAX20 cabin was scaled from the BWB cabin schematic drawn by Liebeck [32]. Similarly, the cargo bay was fitted to the center third of the cabin width and has 877.5 ft^2 of cargo space. The nose and main landing gear bogies are each drawn as a black circle of a diameter equal to that of the tires. The dimensions of the landing gear can be found in Chapter 2, Table 2.4.

Table 1.3: Selected characteristics of SAX21

Parameter	Value
Number of passengers	215
Number of crew	10
Range, nm	5,000
Number of engines	3
SFC, kg/N-hr	0.051
C_{D_0}	0.0060
Planform area, m^2	844.12
Wing span excluding winglets, m	58.22
Cargo bay floor area, m^2	79.70
Passenger cabin floor area, m^2	269.60
Altitude at airport boundary, m	26.24

Using the design methodology described by Hileman et al., airfoils have been developed for each rib shown in Figure 1-4 [26]. Wing twist was determined to minimize control surface deflections at the beginning of cruise, and is thus a function of the airfoils chosen. The parasite drag coefficient, C_{D_0}, for SAX20 in cruise is approximately 0.0060.

1.2.3 The SAX21 design

SAX20 was used as the initial design point for the current work. Using the SAX20 planform and the Granta-3201 propulsion system, the design models were improved, most notably those predicting the weights and center of gravity. Using the updated weight data, wing twist was modified to once again minimize control surface deflections at mid-cruise for the new aircraft. The resulting design is SAX21. Many characteristics of SAX21 are identical to those of SAX20: the entire planform layout, airfoil cross sections, and propulsion system. Defining features such as aircraft weights, center of gravity, and wing twist are described in Sections 2.2, 3.2, and 4.6. A summary of the parameters used to develop SAX21 are given in Table 1.3.

1.3 Objectives

The purpose of this research is to explore tradeoffs in airframe design, engine design, airfoil design, and aircraft operations to develop a quiet aircraft-operations system. From the previous work described in Section 1.1, it is assumed that the noise problem on approach can be addressed by incorporating a steep and slow approach to landing. Therefore, the most noise-critical point is the initial climb after takeoff. To find minimum noise aircraft-operations designs, an aircraft design and analysis model is developed and incorporated in a multidisciplinary design optimization framework. To this end, the objectives addressed in this thesis are:

- Develop an aircraft design model capable of generating Silent Aircraft designs including airframe and engine, weights and center of gravity, takeoff operations, airfoil profiles, and noise prediction.
- Integrate the aircraft design model with a single-level optimization to find minimum noise aircraft-operations system designs.
- Create a distributed optimization framework for the Silent Aircraft problem.
- Evaluate the optimal aircraft-operations system designs obtained from both the single-level and distributed optimization frameworks to determine what design changes can be made to lower the noise observed on the ground during a Silent Aircraft takeoff.

1.4 Outline

The complete aircraft design and analysis model as shown in Figure 1-5 is composed of several modules representing various engineering disciplines: mass properties, airframe design, engine design, flight mechanics, aircraft operations, and noise prediction. Detailed descriptions of the weight and center of gravity models are given in Chapters 2 and 3. Chapter 4 describes the other components of the aircraft design model.

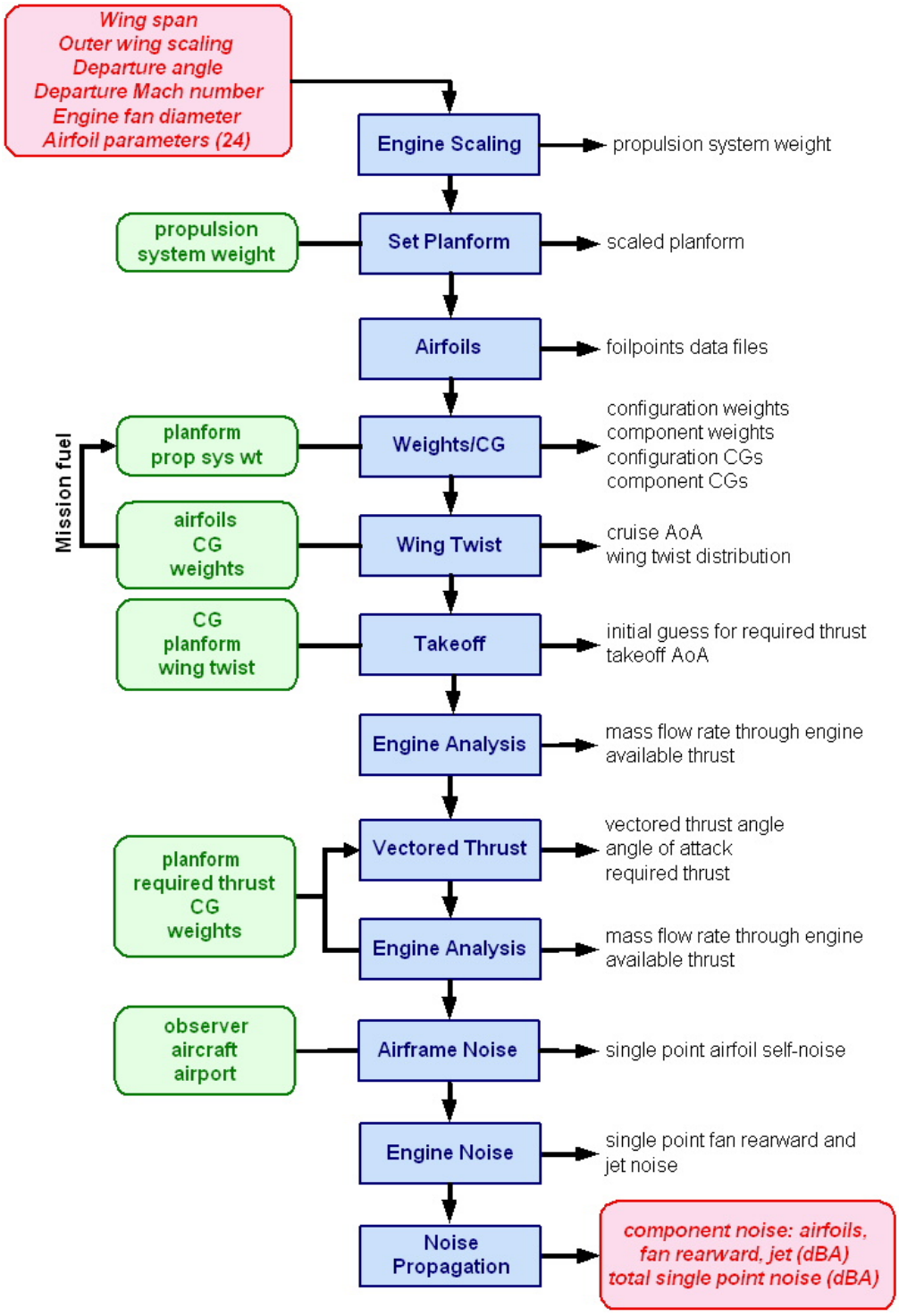

Figure 1-5: Complete aircraft design and analysis model

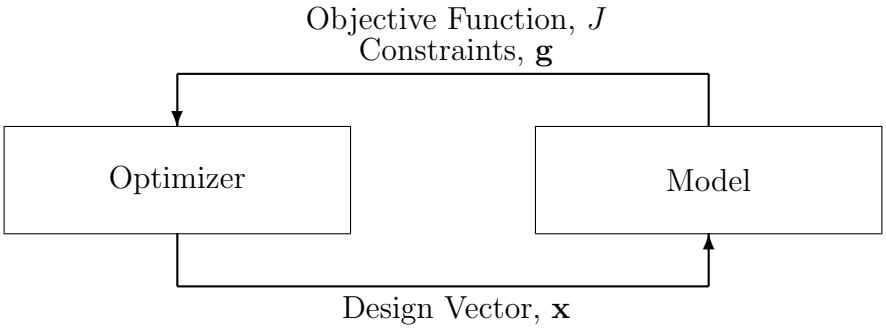

Figure 1-6: Single level optimization framework

To approach the optimization problem, two methods were used: single level optimization and distributed optimization. In a single level optimization framework, one optimizer is linked to a single model as shown in Figure 1-6. The optimizer selects values for the design variables and the model evaluates those values to return a value for the objective function. In distributed optimization, loosely coupled disciplinary models are separated and each controlled individually by a subspace optimizer. At the subspace level, subspace design variables are used to make local design decisions subject to subspace constraints. To coordinate the subspace efforts, a system level optimizer is used to ensure compatibility across the disciplines. The system level optimizer is responsible for minimizing the system objective function subject to the constraint that the disciplines agree on values for the variables that are used in more than one model [29]. A schematic of such a framework is given in Figure 1-7.

Chapter 5 contains the formal problem statement for the silent aircraft optimization problem, summarized in Table 1.4, as well as a description of the single-level optimization framework. In Chapter 6, the distributed optimization problem formulation and framework are explained.

Chapter 7 contains the results from both optimization frameworks. Three optimization subproblems are laid out and solved using a gradient based single-level optimization framework. First, the optimization was performed using only the design variables representing the aircraft design and operations. Secondly, the optimization was performed using only the design variables representing the outer wing airfoil profiles. The third optimization was performed using the complete set of design variables

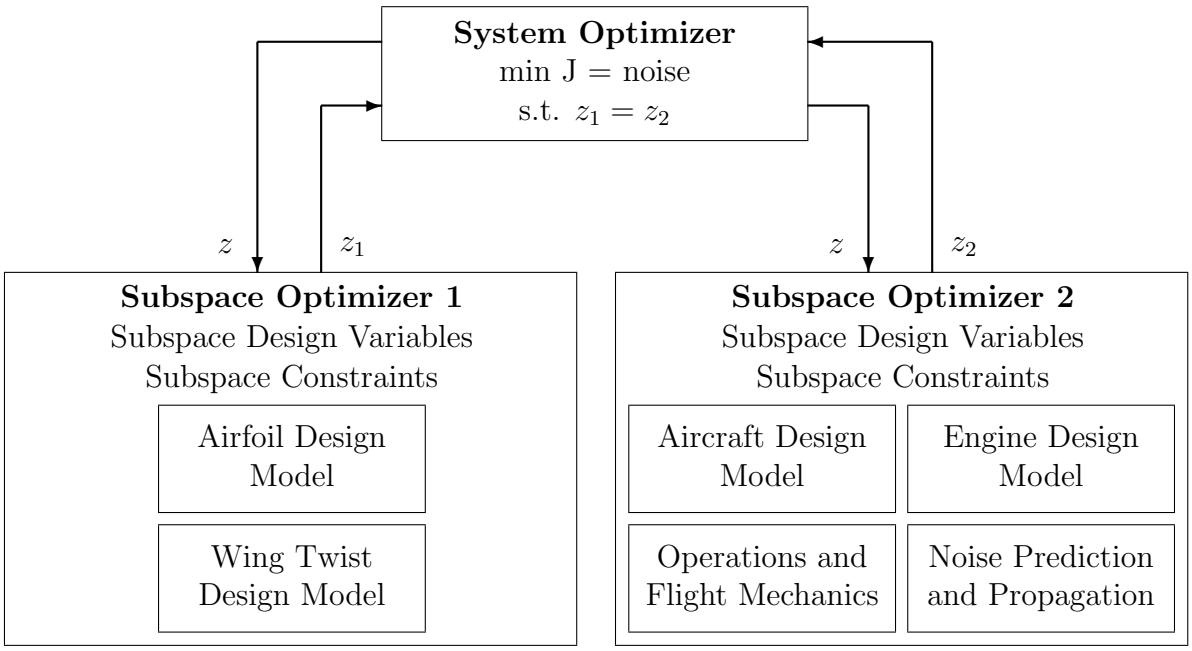

Figure 1-7: Sample distributed optimization framework

Table 1.4: Silent aircraft optimization problem description

Objective:	Total aircraft noise as observed at a single point
Design Variables:	Wing span
	Outer wing chords
	Engine fan diameter
	Departure flight path angle
	Departure flight velocity
	Outer wing airfoil shape
Constraints:	Angle of attack during cruise
	Angle of attack on initial climb
	Thrust vectoring angle on initial climb
	Runway length required for takeoff

representing aircraft design, operations, and airfoil design. The optimal design from the distributed optimization framework is presented and compared to the results from the single-level optimization and the reference aircraft.

Finally, the conclusions of this research are presented in Chapter 8.

Chapter 2

Aircraft Weight Model for the SAX Design

Weight estimation models are readily available for conventional aircraft, but due to the unconventional BWB-type airframe and Granta-3201 distributed propulsion system, a weight model developed for a conventional "tube and wing" aircraft does not apply to the SAX design. To capture the weight differences, a new weight model was developed. In weight categories such as passengers, food, furnishings, and others which are unlikely to differ significantly from one design to another, modifications were made to established empirical formulas to account for SAX weight differences. In some categories such as structure, there is little or no existing data, so new relationships were found. Upon completion of the weight model, a sensitivity analysis was performed to determine which parameters are the most critical to the complete weight analysis.

2.1 Weight Estimation

In general, the aircraft weights of primary interest are the operating empty weight (OEW) and maximum takeoff weight (MTOW). The OEW can be written as the sum

of four system weights,

$$OEW = W_{structure} + W_{propulsion} + W_{landing\ gear} + W_{fixed\ equipment}, \tag{2.1}$$

where $W_{structure}$ is the weight of the airframe structure, $W_{propulsion}$ is the weight of the propulsion system, $W_{landing\ gear}$ is the weight of the landing gear, and $W_{fixed\ equipment}$ is the weight of fixed equipment. Adding the design fuel weight, W_{fuel}, and the payload weight, $W_{payload}$, to the OEW results in the maximum takeoff weight, given by

$$MTOW = OEW + W_{fuel} + W_{payload}. \tag{2.2}$$

2.1.1 Propulsion

The propulsion system weights include bare engines, transmission systems, nacelles, and structure required to support the engine installation. The three thrust vectoring nozzles were assumed to weigh 2,000 lbs and the integration of the three embedded nacelles 2,500 lbs [5]. Incorporating these weights, the propulsion system weight becomes

$$W_{propulsion} = n_{eng}\left(W_{eng} + W_{trans\ sys} + W_{nacelle}\right) + 2,000 + 2,500 \tag{2.3}$$

where n_{eng} is the number of engines, W_{eng} is the weight of a single bare engine, $W_{trans\ sys}$ is the weight per engine of the transmission system as described in Section 1.2.2, and $W_{nacelle}$ is the weight of a single nacelle. Both engine and nacelle weights are scaled from known values according to fan diameter. Transmission system weights are assumed to be constant for engines producing similar amounts of thrust.

As expected, engine weight increases with fan diameter, but due to hollow parts and other components which depend on the fan tip speed rather than fan diameter, weight does not scale with the cube of fan diameter [23]. From existing data, the

relationship between engine weight and fan diameter is

$$W_{eng} \propto n_{eng} D_f^{2.4} \tag{2.4}$$

as discussed by Hall and Crichton [23]. Adjusting for a distributed propulsion system with auxiliary fans, this relationship becomes

$$W_{eng} = N_{core} W_{core} + N_{fan} W_{fan} \left(\frac{D_f}{D'_f} \right)^{2.4} \tag{2.5}$$

where W_{eng} is the weight of one engine including its auxiliary fans, N_{core} is the number of cores per engine, N_{fan} is the number of fans per engine, W_{fan} is the weight of a reference fan, D_f is the diameter of the scaled fan, and D'_f is the diameter of the reference fan.

Similarly, the weight of a scaled nacelle can be found from a reference nacelle weight. Scaling nacelle weight with bare engine weight from an adaption of a statistical weight equation given by Raymer,

$$W_{nacelle} = W'_{nacelle} \left(\frac{W_{eng}}{W'_{eng}} \right)^{0.611}$$

where W_{eng} is the bare engine weight and W'_{eng} is the weight of one engine which is contained by one nacelle of weight $W'_{nacelle}$ [42].

2.1.2 Fuel

The total fuel on board at MTOW includes the fuel that is required to complete the mission as well as that which is reserve or trapped. Assuming reserve and trapped fuel is 10% of mission fuel, the total design fuel is given by

$$W_{fuel} = 1.10 \, W_{mission\ fuel}.$$

For a simple cruise mission, mission fuel weight (lbs) can be found from

$$W_{mission\ fuel} = \frac{1}{2}\rho(Ma)S(C_{D_i} + C_{D_0}) \cdot SFC \cdot R \cdot K_1 \cdot \frac{1}{3600} \tag{2.6}$$

where the atmospheric parameters are those at the average cruise altitude, the range R is in meters, SFC is the specific fuel consumption in kg/N-hr, and the factor $K_1 = 2.2046$ is the number of pounds per kilogram.

As seen above, mission fuel weight is a function of induced drag. In the complete aircraft design model, induced drag is a function of wing twist which is set to provide a zero pitching moment in cruise. Therefore, mission fuel weight is a function of induced drag which is indirectly a function of aircraft weight. To resolve this coupling, a loop was implemented as shown in Figure 2-1. Initially, the aircraft weights and center of gravity (CG) are calculated using an estimated fuel weight. The resulting CG is used to determine wing twist and induced drag, from which the mission and design fuel required can be found. This calculated required fuel weight is then compared to the fuel originally assumed to be onboard when calculating the aircraft weight and CG. If there is more than 1% difference between the fuel assumed onboard and the fuel required, the fuel required weight is used to recalculate the aircraft weight, CG, wing twist, and induced drag.

2.1.3 Payload

Payload weights are broken into two categories: weight located in the cabin and weight located in the cargo bay. Standard average weights from FAA Advisory Circular 120-27E are used to calculate the weight of passengers, hand luggage, and checked luggage. Assuming summer weights, the average weight of an adult passenger and their hand luggage is 190 lbs [1]. Crew members are also considered, thus

$$W_{payload}^{cabin} = 190(N_{cr} + N_{pax})$$

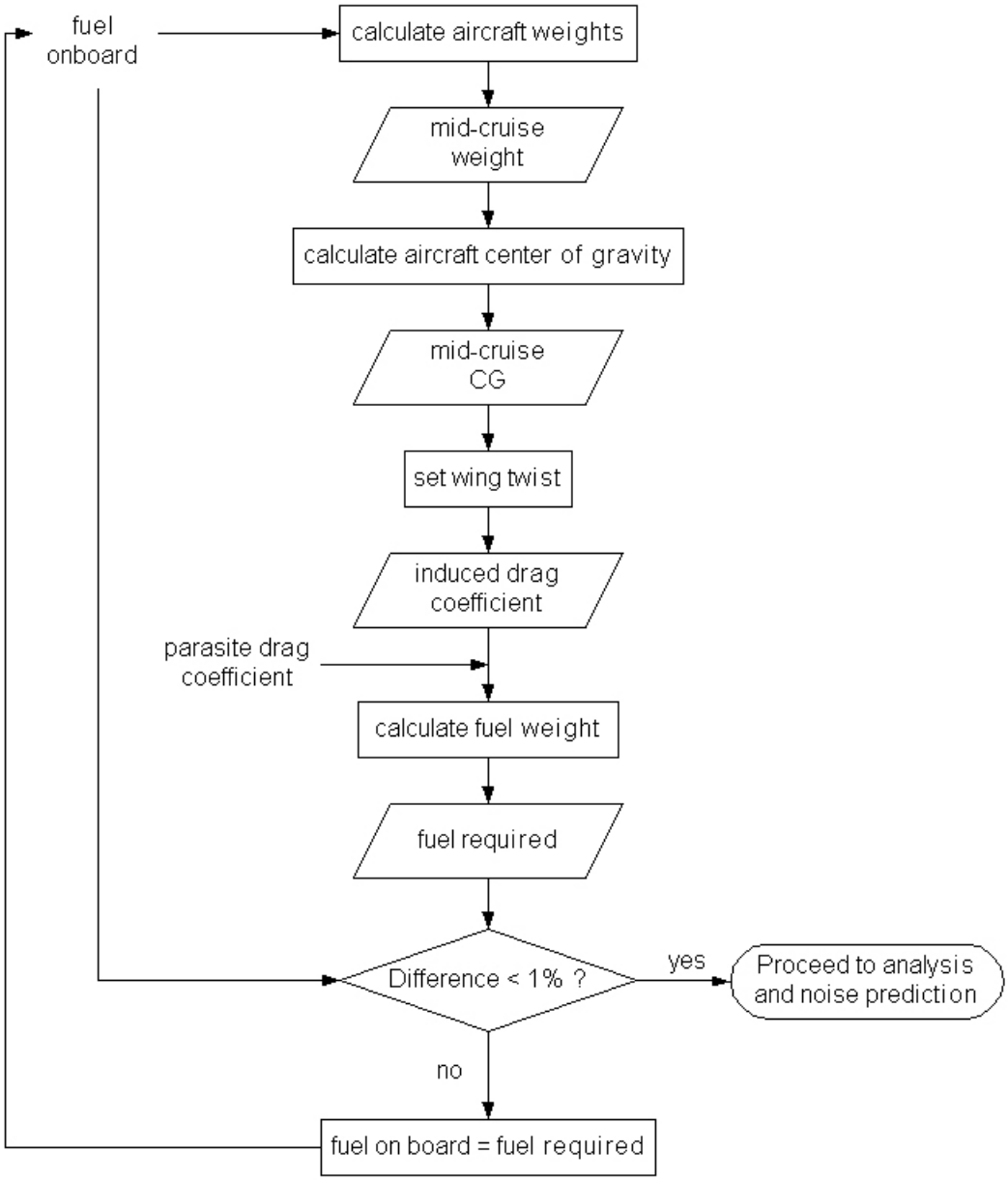

Figure 2-1: Iteration loop for calculation of mission and design fuel weight

where $W_{payload}^{cabin}$ is the payload weight located in the cabin and N_{cr} and N_{pax} are the number of crew and passengers. The average weight per passenger of checked luggage located in the cargo bay is 30 lbs [1]. Crew are not included in this count, so the payload weight located in the cargo bay is given by

$$W_{payload}^{cargo} = 30\ N_{pax}.$$

2.1.4 Structure

There are many empirical relations that can be used to estimate the structural weight of a conventional aircraft, but the SAX airframe is much more similar to a BWB than a conventional tube and wing. Because there is no data published on the structural weight of a BWB-like airframe, WingMOD was used to generate structural weight data [51, 52]. Some versions of the WingMOD structural weight model for a BWB have been validated by Boeing Phantom Works in internal proprietary studies, including high fidelity finite-element analyses. From these studies, it is known that the version of the structural weight model used here is slightly optimistic but within reason when considering the likely advances in composite technology [33]. Using the WingMOD BWB weight model to estimate the structural weight of the SAX, three sets of structural weight values were computed for a range of planform areas, propulsion system weights, and design fuel weights, given in Table 2.1. Data Set #1 represents some of the previous SAX designs. Data Set #2 was selected to cover the range of aircraft designs possible using the design model as described in Chapter 4. Data Set #3 is simply the combination of #1 and #2, dropping data for the two designs in Set #1 which are not within the bounds of Set #2.

A least squares response surface of the form

$$W_{structure} = x_1 P_1 + x_2 P_2 + x_3 P_3 + \ldots$$

where x_i are constant coefficients and P_i are aircraft parameters was fit to each data set. The constant coefficients can be found from a system of linear equations

Table 2.1: BWB structural weight data as found using the WingMOD structural weight model

	Planform Area (ft^2)	Propulsion System Weight (lbs)	Design Fuel Weight (lbs)	Structural Weight (lbs)
Data Set #1	8,071	27,404	72,192	83,940
	8,218	30,447	113,368	87,009
	8,114	27,404	90,745	84,646
	9,068	35,130	162,231	95,989
Data Set #2	6,819	30,636	104,945	97,505
	9,076	30,636	94,656	107,793
	11,421	30,636	97,708	104,742
	11,421	36,951	97,946	98,189
	9,078	36,951	92,870	103,263
	6,819	36,951	101,258	94,876
Data Set #3	8,218	30,447	113,368	87,009
	9,068	35,130	162,231	95,989
	6,819	30,636	104,945	97,505
	9,076	30,636	94,656	107,793
	11,421	30,636	97,708	104,742
	11,421	36,951	97,946	98,189
	9,078	36,951	92,870	103,263
	6,819	36,951	101,258	94,876

Table 2.2: SAX structural weights as calculated from response surfaces

	Planform Area (ft^2)	Propulsion System Weight (lbs)	Design Fuel Weight (lbs)	Structural Weight (lbs)
Data Set #1	9,081	31,905	86,500	95,152
Data Set #2	9,081	31,905	84,128	89,671
Data Set #3	9,081	31,905	86,246	94,549

assembled from the known data,

$$\begin{bmatrix} S^1 & W^1_{propulsion} & W^1_{fuel} \\ \vdots & \vdots & \vdots \\ \vdots & \vdots & \vdots \\ S^n & W^n_{propulsion} & W^n_{fuel} \end{bmatrix} \begin{bmatrix} x_1 \\ x_2 \\ x_3 \end{bmatrix} = \begin{bmatrix} W^1_{structure} \\ \vdots \\ \vdots \\ W^n_{structure} \end{bmatrix},$$

where S, the planform area in square feet, $W_{propulsion}$, the weight of the propulsion system in pounds, and W_{fuel}, the weight of the design fuel in pounds are the aircraft parameters, P_i. Having found the values of the constant coefficients, the structural weight for an aircraft with a given planform area, propulsion system weight, and design fuel weight can be found from

$$W_{structure} = x_1 S + x_2 W_{propulsion} + x_3 W_{fuel}.$$

To decide which of the three response surfaces to use in the final structural weight model, each was used to find the weight of a design similar to SAX21. The SAX21 inputs were provided to the model and the iterations for fuel and landing gear weight were allowed to converge. In Table 2.2 it can be seen that Data Set #2, the one selected to evenly span the possible designs, resulted in a response surface that predicts a structural weight approximately 5.8% lower than the other two surfaces. The response surfaces built from Data Sets #1 and #3 predict structural weights which are only 0.6% different from each other, but Set #1 is undesirable because it contains infeasible design points. Choosing the more conservative of the two response surfaces built completely from feasible aircraft designs, Data Set #3 was selected to build the

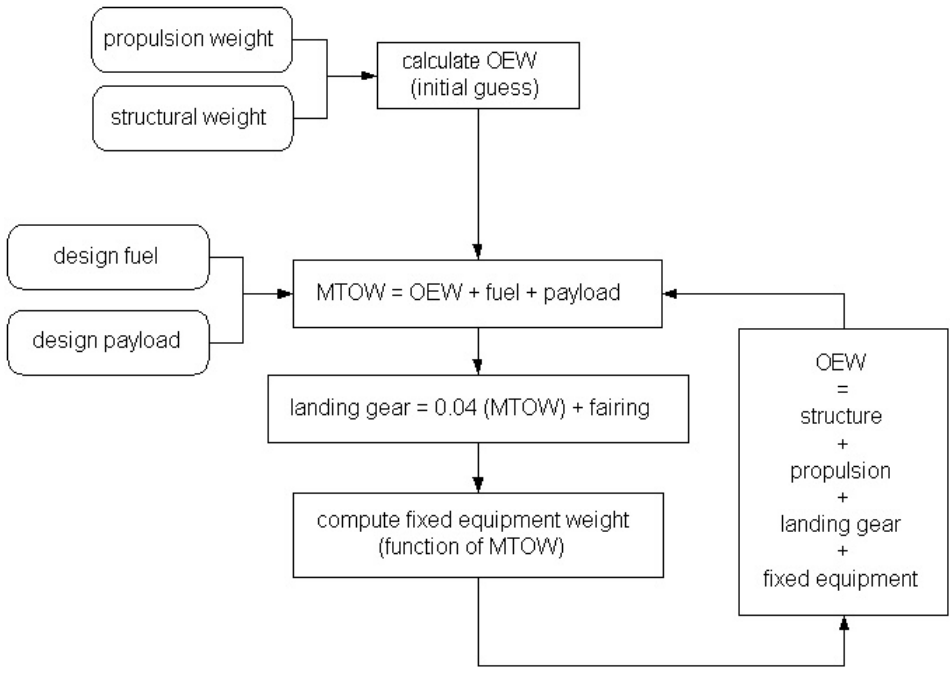

Figure 2-2: Iteration loop for landing gear and fixed equipment weights

final response surface. The structural weight of the SAX designs is related to the selected aircraft characteristics by

$$W_{structure} = 3.3124\ S + 1.9396\ W_{propulsion} + 0.0300\ W_{fuel}.$$

2.1.5 Landing gear

Landing gear weight is estimated as 4% of the calculated MTOW plus a constant fairing weight. Because MTOW is a function of landing gear weight, the loop shown in Figure 2-2 was implemented. Initially, the OEW is estimated as twice the structural weight plus the weight of the propulsion system. Using this estimate, the MTOW is determined according to Equation 2.2. The fixed equipment weight as described in Section 2.1.6 is then calculated and the OEW value updated according to Equation 2.1. The procedure is repeated as shown in Figure 2-2 until the percent difference between the assumed and calculated landing gear weights drops below 0.5%.

To estimate the weight of the landing gear fairing, the geometry was approximated

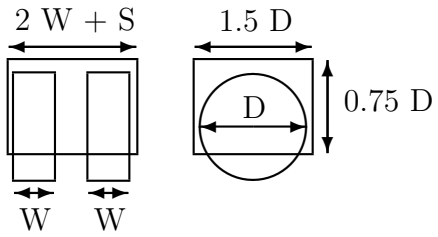

Figure 2-3: Schematic of landing gear fairing

as a rectangular prism of the dimensions shown in Figure 2-3, where D is the wheel diameter, W is the wheel thickness or width, and S is the wheel separation for a two wheel bogey. The weight of the fairing for one bogey can be found from

$$W_{fairing} = \left[\frac{9}{4}D^2 + 3D(2W + S)\right] t\rho_{mat}$$

where t and ρ_{mat} are the thickness and density of the material.

2.1.6 Fixed equipment

The fixed equipment weight was broken into categories according to equipment types. Since fixed equipment weights for a SAX should be similar to those for a conventional aircraft, Roskam's Class II method for commercial transport aircraft was used as a starting point, adjusting some categories to account for the unconventional SAX design [43].

Furnishings and operational items

Equation 2.7 was used to determine the weight of furnishings and operational items. The first three terms of this equation account for the flight deck, passenger, and crew seats which are assumed to weigh 55, 32, and 15 lbs each, respectively [43].

$$W_{furOps} = W_{fds} + W_{paxs} + W_{cs} + W_{food} + W_{water} + W_{galleys} + W_{lav} + W_{misc} + W_{ife} \quad (2.7)$$

To estimate W_{food}, the weight of food onboard, it was assumed that each meal

and associated equipment weighs $W_{meal} = 10$ lbs. The weight of food onboard is thus given by

$$W_{food} = N_{meals} W_{meal} \tag{2.8}$$

where N_{meals} is the total number of meals served during the flight and should account for passengers and crew. For long flights, N_{meals} should allocate more than than one meal per person.

To calculate W_{water}, the weight of water and related equipment onboard, it was assumed that each passenger and crew member requires $C_{water} = 1/2$ gallons of water per hour. The weight of water onboard is given by

$$W_{water} = C_{water}(N_{cr} + N_{pax})\frac{R}{Ma}\rho_w g \tag{2.9}$$

where R is the design mission range, M is the cruise Mach number, a is the speed of sound at the average cruise altitude, and ρ_w is the density of water.

The weight of lavatories and associated water is given by

$$W_{lav} = K_{lav} N_{pax}^{1.33} \tag{2.10}$$

where for a long range aircraft, $K_{lav} = 1.11$ [43].

The final two components of the furnishings and operational items weights are miscellaneous items and in-flight entertainment. W_{misc}, the weight of miscellaneous items, is given by

$$W_{misc} = 7.71 \times 10^{-4} MTOW$$

and accounts for weights which are not itemized above. The Thales TopSeries i-4500 is a 75/90 passenger in-flight entertainment system and weighs 400 lbs, approximately 5 pounds per passenger [14]. Assuming the same per passenger weight for SAX in-flight entertainment,

$$W_{ife} = 5\ N_{pax}. \tag{2.11}$$

Baggage and cargo handling equipment

Baggage and cargo handling equipment was estimated as 3 lbs/ft^2 of freight floor area, thus

$$W_{bc} = 3S_{ff} \tag{2.12}$$

where S_{ff} is the freight floor area in square feet and W_{bc} is the weight of the baggage and cargo handling equipment in pounds [43].

Air-conditioning, pressurization, and anti-/de-icing system

The weight of the air-conditioning, pressurization, and anti-/de-icing system is given by

$$W_{api} = 469 \left(\frac{V_{pax}(N_{cr} + N_{pax})}{10,000} \right)^{0.419} \tag{2.13}$$

where V_{pax} is the volume of the passenger cabin in cubic feet, N_{cr} is the number of crew, and N_{pax} is the number of passengers [43].

Electrical system

The weight of the electrical system can be estimated from

$$W_{els} = 10.8 \, V_{pax}^{0.7}(1 - 0.018 \, V_{pax}^{0.35}) \tag{2.14}$$

where V_{pax} is the volume of the passenger cabin in cubic feet [43].

Instrumentation, avionics, and electronics

The instrumentation, avionics, and electronics weight can be estimated from

$$W_{iae} = 0.575 \, OEW^{0.556} R^{0.25} \tag{2.15}$$

where R is the maximum range in nautical miles. The estimate for this system is most likely conservative as the equation was originally written to estimate the

instrumentation weight of aircraft before modern computer based instrumentation was widely available [43].

Flight control system

The weight of the flight control system can be found from

$$W_{fc} = K_{fc} MTOW^{2/3} + W_{le} \tag{2.16}$$

where, for airplanes with powered flight controls, $K_{fc} = 0.64$ [43]. The addition of $W_{le} = 1,000$ lbs is meant to account for unconventional leading edge devices such as the deployable drooped leading edges on SAX21 [5].

Hydraulic and pneumatic system

The hydraulic and pneumatic system weight is given by

$$W_{hps} = C_{hps}\, MTOW. \tag{2.17}$$

For commercial transport aircraft, C_{hps} has been found to be between 0.0060 and 0.0120 [43]. Since a BWB-type aircraft will require large control surfaces, the upper limit of these C_{hps} values is used.

Auxiliary power unit

Lacking detailed weight data for an APU, the weight was estimated according to

$$W_{apu} = C_{apu} MTOW. \tag{2.18}$$

Roskam suggests that $0.004 \leq C_{apu} \leq 0.013$ [43]. Due to the large amount of power that a SAX would require to properly actuate large control surfaces and thrust vectoring in order to ensure a safe emergency landing, $C_{apu} = 0.013$.

Paint

An estimate of the weight of paint on a well painted aircraft is provided by

$$W_{pt} = C_{pt} MTOW \tag{2.19}$$

where $C_{pt} = 0.0045$ [43].

Oxygen system

The weight of the oxygen system can be estimated from

$$W_{ox} = 7(N_{cr} + N_{pax})^{0.702} \tag{2.20}$$

where $N_{cr} + N_{pax}$ is the total number of people on board [43].

Auxiliary gear

The weight of auxiliary gear is given by

$$W_{aux} = 0.01\ OEW. \tag{2.21}$$

this category was created to estimate the weight of unaccounted items [43].

2.2 Evaluation of SAX21 Weights

The weight model detailed in Section 2.1 was used to determine the system and component weights of the SAX21 design. SAX21 is a 215 passenger and 10 crew member aircraft designed for a 5,000 nautical mile range at Mach 0.8. Further details on the planform layout and propulsion system can be found in Section 1.2.2. The values used for constants in the equations for the landing gear and fixed equipment weights are given in Tables 2.3 and 2.4.

A detailed breakdown of fixed equipment component weights and furnishings and operational items weights can be found in Tables 2.5 and 2.6. The systems weight

Table 2.3: Values used to determine SAX21 landing gear and fixed equipment component weights

Variable	Category	Value	Units
ρ_{mat}	Landing gear	2,700	kg/m^3
t	Landing gear	0.00635	m
C_{apu}	Auxiliary power unit	0.013	
C_{hps}	Hydraulic and pneumatic system	0.012	
C_{pt}	Paint	0.0045	
C_{water}	Furnishings and operational items	0.50	gal/hr
K_{fc}	Flight control system	0.64	
K_{lav}	Furnishings and operational items	1.11	
N_{meals}	Furnishings and operational items	450	
S_{ff}	Baggage and cargo handling equipment	857.83	ft^2
V_{pax}	Air conditioning; Electrical system	18,862	ft^3
W_{galley}	Furnishings and operational items	3,000	lbs
W_{le}	Flight control system	1,000	lbs

Table 2.4: SAX21 landing gear tire dimensions

	diameter, m	width, m	separation, m
nose gear	1.35	0.4	0.5
main gear	1.82	0.4	0.5

Table 2.5: Fixed equipment component weights

Component	Weight, lbs
Furnishings and op items	27,562
Flight controls	4,112
Auxiliary power unit	4,409
Instrumentation, avionics, and electronics	4,320
Hydraulic and pneumatic system	4,070
Baggage and cargo handling equipment	2,574
Auxiliary gear	2,031
Paint	1,523
Air-conditioning, pressurization, and anti-/de-icing system	5,919
Electrical system	4,626
Oxygen system	314
Total	**61,463**

Table 2.6: Furnishings and operational items weights

Component	Weight, lbs
Food	4,500
Water	10,211
Galleys	3,000
Flight deck seats	110
Passenger seats	6,880
Crew seats	120
Lavatories and water	1,404
In-flight entertainment	1,075
Miscellaneous	262
Total	**27,562**

breakdowns for SAX21 at OEW and MTOW are given in Tables 2.8 & 2.7 and Figures 2-5 & 2-4.

2.3 Sensitivity

Because the fixed equipment component weights are partially determined from empirical relationships, there is some uncertainly associated with choosing values for constants in those equations. Upper and lower bounds or discrete values for different aircraft types may be given in the literature, but modern unconventional aircraft of-

Table 2.7: OEW system weights

Component	Weight, lbs
Structure	94,567
Fixed equipment	61,463
Propulsion	31,905
Landing gear	15,020
Total	**202,956**

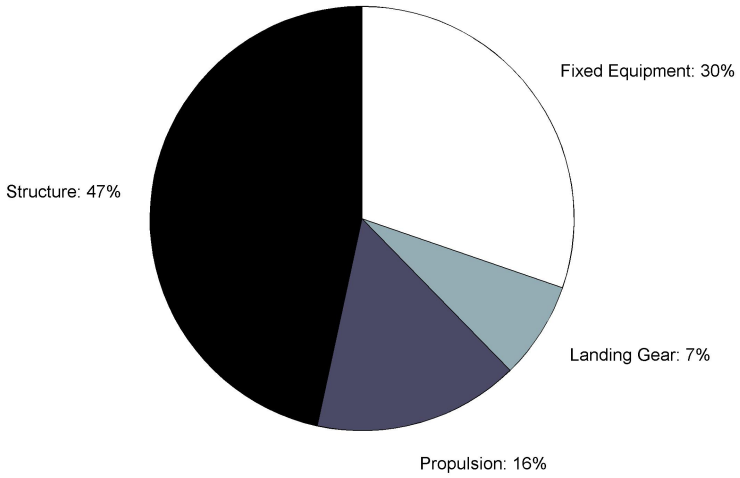

Figure 2-4: OEW system weight breakdown

Table 2.8: MTOW system weights

Component	Weight, lbs
Structure	94,567
Fuel	86,839
Fixed equipment	61,463
Payload	49,200
Propulsion	31,905
Landing gear	15,020
Total	**338,995**

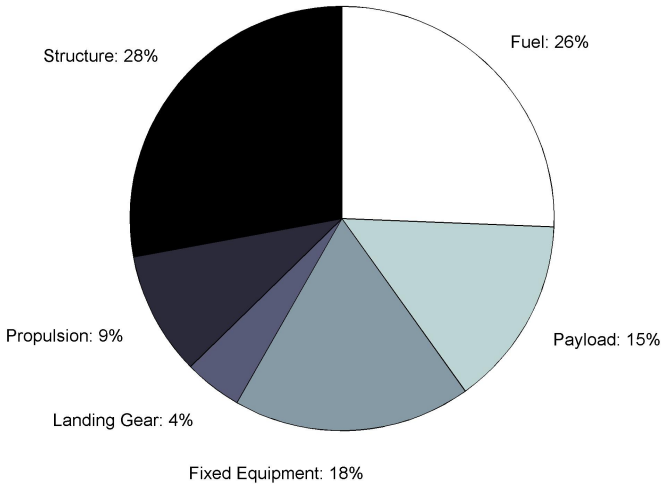

Figure 2-5: MTOW system weight breakdown

Table 2.9: Selected constants in fixed equipment weight equations

C_{apu}	fraction of MTOW used to compute APU weight, Eq. 2.18
C_{hps}	fraction of MTOW used to compute HPS weight, Eq. 2.17
C_{pt}	fraction of MTOW used to compute the weight of paint, Eq. 2.19
C_{water}	gallons of water onboard per person per hour, Eq. 2.9
K_{fc}	empirical factor in determining flight control system weight, Eq. 2.16
K_{lav}	empirical factor in determining lavatory weight, Eq. 2.10
N_{cr}	number of crew, Eqs. 2.7, 2.8, 2.9, 2.13, 2.20
N_{pax}	number of passengers, Eqs. 2.7, 2.8, 2.9, 2.11, 2.13, 2.20
R	aircraft design mission range
S_{ff}	area of freight floor in cargo bay, Eq. 2.12
$W_{galleys}$	weight of galleys, Eq. 2.7
W_{le}	weight of unconventional leading edge devices, Eq. 2.16
W_{meal}	assumed weight of one meal in lbs, Eq. 2.8

ten fall in a gray area. A sensitivity study was performed to investigate the effects of varying the values of the constants given in Table 2.9.

The constants listed in Table 2.9 were perturbed from the values used to evaluate the weight of SAX21. The loops used to determine the fixed equipment and design fuel weights were allowed to converge to find the fixed equipment weight, OEW, and MTOW. The complete aircraft design model described in Chapters 3 and 4 is incorporated in the loops of the weight model described. To compare a change in aircraft weight with a change in a constant value, a normalized sensitivity parameter was defined as

$$NSP \equiv \frac{\%\text{ change in weight}}{\%\text{ change in value of constant}}.$$

The results of this sensitivity study are given in Figure 2-6. It can be seen that the amount of water onboard and the number of passengers are by far the two most important factors in the fixed equipment equations. In most design situations, the number of passengers if a given requirement and therefore is not a source of error in the model. While the amount of water per person onboard is a somewhat arbitrary value, it is not a significant source of error. From Figure 2-6(b), a 10% change in the value of C_{water} results in only a 0.5% change in MTOW.

In the same manner, the sensitivity of MTOW to errors in systems weight values

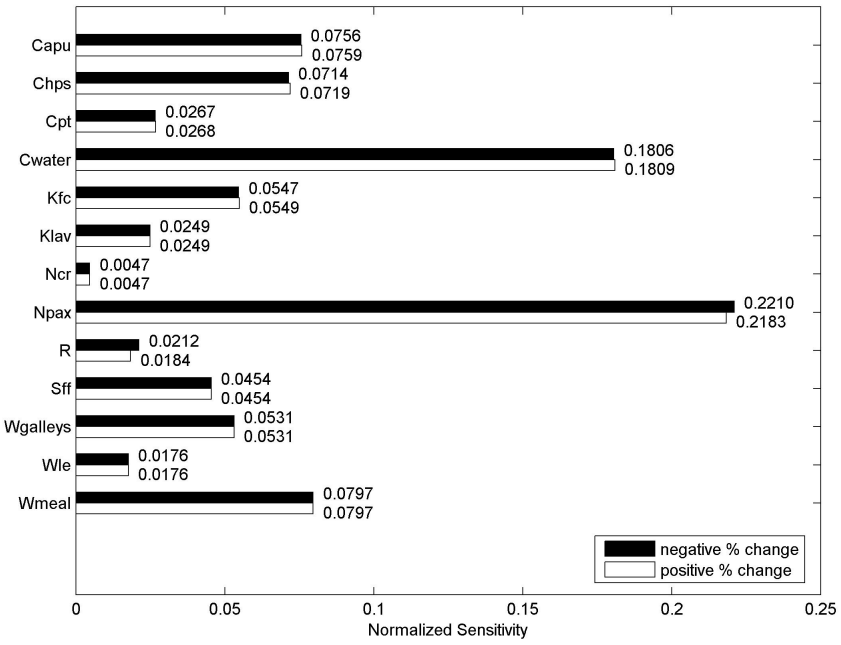

(a) Fixed equipment system weight sensitivity to constants

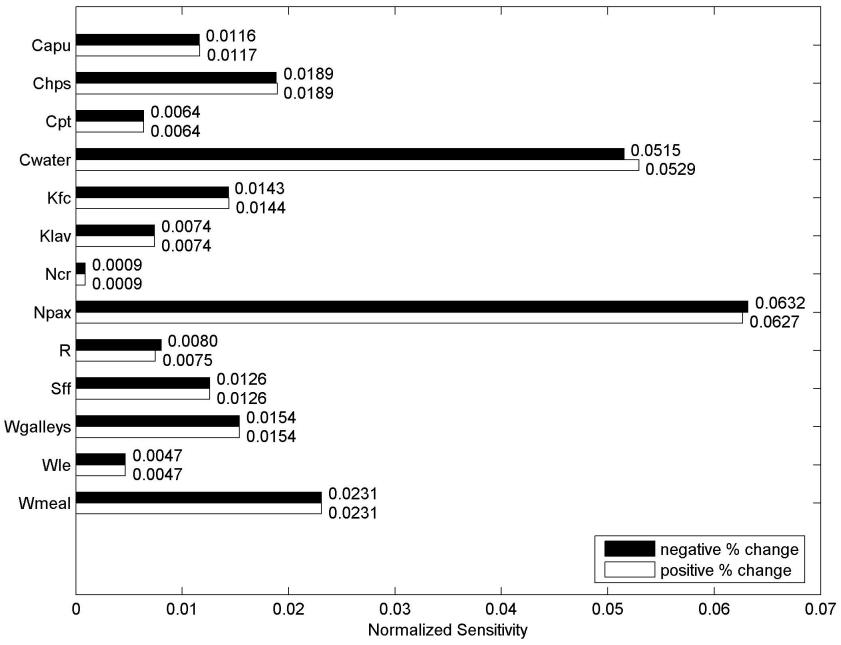

(b) MTOW sensitivity to constants

Figure 2-6: Sensitivity to constants in fixed equipment weight equations. Normalized sensitivity is the % change in weight for a 1% change in the value of a constant. See Table 2.9 for descriptions of constants.

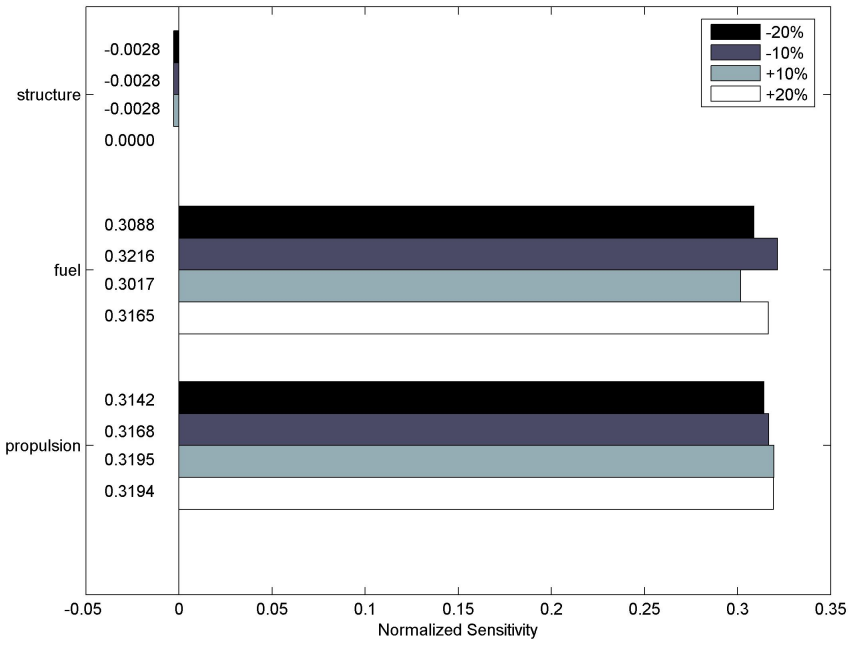

Figure 2-7: MTOW sensitivity to systems weights. Normalized sensitivity is the % change in MTOW for a 1% change in a system weight.

was investigated. Structural weight, design fuel weight, and propulsion system weight were each perturbed ±20% and ±10%. Again, the entire aircraft design model was run to converge on an aircraft design and weights. As before, the normalized sensitivity was calculated and is shown in Figure 2-7.

2.4 Model Fidelity and Risks

The aircraft weight model described in Section 2.1 is built largely from basic aircraft design principles and empirical relations. An effort was made to account for design iterations by calculating the mission fuel, landing gear, and fixed equipment weights. A more detailed weight analysis might calculate individual parasite drag values for each airframe to give a better estimate of mission fuel weight or itemize more components in the fixed equipment category such as overhead bins, partitions, and carpeting. This model was built to provide a best estimate for the overall aircraft

weights and data which can be used to calculate an aircraft center of gravity.

Within the propulsion system weight model, there are two potential sources of error. Equation 2.4, from which Equation 2.5 was derived, was originally intended for application to engines of equal thrust. Applying the resulting Equation 2.5 to engines of different thrust capabilities implies the ability to achieve the resulting thrust to weight ratio. As the fan diameter increases, thrust will increase faster than weight. As a result, the scaled engine will have a higher thrust to weight ratio than did the original design. Therefore, the engine weight may be optimistic but for small changes in fan diameter it can be assumed that the resulting thrust to weight ratio is feasible. Similarly, the transmission system weights are assumed constant and are therefore most accurate for small changes in engine power.

The most likely source of errors in this model are in the structural weight model, but there is very little information on the structural weight of an aircraft such as the SAX. Although the WingMOD BWB structural weight data has been validated, there is no simplified BWB structural weight model suitable for use in this SAX aircraft weights model. The response surface used here is conservative and reasonable given the limited data available, but is likely to contain as much as 6% error. However, from the sensitivity analysis, a +10% error in the structural weight would result in only a -0.02% error in MTOW.

It is encouraging to see that the overall aircraft weights (OEW, MTOW) are not sensitive to the values used for constants in the equations used to determine the fixed equipment weight. Also, the other large contributors to the overall weight such as mission fuel and payload have been estimated using well accepted methods. The aircraft weights model should serve to provide reasonable best estimate values for the Silent Aircraft eXperimental designs.

Chapter 3

Aircraft Center of Gravity Model

Like a BWB, the SAX lacks a horizontal stabilizer to ensure proper balance. Stability and control is a major concern in the design of a tailless aircraft, thus the center of gravity at all mission points is a critical piece of information. To provide a best estimate of center of gravity values, each component of the aircraft weight was placed appropriately within the aircraft and an overall center of gravity calculated. A sensitivity analysis was performed to determine which weight locations are the most critical to the location of the aircraft center of gravity at takeoff and mid-cruise.

3.1 Center of Gravity Estimation

To estimate the aircraft center of gravity, each component of the aircraft weight was assigned a location in the planform. Given N component weights and assuming those weights are point masses at chordwise locations of distance X_i from the aircraft nose, the aircraft center of gravity as measured chordwise from the nose of the aircraft can be computed from

$$CG_x = \sum_{i=1}^{N} \frac{X_i W_i}{W_{total}}$$

where W_i is the component weight. The model used to find the weights is described in Chapter 2. The locations of those weights can be estimated from the planform layout as described below and shown in Figure 3-1.

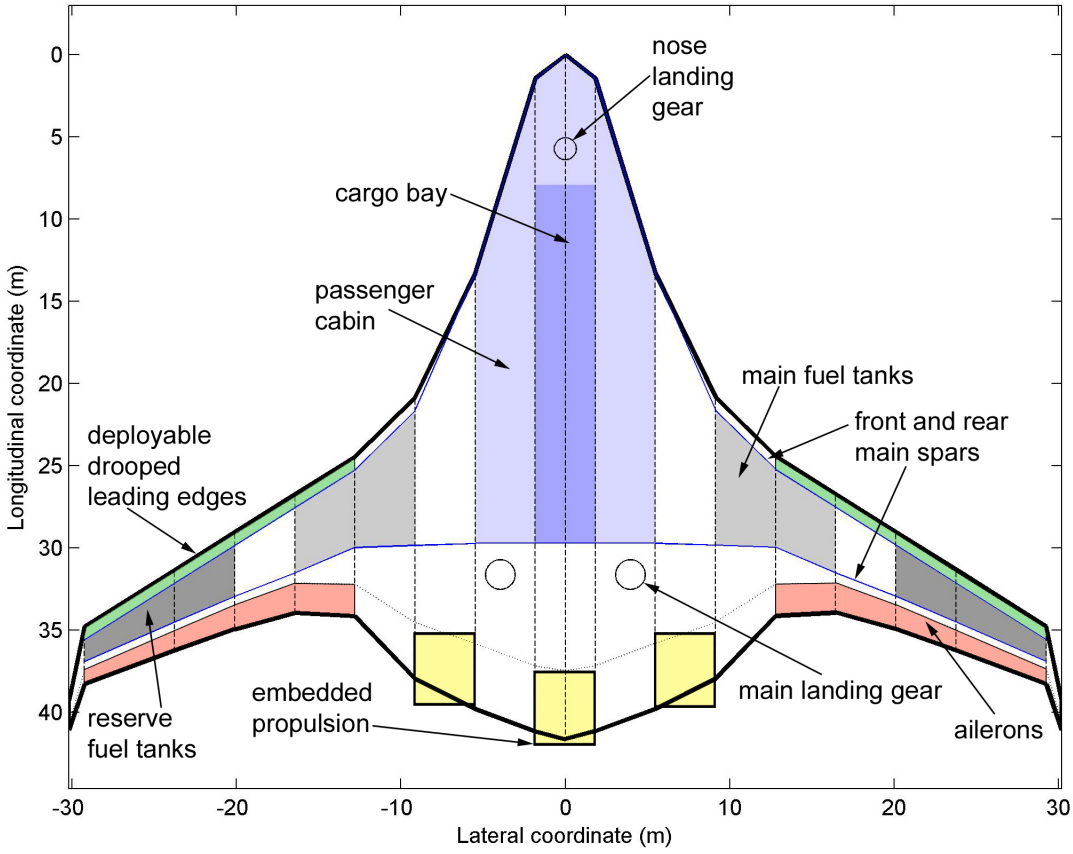

Figure 3-1: SAX21 planform

3.1.1 Passenger cabin

The SAX21 passenger cabin was designed to fit in the center two panels of the airframe, much like the BWB-250 described by Liebeck [32]. The cabin length was determined by the placement of the front and rear spars as shown by the solid blue lines in Figure 3-1. The weights of furniture, operational items, air conditioning and pressurization, auxiliary items, oxygen system, and passengers and hand luggage were assumed to be distributed evenly throughout the cabin and were treated as point masses at the geometric centroid of the cabin floor.

3.1.2 Cargo bay

The cargo bay was designed to fit beneath the passenger cabin in the thickest section of the airframe (Figure 3-1). The weight of the baggage and cargo handling equipment as well as the checked passenger luggage was assumed to be a point mass at the centroid of the cargo bay.

3.1.3 Landing gear

To determine the center of the landing gear weight, the main gear was assumed to account for 85% and the nose gear 15% of the total gear weight [42].

3.1.4 Propulsion

The weight of the entire propulsion system including bare engines, auxiliary fans, transmission systems, and nacelles was assumed to be a point mass at a fixed location. Because the auxiliary power unit is typically located close to the propulsion system, the weight of the APU was also placed at this location.

3.1.5 Cockpit

If most of the instruments and avionics are located forward of the cabin and the display panels are located in the front of the cockpit, these weights can be assumed

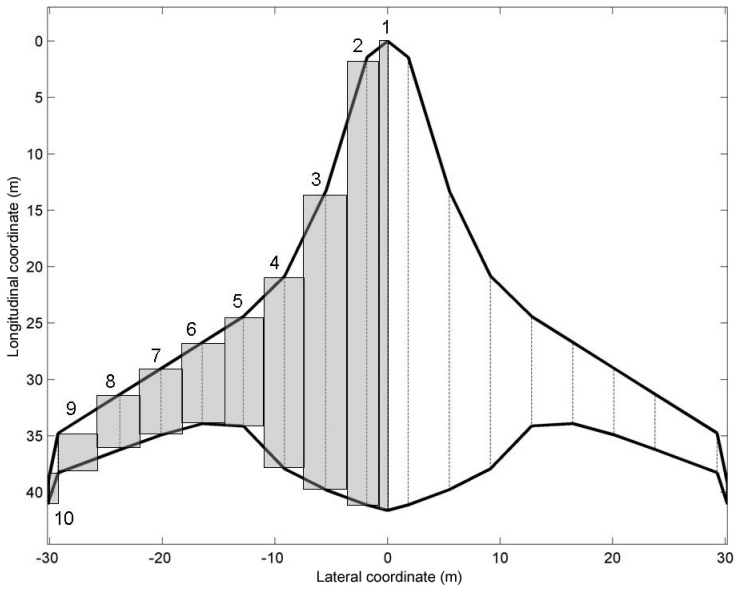

Figure 3-2: Discretized SAX21 planform

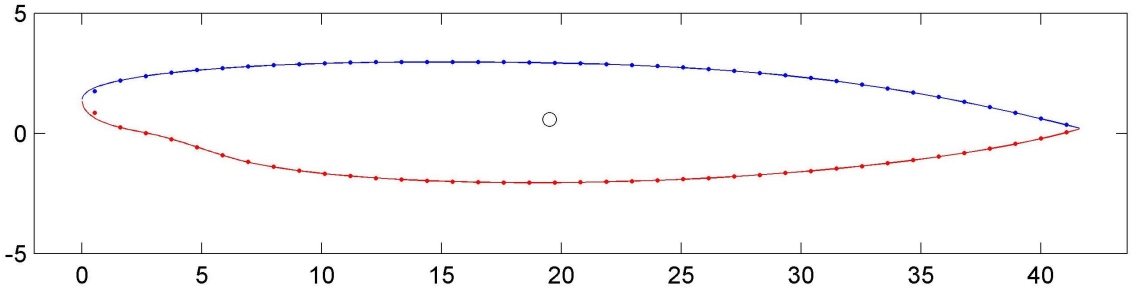

Figure 3-3: Discretized airfoil and airfoil centroid for the first section

to be a point mass located at the forwardmost point of the cabin.

3.1.6 3-D airframe

To determine the three dimensional centroid of the airframe, the airframe was discretized as shown in Figure 3-2. The area and centroid of each sectional airfoil was calculated by discretizing each airfoil as shown in Figure 3-3. The volume of the planform segments, represented by grey rectangles in Figure 3-2, was calculated by multiplying the section width by the sectional airfoil area.

Given the centroid of the airfoil in the chordwise direction for each segment and

the corresponding volume of each segment, the chordwise centroid of the airframe, C_x^{af}, as measured from the aircraft nose was determined from

$$C_x^{af} = \sum_{i=1}^{M} \frac{X_i V_i}{V_{total}}$$

where V_i are the volumes of the planform segments and X_i are the airfoil centroids as measured chordwise from the aircraft nose.

Structure and other distributed weights

It was assumed that the weight of the airframe structure, paint, flight controls, hydraulics and pneumatics, and electrical electrical system is distributed across the aircraft according to volume. More structure is necessary in the thickest sections of the aircraft, namely the centerbody, and more equipment can be stored in thicker sections that more easily accommodate it. Therefore, these system weights were treated as point masses at the centroid of the three dimensional airframe, C_x^{af}.

Fuel tanks

To manage the aircraft center of gravity on a BWB, the fuel onboard is pumped from inboard main tanks to outboard reserve tanks as fuel burns off and the aircraft CG tends to move forward [51]. To size the fuel tanks, the available fuel tank volume was calculated for each wing panel, where a panel is the space between two ribs. First, the cross sectional area of the fuel tank as given by the airfoil area between the front and rear spars was found in the same way as described previously. The available volume for each panel was found by taking the average of the neighboring fuel tank cross sections and multiplying that value by the distance between the ribs, as given by

$$V_{available} = d\frac{A_i + A_{i+1}}{2} \tag{3.1}$$

where d is the spanwise distance between the ribs and A_i and A_{i+1} are the neighboring cross sectional areas. To account for the fact that the wing contains not only fuel, but also the fuel tank itself and airframe structure, it was assumed that only 75% of

the calculated available panel volume is actually tank volume containing fuel, thus

$$V_{tank} = 0.75\ V_{available}.$$

Having determined the fuel capacity of each wing panel, as many panels as necessary were allocated for main fuel tanks starting from the panel adjacent to the cabin and moving outboard. Reserve tanks are allocated from the wingtips and moving inboard. The centroid of each fuel tank was calculated according to

$$C_x^{ft} = \sum_{i=1}^{P} \frac{X_i V_{tank_i}}{V_{tank_{total}}}$$

where X_i is the mean value of the centroids of the two airfoils at the ribs on either side of the current panel and V_{tank_i} is the tank volume of the current panel. At mid-cruise, the fuel on board is assumed to be located in the main tanks, but half of the mission fuel has been burned during cruise such that the fuel on board is given by

$$W_{mid-cruise\ fuel} = \frac{1}{2}(W_{fuel} - W_{reserve\ fuel}) + W_{reserve\ fuel}.$$

3.2 Evaluation of SAX21 Center of Gravity

Using the locations described in Section 3.1, the system and component weights as given in Section 2.2 were placed within the aircraft to determine the center of gravity. Table 3.1 gives the weights and locations for SAX21.

To calculate the aircraft center of gravity on takeoff, it was assumed that the total aircraft weight is MTOW and all of the design fuel is carried in the inboard main tanks. At mid-cruise, it is assumed that half of the mission fuel has been burned, but all fuel is still located in the main tanks. At approach to landing (LAM), only the reserve fuel is still onboard and has been pumped to the outboard reserve tanks. Figure 3-4 shows the CG locations for takeoff at MTOW and landing approach (LAM) with only reserve fuel. Numerical values for four configurations can be found in Table 3.2.

Table 3.1: Aircraft weights and point mass locations for SAX21

		Weight (lbs)	Location (m)	% Center chord
Passenger Cabin	furnishings & op items	27,562	17.85	42.91
	a/c & pressurization	5,919	17.85	42.91
	auxiliary items	2,031	17.85	42.91
	oxygen system	314	17.85	42.91
	passengers	42,750	17.85	42.91
Cargo Bay	checked luggage	6,450	18.81	45.22
	baggage & cargo equipment	2,574	18.81	45.22
Landing Gear	main gear	12,767	31.60	75.96
	nose gear	2,253	5.70	13.70
Propulsion	engines & nacelles	31,905	38.27	92.00
	auxiliary power unit	4,409	38.27	92.00
Cockpit	instruments & avionics	4,320	0.00	0.00
Airframe	structure	94,567	22.72	54.61
	paint	1,526	22.72	54.61
	flight controls	4,112	22.72	54.61
	hydraulics & pneumatics	4,070	22.72	54.61
	electrical system	4,626	22.72	54.61
Fuel	mission fuel	78,155	27.23	65.46
	design fuel	86,839	27.23	65.46
	reserve fuel	8,684	33.12	79.62

Table 3.2: Numerical values for SAX21 center of gravity in meters aft of the aircraft nose

Aircraft configuration	Center of gravity, m
Landing approach	23.54
Mid-cruise	23.85
Takeoff	24.24
OEW	24.48

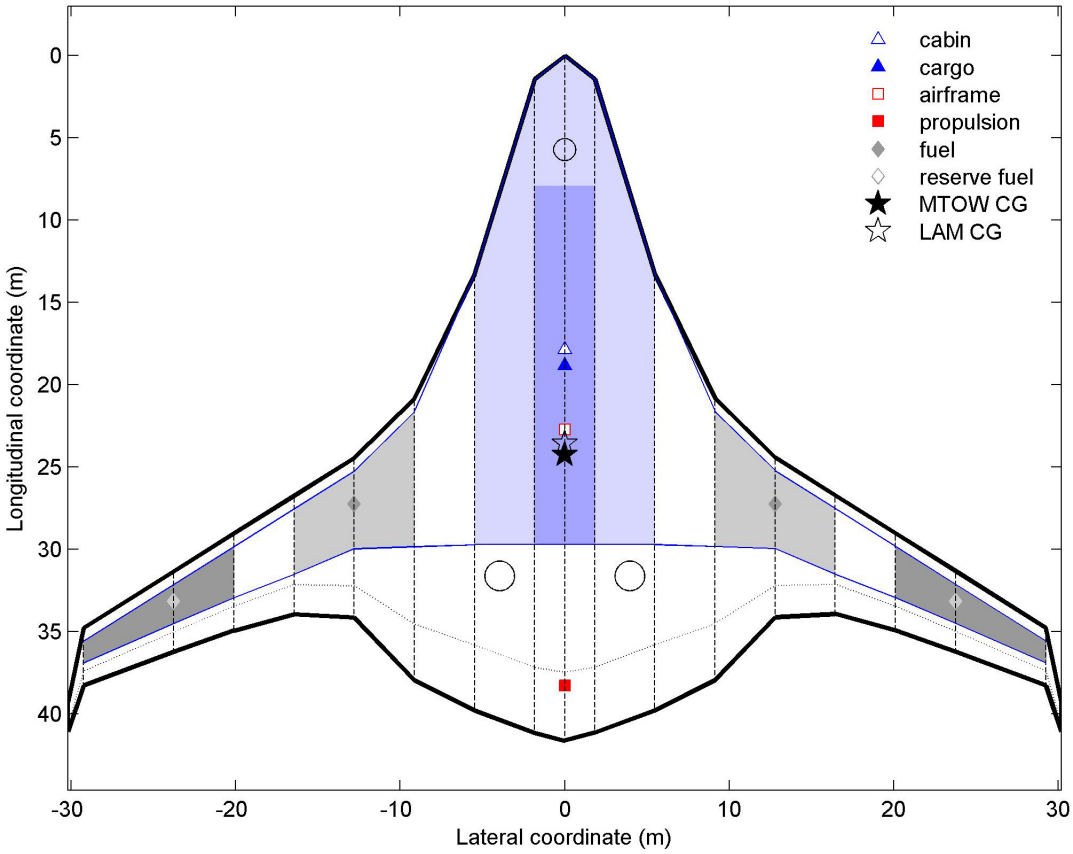

Figure 3-4: SAX21 configuration and center of gravity

3.3 Sensitivity

Because the aircraft center of gravity is a critical piece of information for the design of a tailless aircraft, a sensitivity analysis was performed to determine which weight locations are most likely to affect the aircraft CG. To obtain the results presented below, the aircraft weight, center of gravity, and aircraft design models were combined. In the complete model, the aircraft design is modified to account for changes in aircraft weights and CG with changes in design. For example, a design loop adjusts wing twist to trim the aircraft at mid-cruise. Aircraft trim depends on aircraft CG, but since fuel burn depends on wing twist, the aircraft weight does as well. The complete coupled design-analysis problem was modeled and used to find the aircraft CG. Weight locations were perturbed forward and aft from the baseline SAX21 design and the complete aircraft design model was used to find the resulting change in aircraft CG at both takeoff and mid-cruise. To compare values, a normalized sensitivity parameter was defined as

$$NSP \equiv \frac{\%\text{ change in aircraft CG}}{\%\text{ change in weight location}}.$$

The normalized sensitivities of aircraft CG at takeoff and mid-cruise to system and component weight locations are given in Figure 3-5. It was found that at MTOW, fuel and structure most affect CG, but at mid-cruise propulsion location also becomes important.

3.4 Model Fidelity and Risks

Given accurate weights and locations, the center of gravity calculation is trivial, and for the most part, determining the locations for system weights is relatively simple. Furthermore, even on a highly integrated design such as a BWB or the SAX, components can be shifted to control the aircraft balance. For example, the propulsion system has a significant effect on aircraft balance as fuel is burned off later in cruise, but engines can be placed such that the aircraft balance is controlled. Similarly, fuel tanks placed in the highly swept wings allow the aircraft CG to be controlled simply

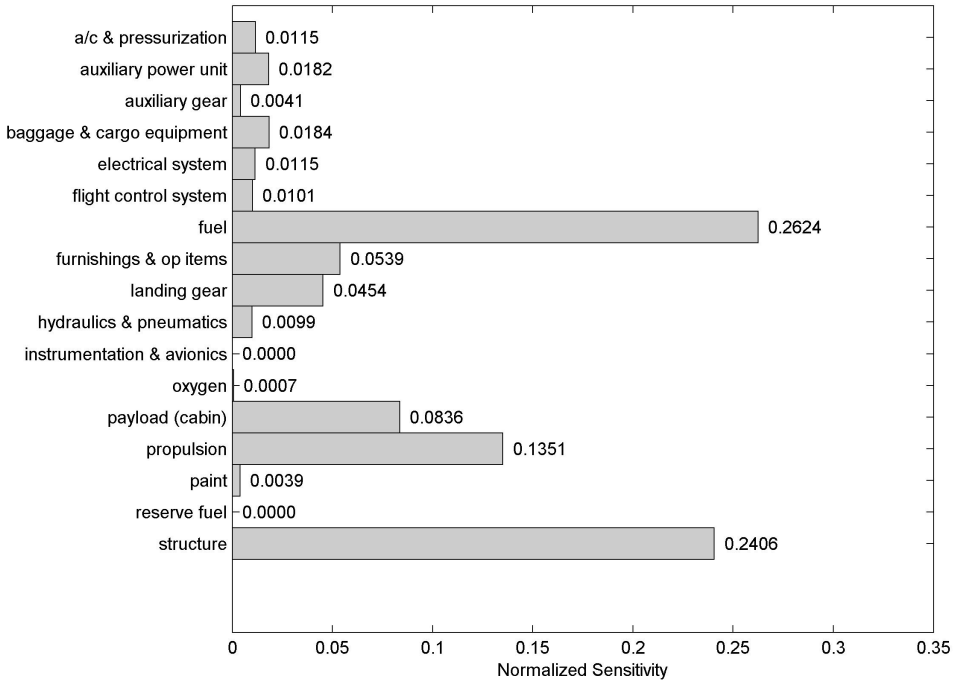

(a) Sensitivity of CG to weight locations at takeoff (MTOW)

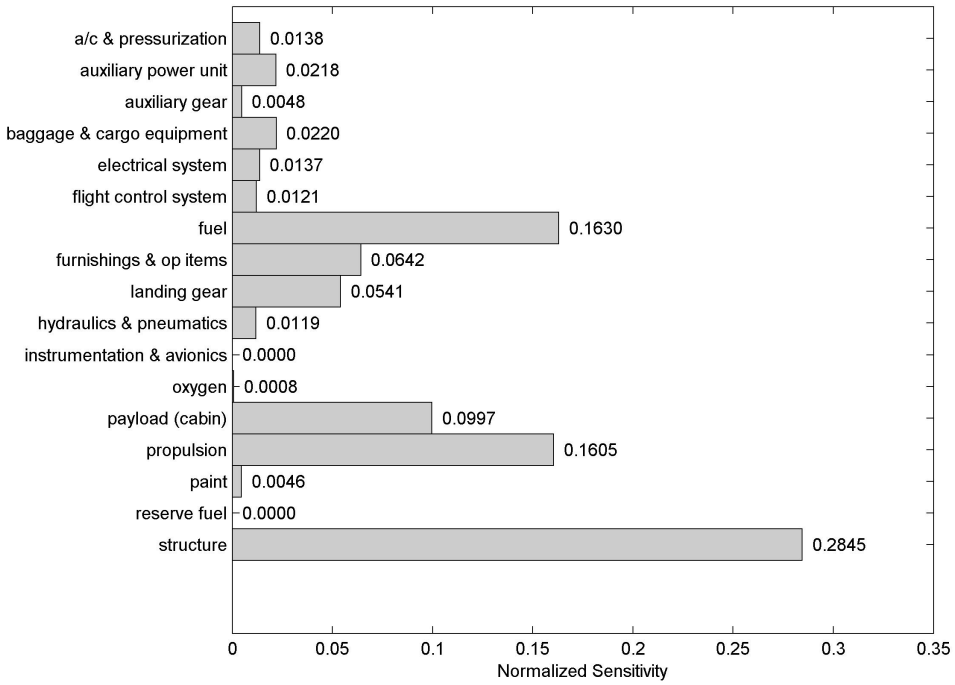

(b) Sensitivity of CG to weight locations at mid-cruise (half mission fuel)

Figure 3-5: Sensitivity of aircraft center of gravity to system and component weight locations. Normalized sensitivity is the % change in CG for a 1% change in a weight location.

by pumping fuel inboard and outboard [51].

For the SAX, the biggest risk in calculating the aircraft CG is that of the structural weight and location of that weight. Unfortunately, this information has one of the largest impacts on the overall aircraft CG. The location chosen for the aircraft structural weight is approximated as the volumetric center of the airframe. Neither the weight nor the design model has the fidelity necessary to accurately compute the weight breakdown of spars, skin, doors, etc. This detailed information would allow the center of gravity of the aircraft structure to be more accurately determined, but presents challenges that require much higher fidelity models. The center of gravity model presented here is intended to provide a best estimate aircraft CG for use in the initial conceptual design of a SAX. To obtain a better CG estimate for a more detailed aircraft design, higher fidelity analysis would have to be performed to more accurately determine the weights of the individual structural components.

Chapter 4

Aircraft Design and Noise Prediction Model for SAX

The purpose of this model is to produce a new design given a baseline aircraft design and predict the noise generated on takeoff climb. The new aircraft design is produced by four modules, each representing an aeronautical engineering discipline: airframe design, engine design, aircraft operations, and flight mechanics. Using the SAX21 and Granta-3201 designs as reference, the airframe is scaled to a given wing span and planform area, airfoil profiles are adjusted to change the aerodynamic characteristics of the airframe, and the engine is scaled to accommodate a given fan diameter. Given a departure flight path and velocity, the aircraft is modeled and trimmed at the point it would cross the airport boundary to determine the altitude and thrust vectoring angle. Once a design has been generated, established noise prediction routines are used to estimate the noise observed on the ground as the aircraft departs the airport.

4.1 Airframe Design

The airframe design module is made up of three functions, each of which is responsible for a distinct section of the airframe. First, the reference planform is scaled to produce an airframe of the appropriate wing span and area. Given a new planform, the airfoils on the outer section of the wing are adjusted and the wing twist is determined to

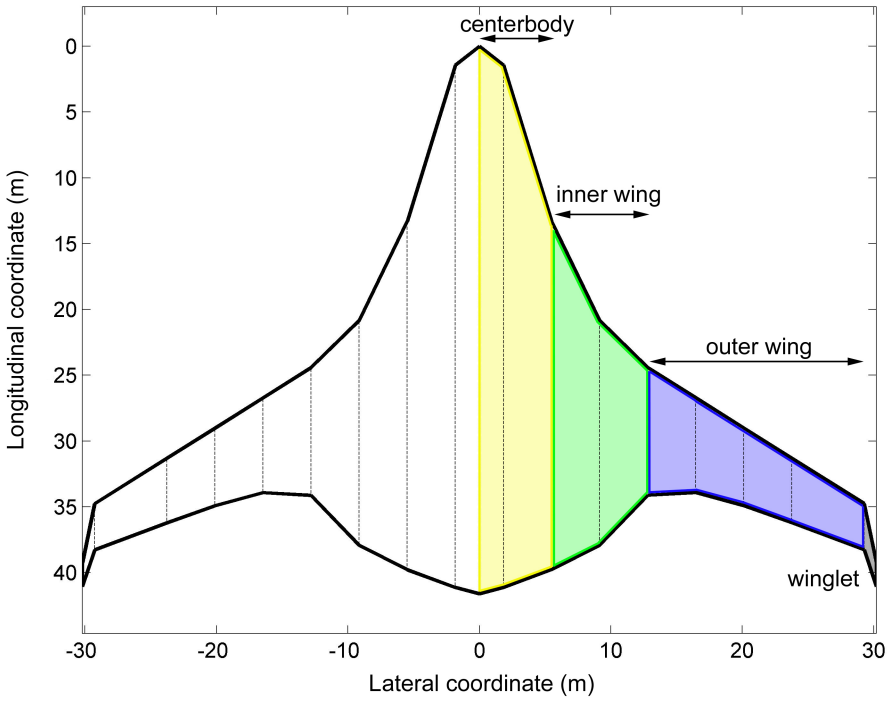

Figure 4-1: Planform sections

reduce control surface deflections during cruise.

4.1.1 Planform scaling

The SAX21 planform was divided into four sections as shown in Figure 4-1. Given this planform, the wingspan is scaled to the desired value by simply scaling the spanwise coordinate of each rib over the inner wing, outer wing, and winglet sections. To modify the planform wetted area, an outer wing chord scaling factor is specified. This factor is applied to the chords of the outer wing and winglet sections of the planform to alter the wing area in these sections. The resulting planform is one that has been scaled from a baseline design to the desired values for wing span and outer wing area. Figure 4-2 illustrates some possible designs using this scaling technique for a constant wing span and three different values of outer wing chord scaling factor.

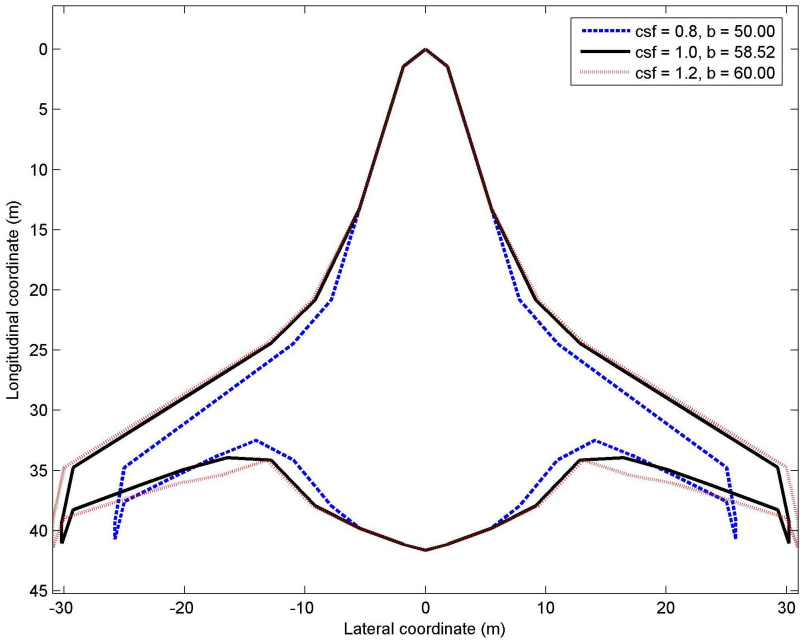

Figure 4-2: Example of planform scaling for various chord scaling factors (csf) and wing spans (b)

4.1.2 Airfoils

Airfoil profiles for this model were generated in the same manner as for the three-dimensional silent aircraft design described by Hileman et al. [26]. The aircraft planform is divided into six sections with one or more ribs in each section as shown in Figure 4-3. Four distinct airfoil profiles are defined and each is applied to the ribs in sections 1, 2, 3, and 4. In regions between distinct airfoils, sections 1/2 and 3/4, linear interpolation is used to create a merged airfoil profile.

The surface of each airfoil is divided into five segments, each represented by a Bézier spline. In Figure 4-4, the SAX21 outer wing airfoil is shown with each spline labeled A through E. The five splines are built from the (x, y) coordinates of five endpoints, six angles θ, and ten lengths L. On spline A in Figure 4-4, the two endpoints are shown as circles and two example control points are shown as squares.

For all five splines, the endpoints are defined by their (x, y) coordinates. These points are shown as circles and labeled 1 through 5 in Figure 4-5. To ensure that the five splines combine to form a smooth airfoil shape, the interior two control points

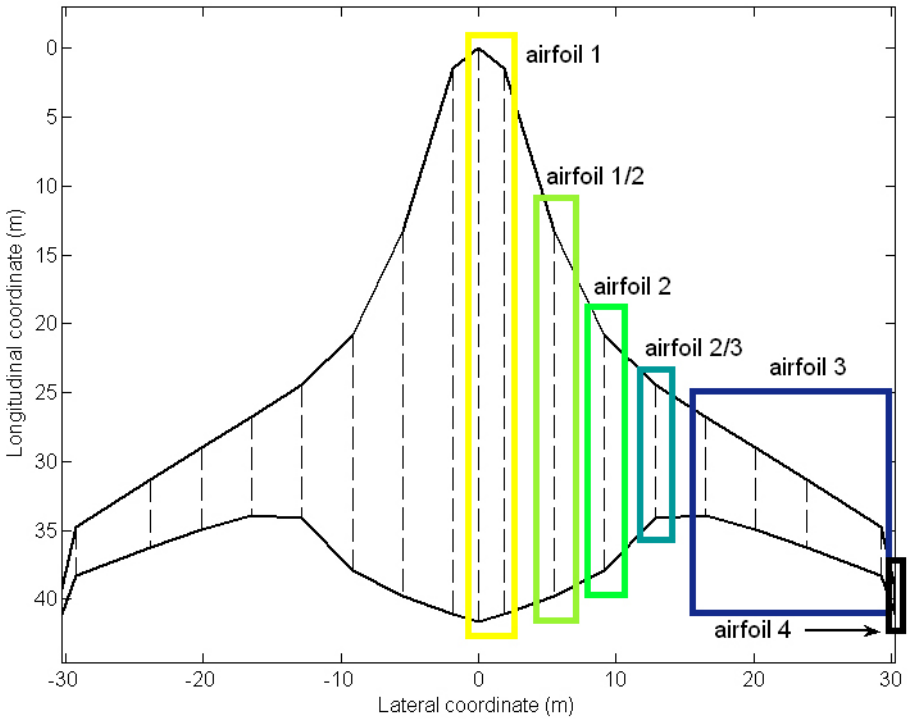

Figure 4-3: Sectioned planform and rib locations for airfoil profiles

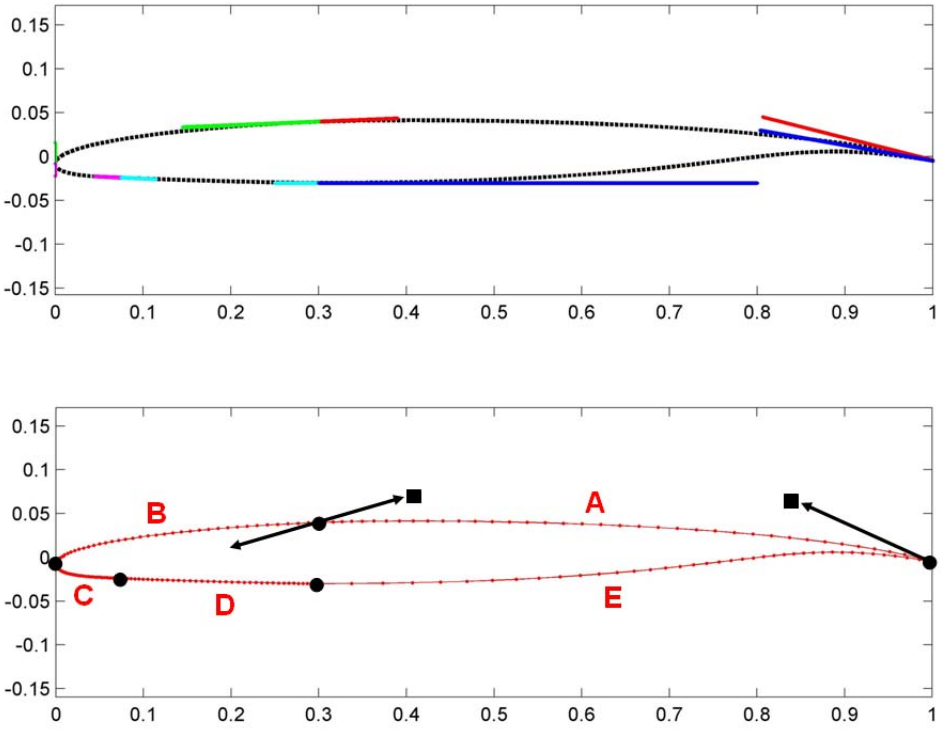

Figure 4-4: Airfoil 3 for SAX21

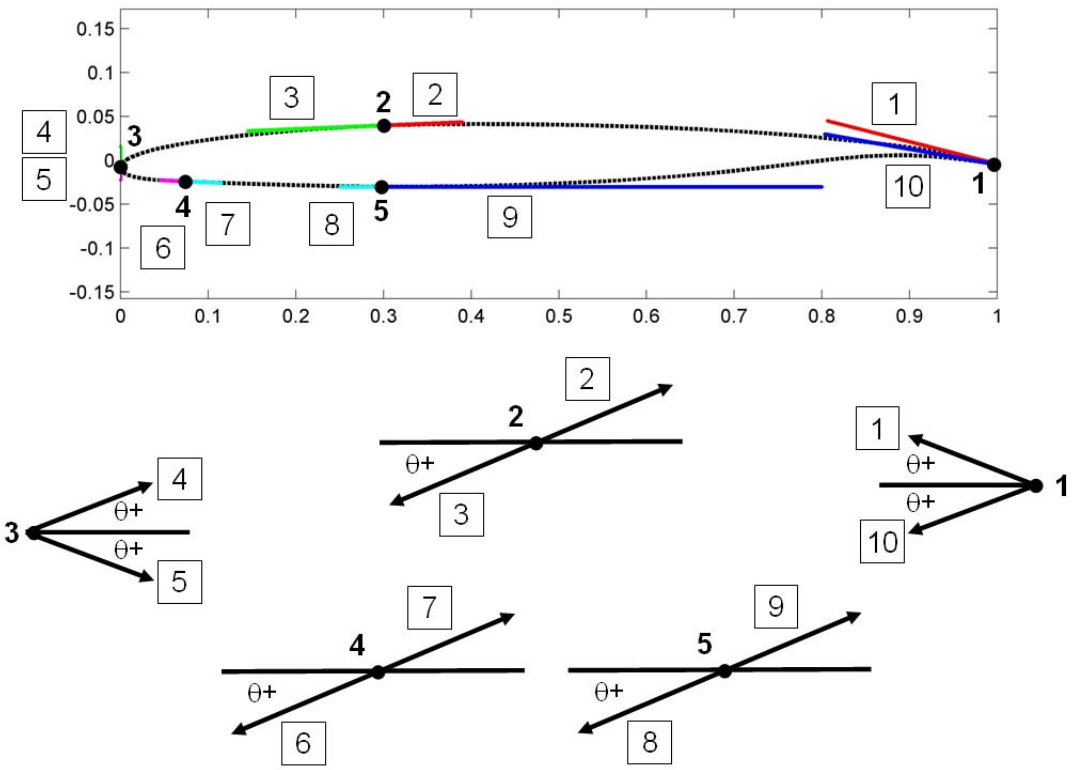

Figure 4-5: Definition of splines used to define airfoil surfaces

for each spline are defined using handles. Take for example spline A in Figure 4-4. In Figure 4-5 it can be seen that the corresponding handles are [1] and [2]. The interior control points for spline A are the endpoints of handles [1] and [2]. Each handle is defined by a length L and an angle θ. Looking more closely at handle [2] in Figure 4-6, (x_e, y_e) is the endpoint of spline A, labeled point 2 in Figure 4-5, and (x_c, y_c) is the handle [2] control point of spline A. Using simple trigonometry, the coordinates (x_c, y_c) can be found according to

$$x_c = x_e + \underbrace{L\cos(\theta)}_{dx}$$

$$y_c = y_e + \underbrace{L\sin(\theta)}_{dy}.$$

To ensure that both surfaces of the airfoil are smooth, handles not at the leading

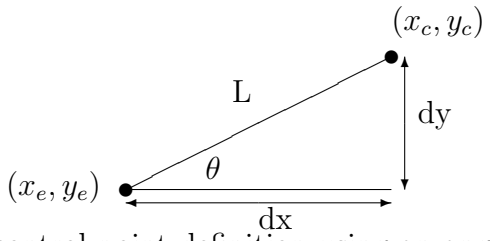

Figure 4-6: Spline control point definition using an angle θ and length L

or trailing edge share share θ values with the other handle at that endpoint. Handles $\boxed{2}$ and $\boxed{3}$ on endpoint 2 are defined by the same value of θ_2. Likewise, handles $\boxed{6}$ and $\boxed{7}$ on endpoint 4 and handles $\boxed{8}$ and $\boxed{9}$ on endpoint 5 are defined by θ_4 and θ_5, respectively. On the trailing edge at endpoint 1, each handle $\boxed{1}$ and $\boxed{10}$ is assigned a separate departure angle θ_1 and θ_{10}. On the leading edge at endpoint 3, each handle $\boxed{4}$ and $\boxed{5}$ is assigned $\theta_4 = \theta_5 = 90°$.

Once four points have been defined for each of the five splines required to produce one airfoil profile, the two dimensional equation for a Bézier spline can be used to generate points on each of the splines and thus a discrete representation of the airfoil surfaces.

4.1.3 Wing twist

The wing twist is designed to trim the aircraft in cruise, thus reducing the need for control surface deflections and reducing drag during cruise. Using an average mission point at the middle of cruise, the lift coefficient necessary to maintain flight is

$$C_{L_{cr}} = \frac{2W_{cr}}{\rho_{cr}(M_{cr}a_{cr})^2 S}$$

where ρ_{cr} and a_{cr} are the air density and speed of sound at the average cruise altitude. The aircraft weight at the middle of the cruise mission is defined as

$$W_{cr} = MTOW - \frac{1}{2}\left(W_{fuel} - W_{reserve\,fuel}\right)$$

to account for the fuel burned during the first half of cruise.

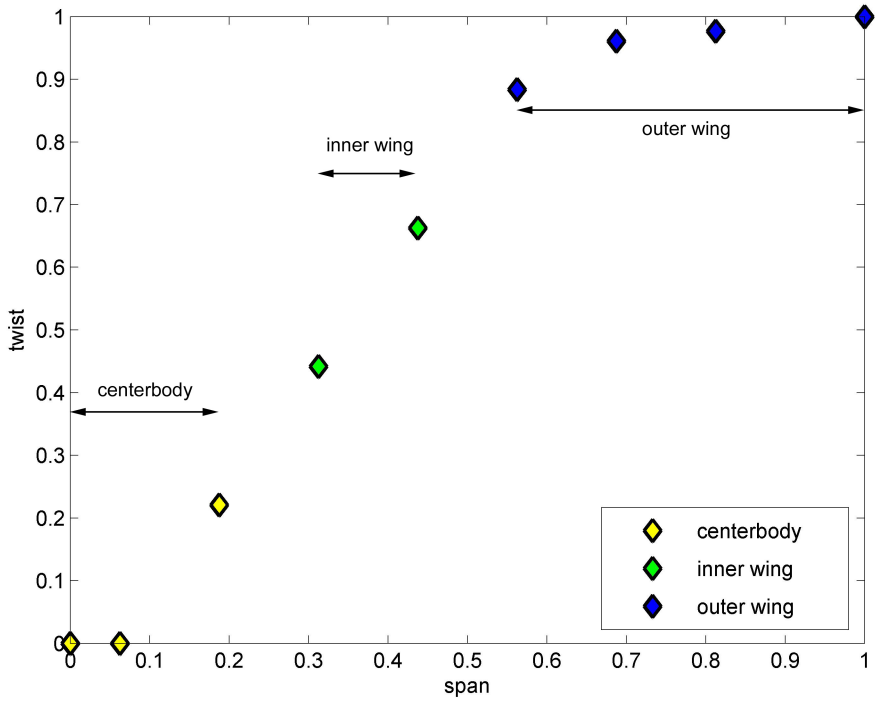

Figure 4-7: Normalized wing twist distribution

A wing twist distribution of three linear segments was defined in the same manner as did Hileman et al. [26]. Let η be the lateral coordinate normalized by the wing semispan. The wing twist distribution is defined such that there is zero twist for $\eta < 0.06$ followed by a linear ramp to 95% of the maximum twist at $\eta = 0.6$, followed by another linear ramp to 100% of maximum twist at $\eta = 1$. As shown in Figure 4-7, the discontinuities in wing twist distribution correspond to the transitions between the centerbody, inner wing, and outer wing.

The aircraft geometry was analyzed using AVL, a vortex lattice code, to determine the proper scaling of the twist distribution to produce the desired zero pitching moment at mid-cruise [18]. Two geometries with different maximum wing twist values T_{max} were analyzed at two different angles of attack. For each combination of α and T_{max}, the lift and moment coefficients C_L and C_m were calculated using AVL. The derivatives of the lift and moment coefficients with respect to angle of attack and

twist were approximated as

$$\begin{aligned} C_{L_\alpha} &\approx \Delta C_L/\Delta\alpha \quad , \quad C_{L_T} \approx \Delta C_L/\Delta T_{max} \\ C_{m_\alpha} &\approx \Delta C_m/\Delta\alpha \quad , \quad C_{m_T} \approx \Delta C_m/\Delta T_{max} \end{aligned}$$

As described by Hileman et al., a system of equations

$$\begin{bmatrix} C_{L_\alpha} & C_{L_T} \\ C_{m_\alpha} & C_{m_T} \end{bmatrix} \begin{bmatrix} \Delta\alpha \\ \Delta T_{max} \end{bmatrix} = \begin{bmatrix} C_{L_{cr}} - C'_L \\ C_{M_{cr}} - C'_M \end{bmatrix} \tag{4.1}$$

can be assembled where $C_{L_{cr}}$ and $C_{m_{cr}}$ are the lift and moment coefficients desired at cruise and C'_L and C'_m are the AVL results for known values of α' and T'_{max} [26]. Equation 4.1 can be solved for $\Delta\alpha$ and ΔT_{max} to find the the desired cruise angle of attack α_{cr} and maximum wing twist T_{max} as given by

$$\begin{aligned} \alpha_{cr} &= \alpha' + \Delta\alpha \\ T_{max_{cr}} &= T'_{max} + \Delta T_{max}. \end{aligned}$$

4.2 Engine Scaling

For a conventional turbofan, the primary aerodynamic design point is top of climb (TOC). At this point, the engine must provide enough thrust to maintain a climb rate despite the unfavorable atmospheric properties at altitude. For a set fan pressure ratio (FPR), the jet velocity is given by

$$V_j \approx \sqrt{2c_p T_{02}(FPR^{\gamma-1/\gamma} - 1) + V_0^2},$$

where T_{02} is the stagnation temperature at the fan face, V_0 is the aircraft velocity, c_p is the specific heat capacity at constant pressure, and γ is the ratio of the specific heats [23]. The thrust equation can be rearranged such that thrust is a function of

the fan area and jet velocity as given by

$$X_N = (V_j - V_0)\frac{n_{eng}A_f p_{02}Q_a}{\sqrt{c_p T_{02}}}, \tag{4.2}$$

where V_j is the jet velocity and n_{eng} is the number of engines. The area of the fan A_f is given by

$$A_f = \frac{D_f^2\pi}{4}(1 - HTR^2)$$

where HTR is the hub-to-tip ratio. The fan capacity Q_a is defined as

$$Q_a \equiv \frac{\dot{m}\sqrt{c_p T_{02}}}{A_f p_{02}}.$$

For a conventional fixed geometry turbofan, the engine is designed such that the fan capacity is largest at TOC and thus is limited by the exhaust nozzle area at takeoff. By incorporating a variable nozzle into the propulsion system design, the flow capacity at takeoff can be increased greatly [23]. Assuming ideal use of such a nozzle, the fan capacity can be considered equal at three mission points, thus $Q_a = Q_{a,TOC} = Q_{a,TO} = Q_{a,CB}$. Given a value for Q_a, it is possible to use Equation 4.2 to compute the thrust at both top of climb and takeoff roll. To later predict jet noise, the jet exhaust velocity is found according to

$$V_j = V_0 + X_N\frac{\sqrt{c_p T_{02}}}{n_{eng}A_f p_{02}Q_a},$$

where X_N is the total net thrust necessary to maintain flight.

To scale the engine design from the baseline Granta-3201, new fan diameters were selected while other parameters such as fan capacity and fan pressure ratio were assumed constant. The characteristics of Granta-3201 can be found in Section 1.2.2.

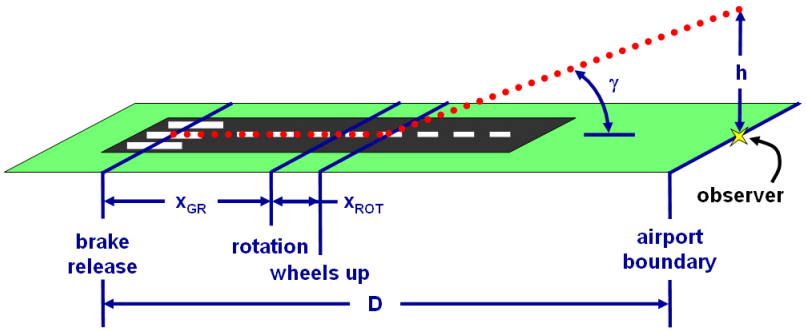

Figure 4-8: Key points on takeoff

4.3 Aircraft Operations

The takeoff procedure is shown in Figure 4-8 and is divided into three segments: ground roll, rotation, and initial climb. To determine the aircraft's altitude as it crosses the airport boundary, the distance traveled during each of these segments must be found.

The ground roll distance is found from

$$x_{GR} = \frac{1}{2gK_A} \ln\left(\frac{K_T + K_A V_f^2}{K_T + K_A V_i^2}\right)$$

$$K_T \equiv \frac{T}{W} - \mu$$

$$K_A = \frac{\rho}{2(W/S)}(\mu C_L - C_{D_0} - K C_L^2),$$

where the coefficient of friction μ is assumed to be approximately 0.04 for tires rolling on dry concrete, T is the total thrust, W is the aircraft weight, and S is the planform area [42]. It was assumed that during ground roll the aircraft accelerates from $V_i = 0$ to a set departure velocity, V_f.

A large aircraft typically requires 3 seconds to complete rotation, thus $x_{ROT} = 3\ V_f$ where V_f is the aircraft's velocity in units of length per second [42].

Assuming that initial climb is a constant slope climb from the moment of rotation until engine cutback past the airport boundary, the aircraft's altitude as it crosses

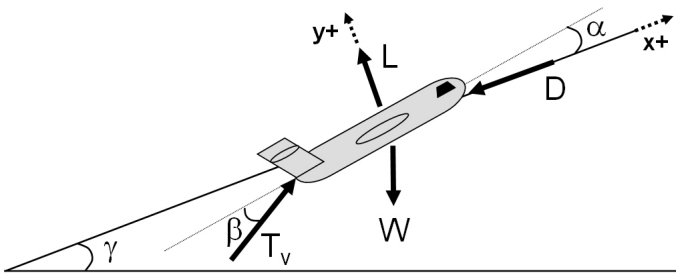

Figure 4-9: Forces acting on an aircraft with thrust vectoring in a constant climb

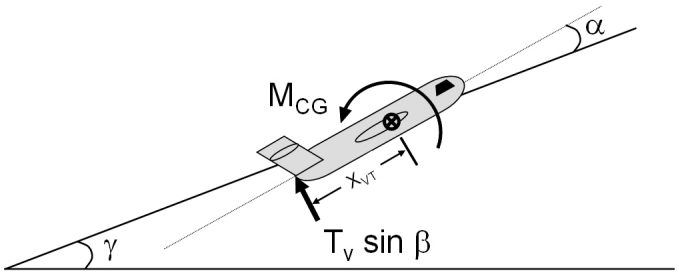

Figure 4-10: Moments acting on an aircraft with thrust vectoring in a constant climb

the boundary is

$$h = (D - x_{GR} - x_{ROT})\ \tan\gamma$$

where D is the distance from brakes off to the airport boundary and γ is the departure flight path angle.

4.4 Flight Mechanics

The forces and moments acting on an aircraft with thrust vectoring in a constant climb are shown in Figures 4-9 and 4-10. Because the vectored thrust angle β is a function of the thrust available and the thrust required is a function of the angle at which it is vectored, the balance of forces and moments must be solved simultaneously. An initial estimate of the required thrust is obtained from a force balance neglecting the effects of vectored thrust. This value is then used as an initial guess to solve the equations of motion simultaneously for the vectored thrust case.

4.4.1 Takeoff force balance

Balancing the forces on initial climb, it is possible to obtain an initial guess for the thrust required to maintain the desired flight path angle γ. The initial force balance does not account for vectoring thrust for pitch trim. The basic forces acting on the aircraft are shown in Figure 4-9 where without thrust vectoring, $\beta = 0$ and $T_{V_y} = 0$ so $T = T_V = T_{V_x}$ and the thrust vector is aligned with the aircraft fuselage line.

4.4.2 Pitch trim with thrust vectoring

Including the effects of thrust vectoring, a force and moment balance for steady state flight results in

$$\sum F_x = \underbrace{\frac{\partial C_L}{\partial \alpha}\alpha + C_{L_{\alpha=0}}}_{lift} + \underbrace{\frac{T_V \sin(\beta - \alpha)}{\frac{1}{2}\rho U^2 S}}_{thrust} - \underbrace{\frac{mg\cos\theta}{\frac{1}{2}\rho U^2 S}}_{weight} = 0$$

$$\sum F_y = \underbrace{\frac{T_V \cos(\alpha - \beta)}{\frac{1}{2}\rho U^2 S}}_{thrust} + \underbrace{\frac{mg\sin\theta}{\frac{1}{2}\rho U^2 S}}_{weight} - \underbrace{C_{Di_{\alpha=10}}\left(\frac{\frac{\partial C_L}{\partial \alpha}\alpha + C_{L_{\alpha=10}}}{C_{L_{\alpha=10}}}\right)^2 - C_{D_0} - C_{D_R}}_{drag}$$

$$\sum M_{CG} = \underbrace{\frac{\partial C_m}{\partial \alpha}\alpha + C_{m_{\alpha=0}}}_{aircraft\ pitching\ moment} + \underbrace{\frac{T_V \sin\beta}{\frac{1}{2}\rho U^2 S}\frac{x_{VT}}{\bar{c}}}_{thrust\ vectoring} = 0.$$

where T_V is the vectored thrust, β is the vectored thrust angle, α is the angle of attack, C_{D_i} is the induced drag coefficient, C_{D_0} is the parasite drag coefficient, C_{D_R} is the ram drag coefficient, x_{VT} is the moment arm of the vectored thrust, and $\bar{c}$ is the reference chord. The definition of net thrust,

$$T_N \equiv \dot{m}(u_{jet} - u_{aircraft}) = \dot{m}u_{jet} - D_R,$$

where D_R is the ram drag and T_N represents the net momentum change produced by the engines, produces a fourth equation

$$\underbrace{\frac{T_V}{\frac{1}{2}\rho U^2 S}}_{vectored\ thrust} - \frac{T_N + D_R}{\frac{1}{2}\rho U^2 S} = 0.$$

The system of four equations given above is solved for the vectored thrust T_V acting on the aircraft, net thrust T_N, angle of attack α, and vectored thrust angle β. Since the net thrust and ram drag are coupled with the angle of attack and thrust vectoring angle, the thrust vectoring model is iterated with the engine scaling model until there is agreement on the net thrust and ram drag values. The net thrust value is then used to predict the noise generated by the engines on initial climb as described in Section 4.5.2.

4.5 Acoustics

As a sound wave propagates away from its source, it disturbs the fluid through which it travels. If the fluid at rest is at pressure p_0, as the sound wave passes the pressure becomes $p_0 + p'(x,t)$ at position x and time t. The sound pressure level (SPL) is a measure of this pressure fluctuation and is defined as

$$\text{SPL in dB} = 20 \log_{10} \left(\frac{\bar{p'^2}}{2 \times 10^{-5}\ \text{N/m}^2} \right)$$

where $\bar{p'^2}$ is the mean value of the pressure fluctuation [17].

The A-weighted decibel (dBA) is an internationally accepted method of accounting for the annoyance of a sound. Because the human ear responds more strongly to some frequencies than others, the A-weighting system adjusts the sound pressure level in each frequency band by a factor which accounts for the human ear's sensitivity to that frequency [17]. The A-weighting bias is shown in Figure 4-11.

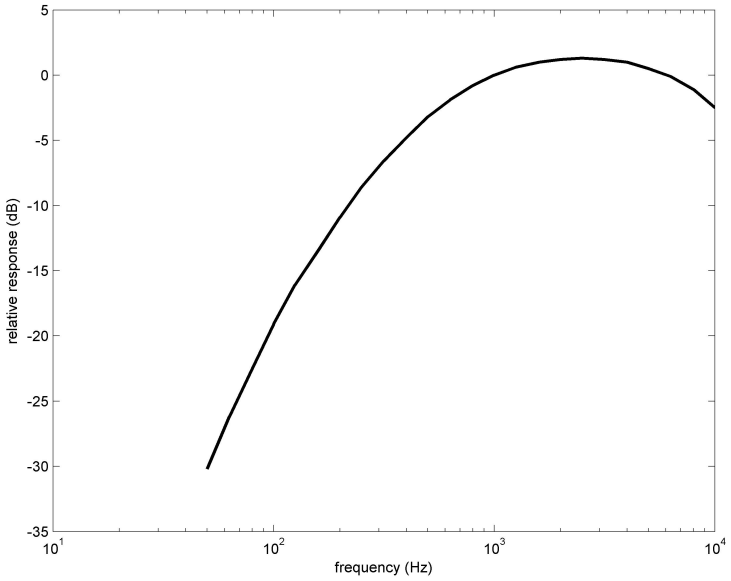

Figure 4-11: A-weighting bias for dBA scale [17]

4.5.1 Airframe noise

Airframe noise is that which is generated by air flow over the surfaces of the aircraft. Because the silent aircraft lacks conventional slats and uses thrust vectoring for pitch control, in a clean takeoff configuration the primary source of airframe noise becomes the airfoils themselves. The noise generated by the airfoil trailing edges was estimated using the ESDU semi-empirical airframe noise prediction model as described in Reference [10].

4.5.2 Engine noise

Because SAX has engines embedded on the upper surface of the aircraft, noise which would ordinarily propagate forward through the engine inlet is shielded by the BWB-like airframe [11]. The two primary components of engine noise are jet noise and rearward propagating fan noise. Estimates for these sources were computed for an aircraft at an angle of attack α and with vectored engines rotated by the vectored thrust angle β.

Jet noise

Jet noise is particularly sensitive to jet velocity as the acoustic power is roughly proportional to jet velocity to the power of 8 [35]. Because the scaled engine designs alter the fan diameter, jet velocity can vary greatly across the possible designs. Jet noise was estimated using the Stone jet noise model [45, 46].

Fan noise

To obtain fan noise estimates for the scaled designs, the ESDU noise correlations were rewritten to allow for variations in thrust and fan diameter from a reference design [22]. The reference noise estimates of rearward propagating fan noise for the Granta-3201 were provided by Crichton from the ESDU fan noise prediction codes based on Heidmann [9, 13, 25].

The ESDU noise correlation can be written

$$N_{BB} = 20\log_{10}(\Delta T_0) + 10\log_{10}(\dot{m}) + K_1$$

where N_{BB} is the broadband noise for a fan with a fixed rotor-stator gap and constant relative Mach numbers at the noise condition of interest. K_1 is a constant. From the steady flow energy equation and neglecting the change in static temperature, the enthalpy change of the flow from the engine inlet to the exhaust is

$$\Delta h_0 = \left(c_p T_j + \frac{V_j^2}{2}\right) - \left(c_p T_{atm} + \frac{V_0^2}{2}\right).$$

The change in total temperature can be written as

$$\Delta T_0 = \frac{1}{2c_p}(V_j^2 - V_0^2) = \frac{1}{2c_p}(V_j - V_0)(V_j + V_0) = \frac{X_N}{\dot{m}}\frac{(V_j + V_0)}{2c_p}$$

and the noise equation becomes

$$N_{BB} = 20\log_{10}(X_N) - 20\log_{10}(\dot{m}) + 20\log_{10}(V_j + V_0) + 10\log_{10}(\dot{m}) + K_2.$$

Because the fan capacity is fixed in the design and the ambient conditions are constant, the fan mass flow rate per area is fixed. Therefore, the mass flow is proportional to the fan diameter squared and the noise equation reduces to

$$N_{BB} = 20\log_{10}(X_N) - 20\log_{10}(D_f) + 20\log_{10}(V_j + V_0) + K_3.$$

Relative to a reference design, this can be written

$$\Delta \text{ SPL} = 20\log_{10}\left(\frac{X_N}{X_{N_{ref}}}\right) - 20\log\left(\frac{D_f}{D_{f_{ref}}}\right) + 20\log_{10}\left(\frac{V_j + V_0}{V_{j_{ref}} + V_0}\right).$$

Considering a jet velocity of approximately 150 m/s and a flight speed of near 100 m/s, the first term on the right hand side of the equation is approximately five times larger than the third term. Therefore, for small changes in thrust a first approximation of the change in fan noise can be obtained by neglecting the third term [22].

4.5.3 Propagation

To account for the sound propagation from the source through the atmosphere to a point on the ground under the aircraft, sound levels were corrected for geometric and atmospheric attenuation. Geometric attenuation occurs because there is a loss of energy as the sound waves radiate outwards. The relationship between the mean-square acoustic pressure $\bar{p'^2}$ and the distance from the noise source to the observer r is given by $\bar{p'^2} \propto \frac{1}{r^2}$. The mean-square acoustic pressure is related to the sound pressure level (SPL) logarithmically, thus $SPL \propto k\, r$ where k is a constant [47].

Furthermore, as sound waves pass through the atmosphere, some energy is transferred to air molecules. This reduction in sound energy, atmospheric attenuation, is a function of temperature and humidity. To determine the energy loss due to atmospheric attenuation, the atmosphere was assumed to be a single layer of air at 298 K with 70% humidity. Atmospheric attenuation values were obtained using the ESDU model described by Evans [19].

Table 4.1: Model inputs to generate the SAX21 planform design and takeoff operations

Variable	Parameter	Value
K_{ow}	chord scaling factor	1.00
b	span, m	58.52
γ	flight path angle, degrees	2.41
M	departure Mach number	0.22
D_f	fan diameter, m	1.292

Table 4.2: Model inputs to generate the SAX21 outer wing airfoil

Endpoint #	Handle #	θ (deg)	L
1	1	14.5	0.200
	10	-10.0	0.090
2	2	2.4	0.155
	3	2.4	0.024
3	4	90.0	0.014
	5	90.0	0.030
4	6	-2.7	0.040
	7	-2.7	0.050
5	8	0.0	0.500
	9	0.0	0.200

4.6 Application to SAX21

The SAX21 design is the result of applying the aircraft weights, center of gravity, and design models described in Chapters 2, 3, and 4 to the inputs given in Tables 4.1 and 4.2. The SAX20 design was used as the reference aircraft and the SAX20 and SAX21 planform area, wing spans, airfoils, and engines are identical. The aircraft have different weights and centers of gravity, and as such have different wing twists and aerodynamic characteristics. The wing twist and other characteristics of SAX21 are given in Figure 4-12 and Table 4.3

The acoustics models described in Section 4.5 were used to predict the noise as observed at a single point under SAX21 as it crosses the airport boundary on takeoff. The observation point was defined as 4,000 meters from brake release. The takeoff ground roll and rotation distances were found to be 3,152 meters and 225 meters. Departing the airport at a flight path angle of 2.41°, the aircraft's altitude at the

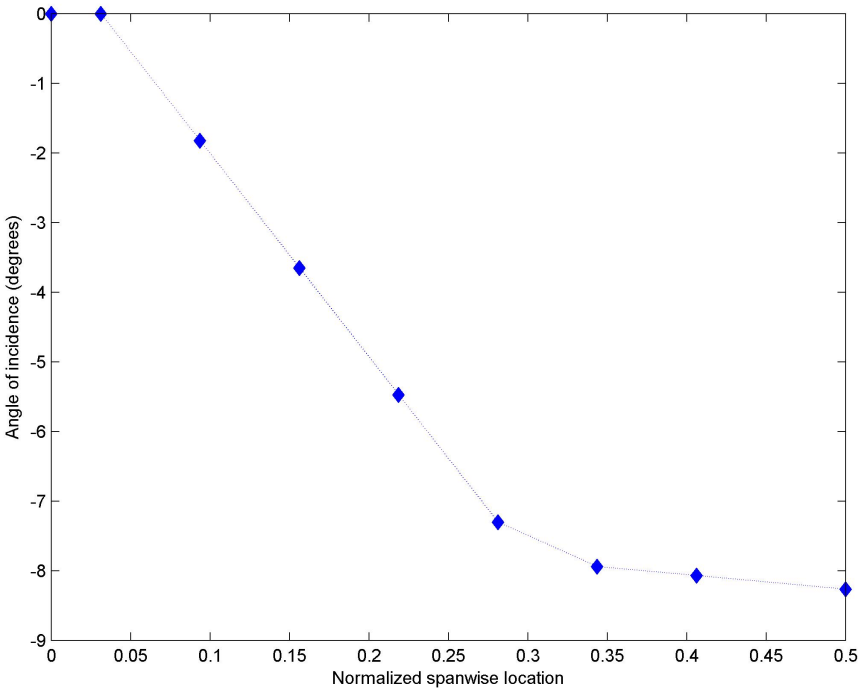

Figure 4-12: Wing twist for SAX21 design

Table 4.3: Selected characteristics of the SAX21 design

Parameter	Value	Units
planform area	843.63	m^2
angle of attack at cutback	12.16	degrees
thrust vectoring angle at cutback	18.07	degrees
angle of attack at mid-cruise	5.72	degrees
L/D at mid-cruise	20.73	
total thrust at cutback	149.62	kN
MTOW	338,995	lbs

Table 4.4: SAX21 noise as observed at a single point on the ground directly below the aircraft 4,000 past brake release

Airframe	77.87	dBA
Fan rearward	79.81	dBA
Jet	61.02	dBA
Total	**81.99**	**dBA**

observation point was found to be 26.24 meters. Propagating the airframe, rearward propagating fan, and jet noise to the observer point, the total observed SAX21 noise was found to be 81.99 dBA and the component noise is given in Table 4.4.

4.7 Sensitivity

Because an in-depth sensitivity analysis was performed on both the weights and center of gravity models, the most interesting effect to examine here is that of aircraft weight on noise. To perturb the MTOW for this analysis, MTOW was multiplied by a factor after the iterations to find the design fuel were complete so as not to alter the aircraft center of gravity. Figures 4-13 and 4-14 show the normalized sensitivity,

$$NSP \equiv \frac{\%\text{ change in noise}}{\%\text{ change MTOW}},$$

of each noise component with respect to MTOW.

The noise as observed on the ground is a function of three variables: noise generated at the source, aircraft orientation, and aircraft altitude. The data presented in Figure 4-13 accounts for the effects of MTOW on source noise and aircraft orientation only. Here, the aircraft altitude was fixed at 34.43 meters. The airframe noise sensitivity is slightly negative due to the increase in angle of attack with MTOW in order to maintain lift. Figure 4-14 shows the complete effect of MTOW on observed noise. To obtain this data, the aircraft altitude was computed as described in Section 4.3.

From Figure 4-14, the total aircraft noise can be quite sensitive to MTOW. A 10% increase in MTOW can result in a 10.7% increase in total noise. This dependency

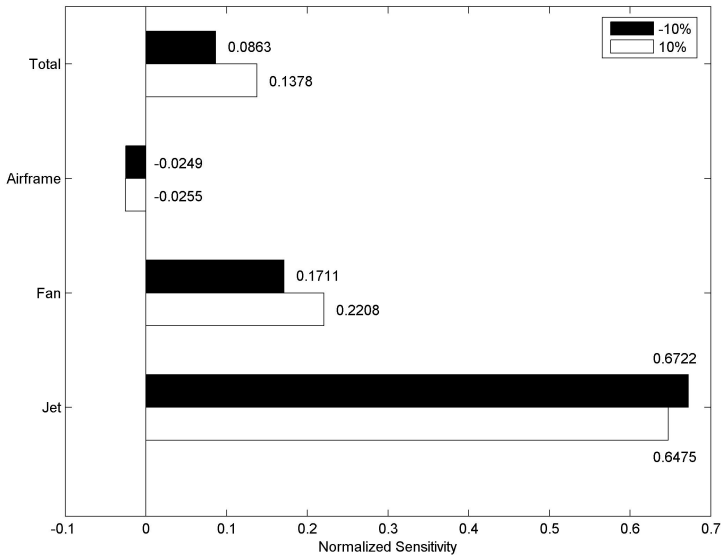

Figure 4-13: Single point noise sensitivity to MTOW with aircraft at a fixed altitude, accounting only for effects of changes in thrust. Normalized sensitivity is the % change in noise for a 1% change in MTOW.

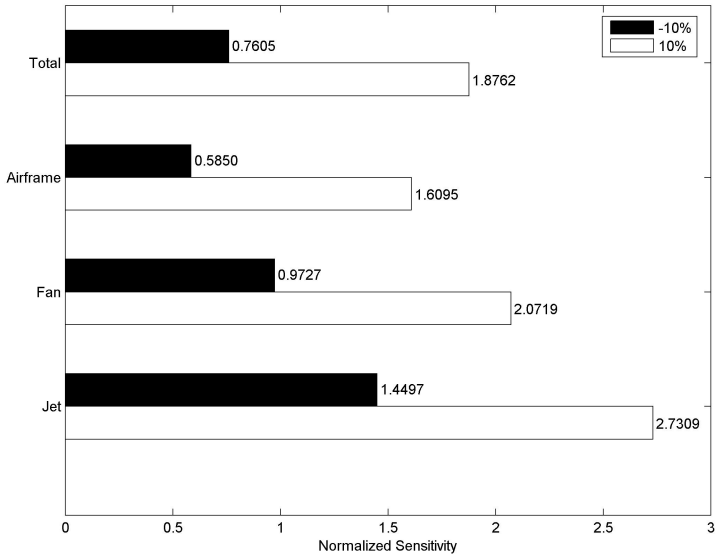

Figure 4-14: Single point noise sensitivity to MTOW, accounting for both altitude and thrust changes. Normalized sensitivity is the % change in noise for a 1% change in MTOW.

is likely driven by the jet noise as a heavier aircraft will both require more thrust to maintain flight as well as require a longer ground roll on takeoff. This results in an engine exhausting a jet of higher velocity at a lower altitude.

4.8 Model Fidelity and Risks

The aircraft design model was intended to be simple-physics and empirical model capable of capturing design trades and generating reasonable aircraft designs in minimal run time. To this end, AVL was used to perform the aerodynamic analysis, a baseline airframe and engine were scaled to provide a range of possible designs, and first principles were used to analyze the flight mechanics. Perhaps the weakest part of the design model is the lack of ability to account for three-dimensional aerodynamic effects. The SAX design, like a BWB, should experience strong three-dimensional flow in the centerbody region. Due to the run time necessary to conduct such an analysis, it was not possible to account for these effects. As such, the drag estimation includes only induced drag and a constant parasite drag value and is not as accurate as it might otherwise be.

Similarly, the noise prediction and propagation models are intended to provide accurate but basic information. Airframe, rearward propagating fan, and jet noise were selected as the primary noise sources for a BWB-like design where forward propagating noise is shielded by the airframe. To simplify noise prediction, well accepted models were used to predict airframe and jet noise and fan noise was scaled from known data. The noise propagation model was built to capture only effects that change with aircraft design. For example, noise is corrected for atmospheric and geometric attenuation because they are a function of the distance between the noise source and the observer, but the effect of ground reflections is not computed as it should not change significantly with aircraft design or flight path.

Chapter 5

Single-Level Optimization Setup

The primary goals of this silent aircraft optimization are to find the aircraft design-operations system with minimum noise while satisfying a set of constraints and to gain insight into the design tradeoffs that must be made in order to achieve a "silent" aircraft and how those tradeoffs affect the design process. To this end, two optimization frameworks, one single-level and one distributed, were developed and applied to the silent aircraft problem.

A general design optimization problem can be written as

$$\min J(\mathbf{x})$$

where J is the objective function and $\mathbf{x}$ is the design vector. The minimization problem is subject to constraints

$$\begin{aligned} g_j(\mathbf{x}) &\leq 0 \qquad j = i, \ldots, m_1 \\ h_k(\mathbf{x}) &= 0 \qquad k = 1, \ldots, m_2 \\ x_i^l \leq x_i &\leq x_i^u \quad i = 1, \ldots, n \end{aligned}$$

where $g_j(\mathbf{x})$ and $h_k(\mathbf{x})$ are the inequality and equality constraints and the optimization is required to satisfy a total of $m = m_1 + m_2$ constraints. The n design variables are bounded by upper and lower bounds $\mathbf{x}^u$ and $\mathbf{x}^l$.

In a single-level optimization framework, the optimizer is linked to a single inte-

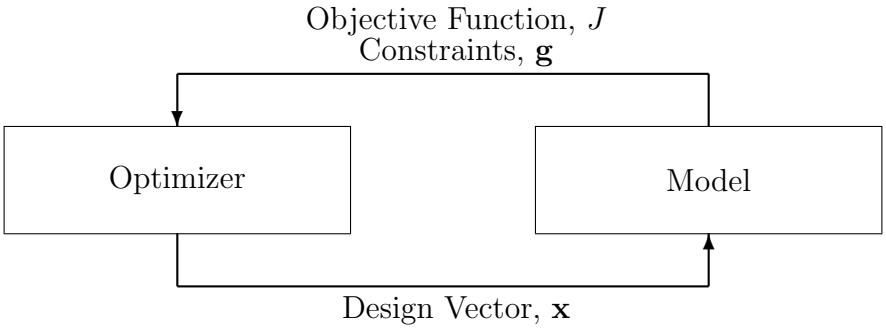

Figure 5-1: Single level optimization framework

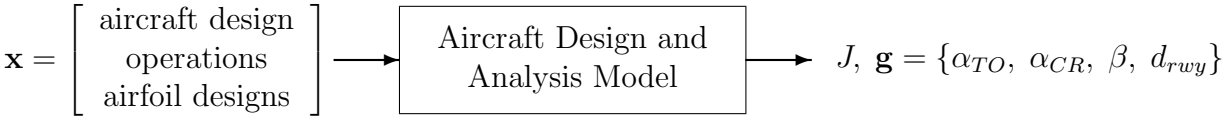

Figure 5-2: Relationship between design vector and objective function

grated set of models as shown in Figure 5-1. The optimizer specifies values to fill the design vector and the model evaluates those values to returns the values of the objective function and constraints (Figure 5-2).

For an iterative optimization procedure, the initial design vector $\mathbf{x}^0$ is given and subsequent steps are computed from

$$\mathbf{x}^q = \mathbf{x}^{q-1} + \alpha^q \mathbf{S}^q$$

where q is the iteration number, $\mathbf{x}^q$ is the design vector at the q^{th} iteration, α is a scalar distance, and $\mathbf{S}$ is the vector search direction.

In this work, sequential quadratic programming (SQP) was used to solve the optimization problem. The SQP algorithm creates and solves a sequence of sub-problems in which the objective function is replaced with a quadratic approximation, the constraints with linear approximations, and the Hessian is approximated using a quasi-Newton method with the Broyden-Fletcher-Shanno-Goldfarb update [39].

5.1 Problem Statement

The goal here is to find the quietest possible SAX design-operations system on takeoff. The optimization for low noise can be written

$$\begin{aligned} \min \quad & J(\mathbf{x}) \\ \text{s.t.} \quad & \alpha_{TO} < 16^\circ \\ & \alpha_{CR} < 6^\circ \\ & \beta < 30^\circ \\ & d_{rwy} < 3,600 \end{aligned}$$

where J is the noise as observed at a single point under the aircraft as it crosses the airport boundary and $\mathbf{x}$ is a vector of design variables representing the aircraft design, operations and airfoil design. The constrained values are the angle of attack on initial climb from takeoff α_{TO}, the mid-cruise angle of attack α_{CR}, the thrust vectoring angle β, and the runway distance needed for ground roll and rotation $d_{rwy} = d_{GR} + d_{ROT}$. The aircraft design is modeled as described in Chapters 2 through 4.

5.2 Design Variables

The design vector shown in Figure 5-2 is made up of 29 design variables from three aeronautical engineering disciplines. Aircraft design is represented by 3 variables, operations by 2 variables, and airfoil design by 24 variables. The complete set of 29 design variables is given in Table 5.1.

The aircraft design variables are responsible for both the airframe and engine sizing. As described in Section 4.1.1, a reference airframe outer wing chords and wingspan are scaled to create a new design. The engine design is scaled by changing the fan diameter as described in Section 4.2.

Takeoff operations are modeled with two design variables: departure flight path angle and departure Mach number. As described in Section 4.3, these two values define the flight path as the aircraft departs the runway on initial climb.

Table 5.1: Design variable values for the initial design point, $SAX31_0$

Aircraft Design	Outer wing chord scaling factor	K_{ow}	1.0046
	Wing span, excluding winglets, m	b	60.0000
	Engine fan diameter, m	D_f	1.2971
Aircraft Operations	Departure flight path angle, degrees	γ	6.2498
	Mach number on initial climb	M	0.1938
Airfoil Design	Control point 1 upper surface handle angle, degrees	θ_{1u}	14.5000
	Control point 1 lower surface handle angle, degrees	θ_{1l}	-8.6229
	Control point 2 handle angle, degrees	θ_2	2.4000
	Control point 4 handle angle, degrees	θ_4	-2.2950
	Control point 5 handle angle, degrees	θ_5	1.3599
	Control point 1 x-coordinate	x_1	0.9844
	Control point 2 x-coordinate	x_2	0.3052
	Control point 4 x-coordinate	x_4	0.0638
	Control point 5 x-coordinate	x_5	0.2997
	Control point 1 y-coordinate	y_1	-0.0049
	Control point 2 y-coordinate	y_2	0.0370
	Control point 3 y-coordinate	y_3	-0.0079
	Control point 4 y-coordinate	y_4	-0.0238
	Control point 5 y-coordinate	y_5	-0.0345
	Handle 1 length	L_1	0.1983
	Handle 2 length	L_2	0.0936
	Handle 3 length	L_3	0.1492
	Handle 4 length	L_4	0.0241
	Handle 5 length	L_5	0.0140
	Handle 6 length	L_6	0.0255
	Handle 7 length	L_7	0.0460
	Handle 8 length	L_8	0.0492
	Handle 9 length	L_9	0.4998
	Handle 10 length	L_{10}	0.2000

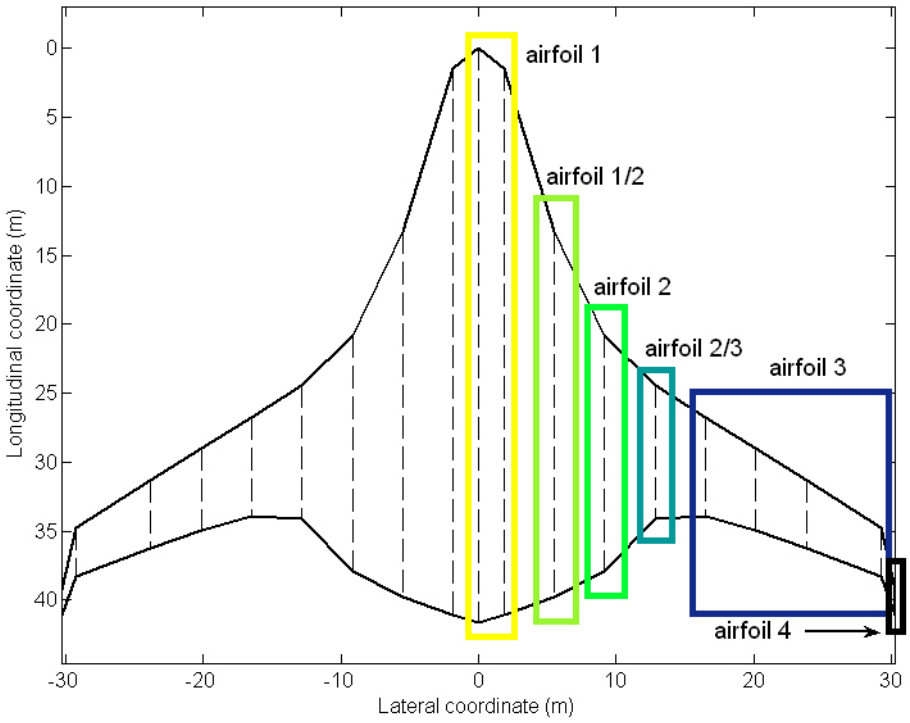

Figure 5-3: Sectioned planform and rib locations for airfoil profiles

The airfoil design variables define the endpoints and control points of the five splines that make up the outer wing airfoil profile. Section 4.1.2 provides a detailed description of the method used to generate the airfoil profiles from these values. Only the outer wing airfoils ("airfoil 3" in Figure 5-3) are explicitly defined by design variables. Airfoils 1, 2, and 4 in the centerbody, mid-wing, and winglet have constant profiles. Because airfoil 2/3 is a linear interpolation of airfoil 2 and airfoil 3, it is indirectly affected by the choice of values for the airfoil design variables. The airfoil shapes are defined by a total of twenty-seven variables: five spline endpoint x-coordinates, five spline endpoint y-coordinates, seven handle departure angles, and ten handle lengths. For the optimization, the endpoint located at the airfoil leading edge has a constant x-coordinate of 0 and handle departure angles of 90°. Because of these constraints, the airfoil design variables are limited to twenty-four: four spline endpoint x-coordinates, five spline endpoint y-coordinates, five handle departure angles, and ten handle lengths.

Table 5.2: General characteristics of the Granta-3201 engine

Parameter	Value
Number of cores	1
Number of fans	3
Fan diameter, m	1.292
Length, m	1.98
Weight of 1 core, lbs	4,190
Weight of 1 fan, lbs	242.5
Hub-to-tip ratio (HTR)	0.25
Axial Mach number	0.675
Fan capacity	1.1502
Begin cruise SFC, kg/N-hr	0.051

Table 5.3: Performance characteristics of the Granta-3201 engine

	Top of climb	Cutback	Takeoff roll
Fan pressure ratio (FPR)	1.5000	1.1788	1.1863
Pressure loss across inlet (η_{inlet})	0.94	0.98	0.98
Pressure loss across fan (η_{fan})	0.92	0.94	0.94
Thrust per engine, kN	20.33	44.33	76.73

5.3 Objective Function

The objective function is defined as the single point noise as observed directly under the aircraft as it crosses the airport boundary 4,000 meters from brake release. This noise value, measured in A-weighted decibels, accounts for airfoil self-noise, rearward propagating fan noise, and jet noise. Details on the noise prediction and propagation models can be found in Section 4.5.

5.4 Parameters

The reference aircraft and engine designs define all of the remaining parameters in the problem. For example, the primary characteristics of the reference engine design are given in Tables 5.2, 5.3, and 5.4. The new engine designs produced by the model are the Granta-3201 inlet and core with a scaled fan diameter. It is assumed that within the bounds of the optimization, the new fan diameter can be achieved with

Table 5.4: Component weights for one Granta-3201 engine (1 core, 3 fans)

Component	Weight, lbs
1 core	4,190
1 fan	242.5
Transmission gearbox to fans	882
Connecting shafts	287
Reduction gearboxes	827
Support and bearing for auxiliary fans	154
Nacelle	2,068

Table 5.5: Parameters defined by the SAX31 design

Mission	Begin cruise altitude, ft	40,000
	End cruise altitude, ft	45,000
	Cruise Mach number	0.8
	Range, nm	5,000
Payload	Number of passengers	215
	Number of crew	10
	Reserve fuel, % total fuel	10
Configuration	Number of engines	3
	Parasite drag coefficient, C_{D_0}	0.0060

the same technology level used to develop the Granta-3201. As such, the fan pressure ratio, pressure losses, specific fuel consumption, and other parameters given in the tables are constant for all scaled engine designs.

The aircraft mission, payload, and configuration given in Table 5.5 are set by the reference SAX design. The SAX31 design, an updated version of SAX21, was used to define the aircraft configuration in the centerbody. In this region, both the rib placement and airfoil profiles are fixed, allowing for a fixed cabin and cargo bay layout. Relative to the SAX21, the SAX31 wing is slightly forward and has less sweep (Figure 5-4). Also, the SAX31 airframe makes use of an updated wing twist distribution, shown in Figure 5-5. The SAX31 center of gravity locations are shown in Figure 5-6.

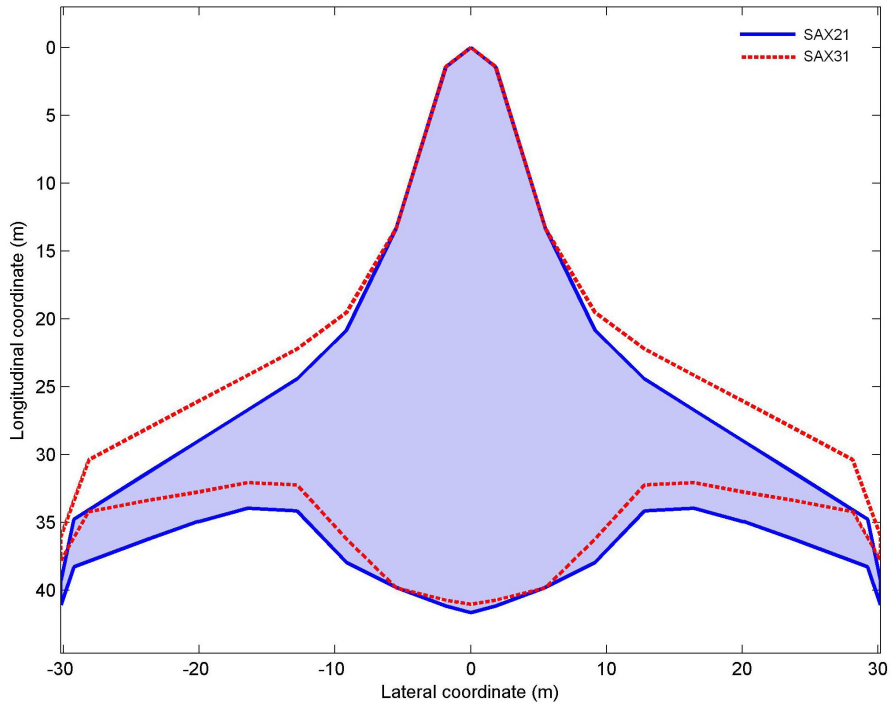

Figure 5-4: Comparison of SAX21 and SAX31 planforms

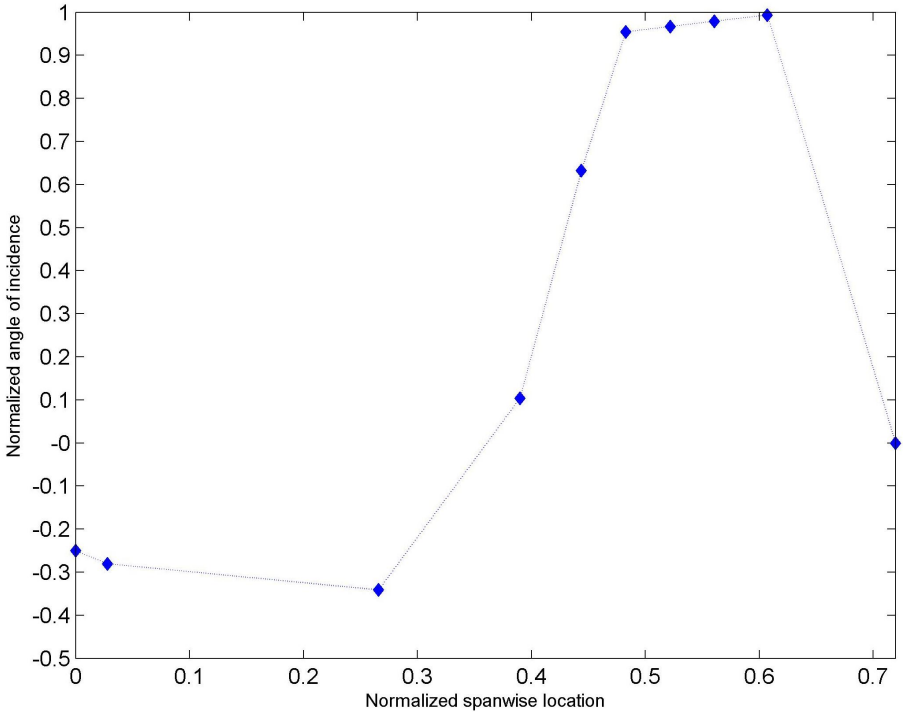

Figure 5-5: SAX31 wing twist distribution

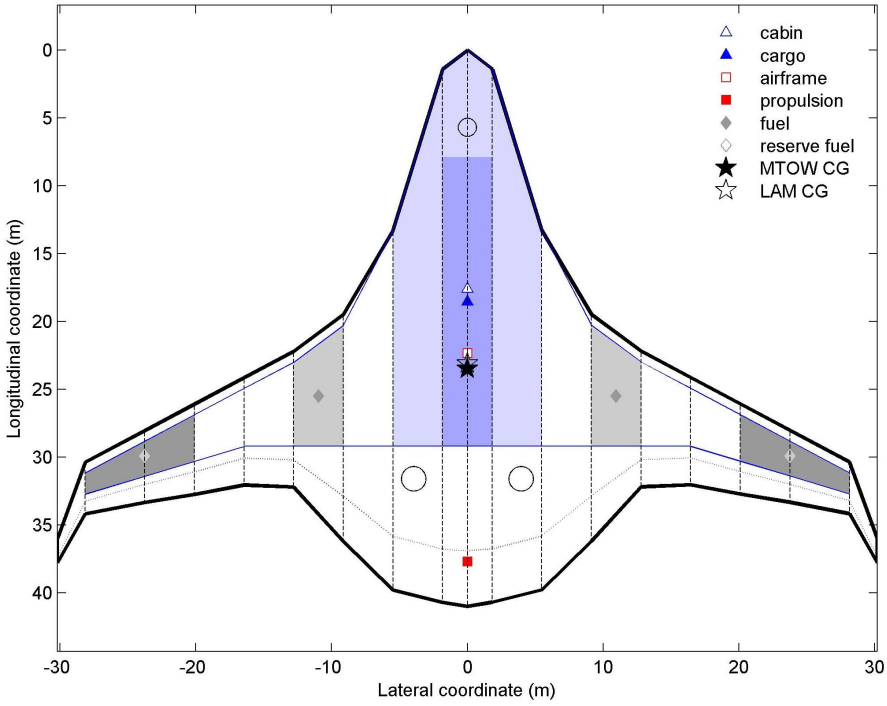

Figure 5-6: SAX31 planform layout and center of gravity locations

5.5 Constraints

As discussed in Chapter 1, the Boeing Company's Wing Multidisciplinary Optimization Design (WingMOD) code was used to optimize the first Silent Aircraft designs for minimum maximum takeoff weight. Because WingMOD was used from the beginning of the Silent Aircraft design process, the early SAX designs adhere to the 930 constraints imposed by the WingMOD optimization [51]. Due to the relatively minor scalings in the airframe design, is it assumed that constraints such as structural loads, spar placement, yaw stability, and buffet, which have already been addressed by WingMOD in the initial design, are still satisfied. WingMOD does not, however, allow for the thrust vectoring capabilities that the SAX designs rely on for pitch-trim. The vectored thrust angle, which in itself must be constrained, has a significant impact on the aircraft angle of attack at any flight condition. To represent limitations due to stall, constraints were imposed on the angle of attack on initial climb and at

mid-cruise such that

$$\begin{aligned} \alpha_{TO} &< 16^\circ \\ \alpha_{CR} &< 6^\circ \end{aligned}$$

while the thrust vectoring angle is constrained such that

$$\beta < 30^\circ.$$

To ensure a reasonable takeoff roll while allowing the engine size as a variable, the total runway length needed for roll and rotation was constrained to

$$d_{rwy} = d_{GR} + d_{ROT} < 3,600.$$

5.6 Bounds

Each of the design variables described in Section 5.2 are bounded by the values given in Table 5.6.

The airframe and engine design variables are bounded by the limits of the modeling capabilities. The airframe design variable bounds were chosen to allow the maximum design freedom while still ensuring that the resulting wing is of sufficient aspect ratio to contain both the main spars and the fuel tanks.

The engine design model and noise predictions are accurate only for small changes from the baseline Granta-3201 design. An acceptable perturbation in mass flow rate is approximately $\pm 10\%$, or $\pm 5\%$ in fan diameter [22].

The most critical operations bounds are the maximum flight path angle and the minimum Mach number. The lower bound on the takeoff Mach number is approximately 1.2 times the stall speed of SAX21. The upper bounds on the departure flight path angle and Mach number result in a climb rate of approximately 2,500 feet per minute–steeper than a conventional climb-out, but within the capabilities of modern airliners.

Table 5.6: Design variable bounds for optimization of the SAX31 design

	DV	Lower	Upper
Aircraft Design	K_{ow}	0.8000	1.2000
	b	50.00	65.00
	D_f	1.2274	1.3566
Aircraft Operations	γ	2.0000	8.0000
	M	0.1800	0.2600
Airfoil Design	θ_{1u}	12.3250	16.6750
	θ_{1l}	-11.5000	-8.5000
	θ_2	2.0400	2.7600
	θ_4	-3.1050	-2.2950
	θ_5	-2.7600	2.7600
	x_1	0.8500	1.1500
	x_2	0.2550	0.3450
	x_4	0.0638	0.0863
	x_5	0.2550	0.03450
	y_1	-0.0058	-0.0043
	y_2	0.0340	0.0460
	y_3	-0.0092	-0.0068
	y_4	-0.0276	-0.0204
	y_5	-0.0335	-0.0255
	L_1	0.1700	0.2300
	L_2	0.0765	0.1035
	L_3	0.1318	1783
	L_4	0.0204	0.0276
	L_5	0.0119	0.0161
	L_6	0.0255	0.0345
	L_7	0.0340	0.0460
	L_8	0.0425	0.0575
	L_9	0.4250	5750
	L_{10}	0.1700	2300

The airfoil parameters are simply allowed a $\pm 15\%$ deviation from the nominal values.

Chapter 6

Distributed Optimization Setup

Multidisciplinary design optimization (MDO) is known to exploit simplifications in numerical models. The models used in an optimization must be robust within the entire design space, often requiring a great deal of effort to develop and integrate with other models. Furthermore, simple design decisions often require high fidelity analysis which tends to increase runtime and complexity. As complexity increases, communication between analysis modules and the people involved becomes more difficult [28].

To reduce complexity, research has been directed at finding ways to decompose the optimization problem. One such method is the collaborative optimization (CO) architecture [30]. CO can be likened to the organizational structure of a large engineering company. At the top level, a project coordinator makes decisions that affect all of the disciplinary groups. In each discipline, experts work with their subordinates to find the design that most closely satisfies the project coordinator's demands. In this manner, collaborative optimization was designed to allow disciplinary experts to retain control of their models while coordinating interdisciplinary data at a higher level. The optimization problem is decomposed along disciplinary lines making it easier to integrate models and reducing the amount of communication necessary [6]. The autonomy afforded to each discipline allows for models to be updated and controlled independent of each other and members of disciplinary design groups can be more closely involved in the optimization process.

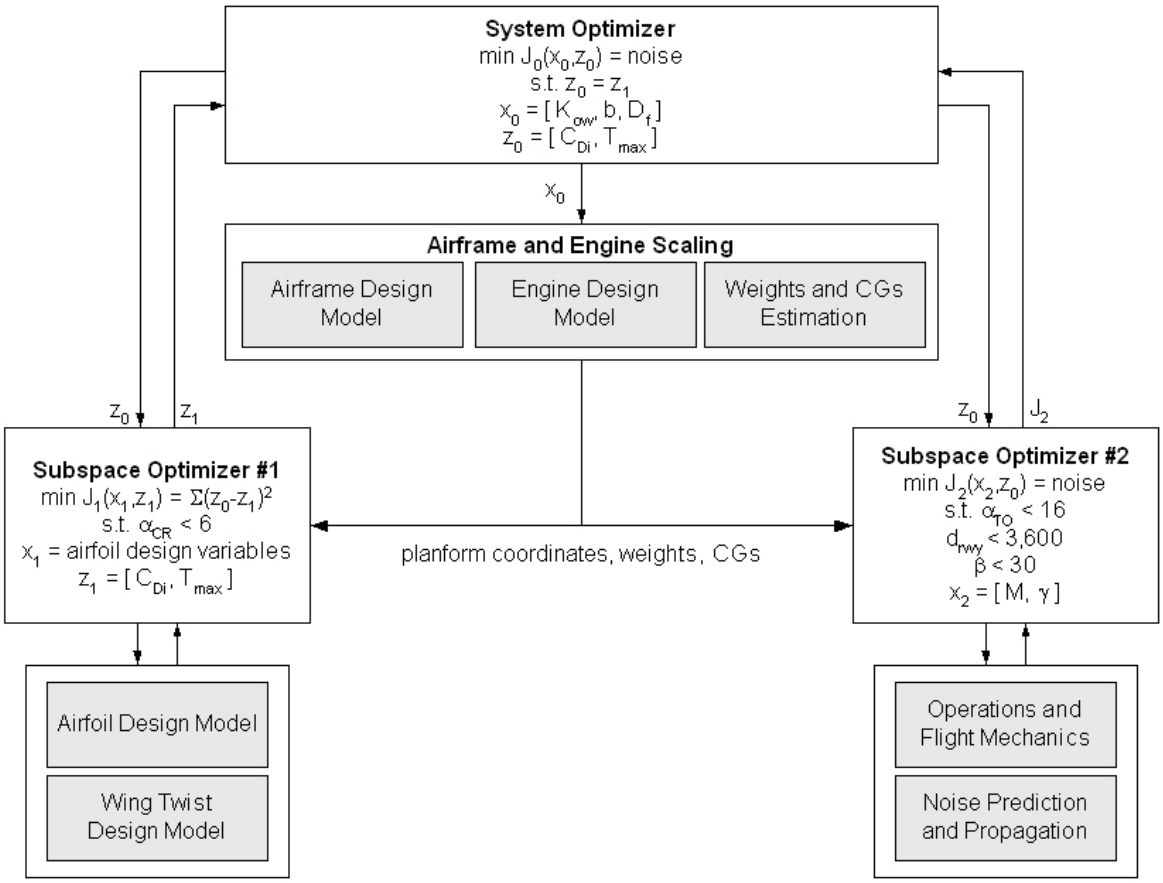

Figure 6-1: Distributed optimization framework

6.1 Problem Decomposition

The distributed optimization framework used here (Figure 6-1) is based on the collaborative optimization architecture, but is not CO in its purest form.

At the highest level, a system optimizer is responsible for minimizing noise. The system optimizer has a predetermined set of design and target variables, all of which it is allowed to change in order to find the minimum noise design. The design variables that make up $\mathbf{x}_0$ are the outer wing chord scaling factor, wingspan, and engine fan diameter. The target variables that make up $\mathbf{z}_0$ are the induced drag coefficient and the maximum wing twist:

$$\mathbf{x}_0 = [K_{ow}, b, D_f]$$

$$\mathbf{z}_0 \;=\; [C_{D_i}, T_{max}].$$

The system level design variables, responsible for the planform and engine scaling, are passed directly to a module which performs the scaling and passes the results on to the sub-optimizers at the lower level. The system level target variables are passed directly to the sub-optimizers.

At the system level, the optimization problem can be written

$$\begin{aligned} \min \quad & J_0(\mathbf{x}_0, \mathbf{z}_0) \\ \text{s.t.} \quad & \mathbf{z}_0 \;=\; \mathbf{z}_1 \end{aligned}$$

where the system level objective function J_0 is the single point noise as observed on the ground 4,000 meters from brake release. The constraints require that at the design solution the sub-optimizations return a design with values for the target variables $\mathbf{z}_1$ that match the values set by the system-level optimizer, $\mathbf{z}_0$.

At the lower level, there are two sub-optimizations decomposed along disciplinary lines: wing design and takeoff operations. Each of these optimizations has a separate problem to solve with different design variables and objective functions. The four constraints that were imposed on the single-level optimization still apply but are divided between the two sub-optimizations in the decomposed problem. The bounds on the design variables are the same as in the single-level optimization setup described in Chapter 4.

The first sub-optimization is responsible for the wing design. Local design variables are used to create the outer wing airfoil profiles and a reference wing twist distribution is scaled to the wing twist necessary for zero elevator deflection at mid cruise. The wing design optimization problem can be written

$$\begin{aligned} \min \quad & J_1(\mathbf{x}_1, \mathbf{z}_1) \;=\; (C_{D_{i_0}} - C_{D_{i_1}})^2 + (T_{max_0} - T_{max_1})^2 \\ \text{s.t.} \quad & \alpha_{CR} \;<\; 6^\circ \end{aligned}$$

where the local vector of design variables consists of the airfoil design variables described in Section 4.1.2, $\mathbf{x}_1 = [\text{airfoil design variables}]$. The constraint that appears in this optimization is the limit on the cruise angle of attack.

The second sub-optimization focuses on takeoff operations and noise prediction. Here, the local design variables are the departure Mach number and flight path angle, $\mathbf{x}_2 = [M, \gamma]$. In the disciplinary analysis, the target values for induced drag coefficient and wing twist are used to determine the ground roll distance and flight characteristics on initial climb. The thrust vectoring model described in Section 4.4.2 is used to trim the aircraft in pitch and calculate the angle of attack, thrust vectoring angle, and thrust required to maintain the given flight path. The optimization problem can be written

$$\begin{aligned} \min \quad & J_2(\mathbf{x}_2, \mathbf{z}_0) \\ \text{s.t.} \quad & d_{rwy} < 3,600 \\ & \alpha_{TO} < 16^\circ \\ & \beta < 30^\circ \end{aligned}$$

where the objective function is the same as at the system level, and the constraints are the remainder of the constraints imposed on the single-level optimization.

Chapter 7

Optimization Results for the SAX31 Design

The two optimization frameworks described in previous chapters were used to solve the silent aircraft optimization for minimum noise based on the SAX31 reference design. To find a design from which to initialize the optimizations, a preliminary exploration of the design space was conducted. More than fifty random designs were used to initialize a preliminary single-level optimization. Of these points, the one which reliably converged to the quietest design was chosen as SAX31_0, defined in Table 5.1.

The single-level optimization was broken into three problems, optimizations A through C. In optimization A, optimization for low noise was performed using only the design variables corresponding to the aircraft design and operations. For this case, the airfoils were set to a constant profile to obtain the solution SAX31A^*. In optimization B, the planform and operations were fixed and only the outer wing airfoil profiles were allowed to vary, resulting in the solution SAX31B^*. Finally, the complete optimization problem was solved using all 29 design variables described in Section 5.2. The low noise design produced by this optimization is referred to as SAX31C^*. The distributed optimization is labeled optimization D.

For each of the three optimizations described below, the initial and final values of the design variables are given in Table 7.1 and the noise predictions in Table 7.2. To

Table 7.1: Optimization results for the SAX31 design family

		SAX31	$SAX31_0$	SAX31A*	SAX31B*	SAX31C*	SAX31D*
Aircraft Design and Ops	K_{ow}	1.0000	1.0046	1.0046	1.0046	1.0046	0.800
	b	56.30	60.00	59.98	59.98	59.98	60.00
	D_f	1.2920	1.2971	1.3566	1.3566	1.3566	1.3566
	γ	2.4100	6.2498	6.2560	6.2560	6.2577	5.9782
	M	0.2200	0.1938	0.1938	0.1938	0.1938	0.1800
Airfoil Design	θ_{1u}	14.5000	14.5000	14.5000	12.3330	12.3250	14.5000
	θ_{1l}	-10.0000	-8.6229	-8.6229	-8.5000	-8.5664	-8.6229
	θ_2	2.40000	2.4000	2.4000	2.4053	2.1249	2.4000
	θ_4	-2.7000	-2.2950	-2.2950	-2.8316	-2.6824	-2.2950
	θ_5	0.0000	1.3599	1.3599	-2.7600	-2.5310	1.3599
	x_1	1.0000	0.9844	0.9844	0.9844	0.9851	0.9845
	x_2	0.3000	0.3052	0.3052	0.3044	0.3052	0.3053
	x_4	0.7500	0.0638	0.0638	0.0662	0.0844	0.0638
	x_5	0.3000	0.2997	0.2997	0.2997	0.2997	0.2997
	y_1	-0.0050	-0.0049	-0.0049	-0.0049	-0.0044	-0.0049
	y_2	0.0400	0.0370	0.0370	0.0370	0.0370	0.0370
	y_3	-0.0080	-0.0079	-0.0079	-0.0077	-0.0082	-0.0079
	y_4	-0.0240	-0.0238	-0.0238	-0.0234	-0.0204	-0.0238
	y_5	-0.3000	-0.0345	-0.0345	-0.0345	-0.0342	-0.0344
	L_1	0.2000	0.1983	0.1983	0.1983	0.2018	0.1983
	L_2	0.0900	0.0936	0.0936	0.0936	0.0936	0.0936
	L_3	0.1550	0.1492	0.1492	0.1783	0.1783	0.1492
	L_4	0.0240	0.0241	0.0241	0.0240	0.0209	0.0241
	L_5	0.0140	0.0140	0.0140	0.0140	0.0135	0.0140
	L_6	0.0300	0.0225	0.0225	0.0255	0.0255	0.0255
	L_7	0.0400	0.0460	0.0460	0.0458	0.0340	0.0460
	L_8	0.0500	0.0492	0.0492	0.0454	0.0412	0.0492
	L_9	0.5000	0.4998	0.4998	0.4998	0.4998	0.4998
	L_{10}	0.2000	0.2000	0.2000	0.2000	0.2000	0.2000

Table 7.2: Aircraft noise predictions (dBA) for optimized designs

	Airfoil	Fan	Jet	Total
SAX31	74.23	72.04	56.09	76.32
$SAX31_0$	55.72	58.41	59.56	62.95
SAX31A*	54.46	56.63	55.47	60.38
SAX31B*	54.44	56.43	54.93	60.12
SAX31C*	54.43	56.43	54.95	60.13
SAX31D*	50.83	56.16	57.50	60.40

Table 7.3: Definition of design characteristics

Planform area, m^2	S
Angle of attack at mid-cruise, degrees	α_{CR}
Thrust vectoring angle on initial climb, degrees	β
Maximum takeoff weight, lbs	MTOW
Altitude crossing the airport boundary, m	h
Lift to drag ratio	L/D
Runway length required for ground roll and rotation, m	d_{rwy}
Maximum wing twist at wingtip, degrees	T_{max}
Weight of fuel onboard, lbs	W_{fuel}
Thrust required on initial climb, kN	T_N

Table 7.4: Characteristics of optimized designs

	S	α_{CR}	β	MTOW	h	L/D	d_{rwy}	T_{max}	W_{fuel}	T_N
SAX31	845	3.63	0.44	326,606	40.57	22.55	3,036	-4.52	75,823	143.1
$SAX31_0$	892	3.55	1.79	332,089	191.9	21.96	2,247	-4.15	79,007	254.1
SAX31A*	892	3.55	1.68	333,179	218.0	21.99	2,012	-4.14	79,073	255.9
SAX31B*	892	3.42	2.03	332,078	219.3	22.19	2,000	-2.74	78,088	252.0
SAX31C*	892	3.43	2.01	332,078	219.3	22.20	2,000	-2.81	78,088	252.2
SAX31D*	856	3.52	-3.00	328,770	244.7	22.53	1,664	-4.14	76,405	282.9

evaluate the design results of the optimizations, a set of characteristics is presented in Tables 7.3 and 7.4.

There are six primary members of the SAX31 design family. First, there is the baseline SAX31 design, designed by members of the Silent Aircraft Initiative from the results of WingMOD optimizations. All other designs are a scaled version of the SAX31. $SAX31_0$ is the result of a preliminary design space exploration and is the design used to initialize optimizations A, C, and D. SAX31A*, SAX31B*, SAX31C*, and SAX31D* are the results of the optimizations. The result of optimization A, SAX31A*, was used to initialize optimization B, thus $SAX31B_0 \equiv$SAX31A*.

7.1 Optimization A: Aircraft Design and Operations

In order to investigate the effects of aircraft design and operations on noise independent of airfoil design, optimization A was performed using only the aircraft design and operations design variables. The outer wing airfoils were set to a constant profile defined by the airfoil design variables for the $SAX31_0$ initial design point given in Table 5.1.

The aircraft design and operations optimization resulted in an optimal design with a noise value 2.57 dBA less than $SAX31_0$ or 15.94 dBA less than the baseline SAX31 design. In this optimization there are two possible ways to reduce the overall aircraft noise: lower the acoustic power generated at the source and increase the distance between the noise source and observer.

The two noise sources which can most easily be controlled by the available design variables are the airfoils and jet. Airfoil self-noise scales with aircraft velocity to the fifth power. By lowering the Mach number from 0.22 (SAX31) to 0.19 (SAX31A*), the actual pressure fluctuations which cause noise are reduced. Similarly, jet noise increases with jet velocity to the eighth power. For equal thrusts, jet exit area and velocity are inversely proportional. In the aircraft design model used here, the jet exit area is the equal to the fan diameter, thus increasing the fan diameter even a small amount decreases jet noise significantly.

Because the noise observed on the ground is inversely proportional to altitude squared, it is be beneficial to gain as much altitude as possible before leaving the airport perimeter. One simple way to gain altitude is to simply provide more lift. Lift is proportional to the wing area, therefore increasing both the wingspan and outer wing chords increases lift and gains altitude with little or no noise penalty. Another obvious way to gain altitude is to increase the flight path angle γ. However, while a steeper flight path gains altitude, it also requires more thrust and thus louder engines. This tradeoff is clearly seen in Figure 7-1, where all of the design variables except flight path angle have been frozen to the SAX31A* design. As the flight path

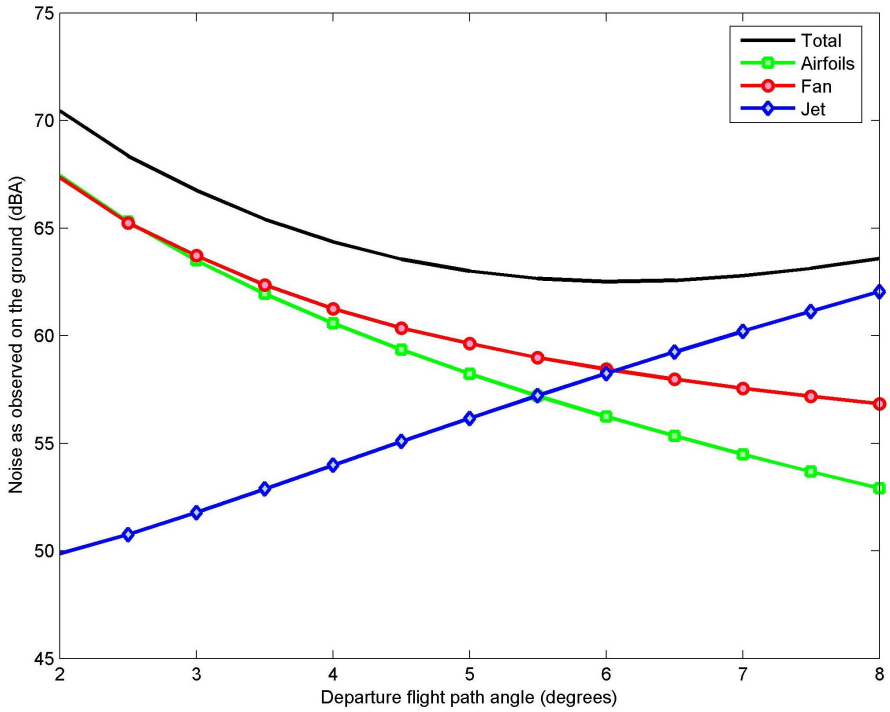

Figure 7-1: Observed noise versus departure flight path angle

steepens, airfoil and fan noise decreases due to the increased altitude, but jet noise increases due to the increase in required thrust. The ideal flight path angle is not the upper bound, but just over 6 degrees. In Table 7.1 it can be seen that all of the optimized designs have converged near the ideal flight path angle.

Relative to SAX31, the SAX31A* improvement in noise is promising, but comes at a large cost in fuel burn. SAX31A* is about 6,600 pounds heavier at MTOW and requires 4.3% more fuel than does SAX31. The increase in fuel burn is due to a combination of a heavier structure (larger engines and wings) and a lower lift-to-drag ratio.

7.2 Optimization B: Airfoil Design

To investigate the effects of the airfoil design on noise, optimization B was performed using only the airfoil design variables. The airfoil optimization results in a 16.20 dBA noise reduction relative to SAX31 but only a 0.26 dBA reduction relative to SAX31A*.

Table 7.5: Comparison of aerodynamic coefficients and 0.1% accurate fuel weights moving from $SAX31B_0$ to $SAX31B^*$

	$SAX31B_0$	$SAX31B^*$	% Change
C_L	0.19442	0.19353	-0.5
C_{D_i}	0.00284	0.00272	-4.2
C_D	0.00884	0.00872	-1.4
W_{fuel}, lbs	79,163	78,088	-1.4

The noise prediction model used for the optimization is not of high enough fidelity to consider anything less than about 1 dBA significant, so the noise reduction in optimization B relative to SAX31A* is negligible. It is of interest, however, that the airfoil optimization for low noise resulted in a design ($SAX31B^*$) requiring 1.2% less fuel than $SAX31A^*$. From Section 2.1.2, the error in fuel weight is approximately 1%, thus to confirm the apparent improvement in fuel burn, the $SAX31B_0$ and $SAX31B^*$ designs were re-evaluated allowing only a 0.1% error in the fuel weight design loop. The analysis confirmed the fuel burn improvement as shown in Table 7.5.

A close look at the initial and final airfoil profiles shown in Figure 7-2 reveals that the region from 40% to 90% of chord has thickened, effectively reducing the camber in that region. For both $SAX31B_0$ and $SAX31B^*$, the aspect ratio $\mathcal{AR} = 4.04$. From Table 7.5 and the induced drag equation,

$$C_{d_i} = \frac{C_L^2}{\pi \mathcal{AR} e},$$

the Oswald efficiency factor e can be found:

$$\begin{aligned} e(\text{SAX31B}_0) &= 1.05 \\ e(\text{SAX31B}^*) &= 1.08. \end{aligned}$$

$SAX31B^*$ has a higher efficiency and is thus expected to have a lower fuel burn. To confirm this, the total drag coefficient can be found as the sum of the induced and parasite drag coefficients:

$$C_D = C_{D_i} + C_{D_0}.$$

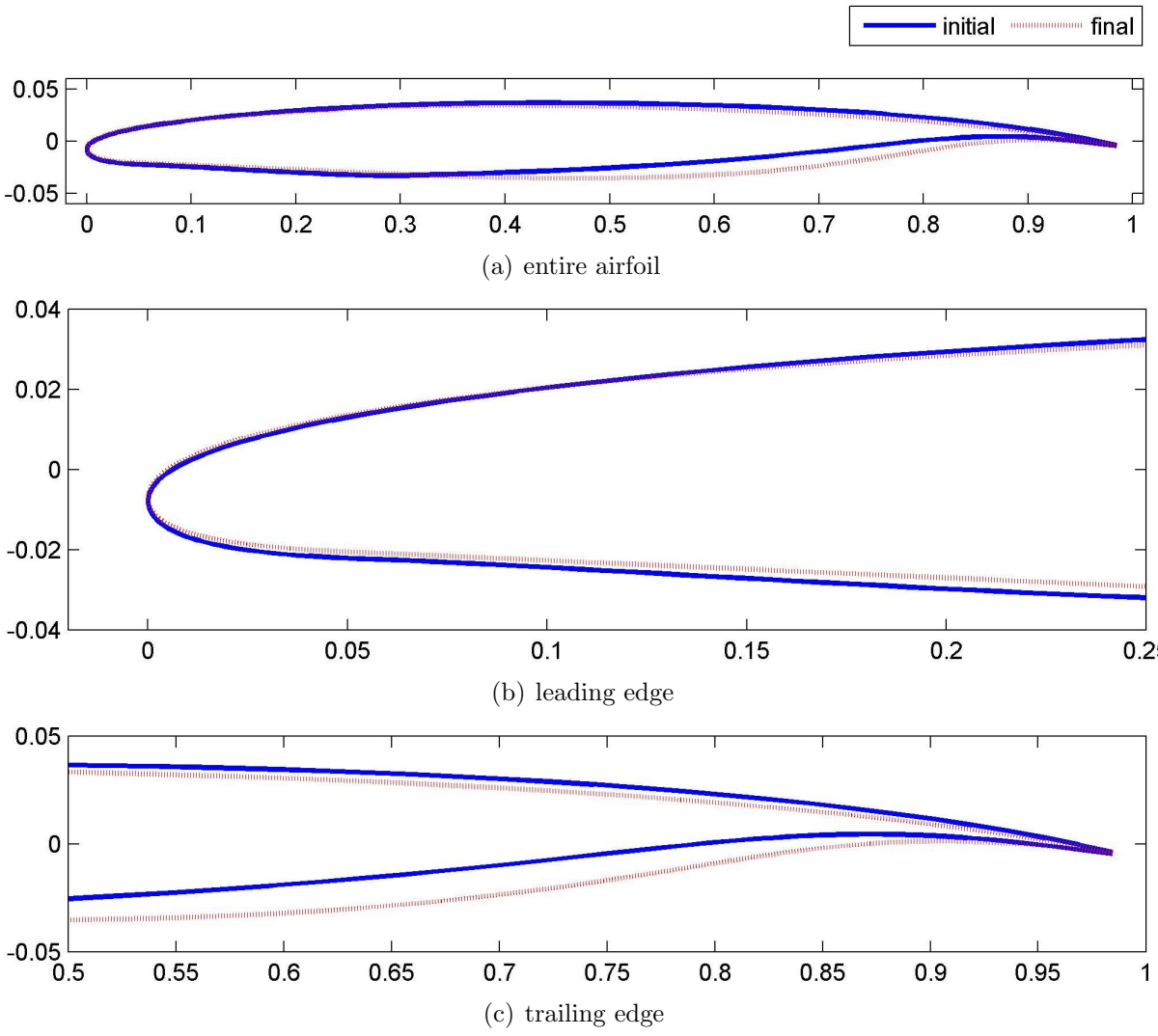

(a) entire airfoil

(b) leading edge

(c) trailing edge

Figure 7-2: Comparison of outer wing airfoil profiles for $SAX31B_0$ and $SAX31B^*$

For a constant $C_{D_0} = 0.0060$, the total drag coefficient decreases 1.4% from SAX31B$_0$ to SAX31B* as given in Table 7.5. From Section 2.1.2, the fuel weight is proportional to the total drag coefficient, and as expected, the 0.1% accurate fuel weights differ by 1.4%.

In optimization A, only the aircraft design and operations design variables were used and it was found that a large fuel burn penalty must be accepted to achieve a low noise design. By optimizing the airfoil profiles separately from the aircraft design and operations, it was found that airfoil design does not have a significant effect on noise, but can be used to improve fuel burn. Airfoil optimization could, without adversely affecting noise, be incorporated in the design process to mitigate the increase in fuel burn that results from a low noise design.

7.3 Optimization C: Aircraft Design, Operations, and Airfoil Design

Finally, an optimization was performed using the complete set of twenty-nine design variables. By optimizing for all design variables simultaneously, it should be possible to exploit tradeoffs amongst the three disciplines. From SAX31$_0$ to SAX31C*, a 2.82 dBA noise reduction was achieved with only a 1.2% increase in fuel burn. Relative to the baseline SAX31 design, the SAX31C* design represents a 16.19 dBA noise reduction with a 3.0% increase in fuel burn. As in the other two optimizations, the final result is a heavier aircraft with higher fuel burn and lower noise.

For each member of the SAX31 design family, Figure 7-3 shows the noise and required fuel relative to the reference SAX31 design. The biggest change in noise levels occurs in the step from SAX31 to SAX31$_0$, but there is also a significant noise reduction from SAX31$_0$ to the SAX31A* and SAX31C* designs. (The SAX31D* is discussed in Section 7.4.)

The SAX31B* and SAX31C* designs lie very nearly on top of each other on the fuel versus noise plot. Looking back at Tables 7.1, 7.2, and 7.4, the results of optimizations

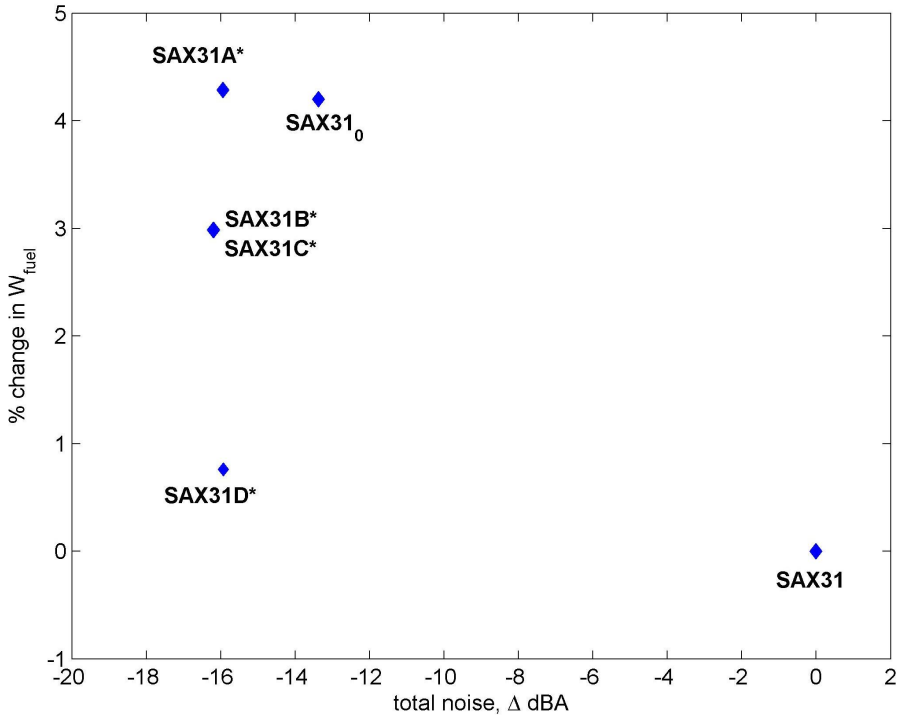

Figure 7-3: Relative fuel burn versus noise for SAX31 design family

B and C are almost identical designs. Taking a very close look at the different airfoil profiles as shown in Figure 7-4, there is a slightly carved out region near the leading edge of the optimization C airfoils. This slight increase in camber near the leading edge causes the wing loading to shift forward slightly, resulting in a slightly larger nose-up pitching moment. SAX31C* requires slightly less thrust vectoring for pitch-trim on initial climb, but the effect is so small that there is no practical difference in the designs.

7.4 Optimization D: Distributed Optimization

The result of the distributed optimization is SAX31D*, a design that has a 15.92 dBA noise reduction and only a 0.8% increase in fuel weight with respect to SAX31. Looking back at Figure 7-3, it can be seen that the SAX31D* noise is very similar to that of the other low noise designs but has a much more favorable fuel weight. From Figure 7-5 it can be seen that SAX31D* wings are a higher aspect ratio and smaller

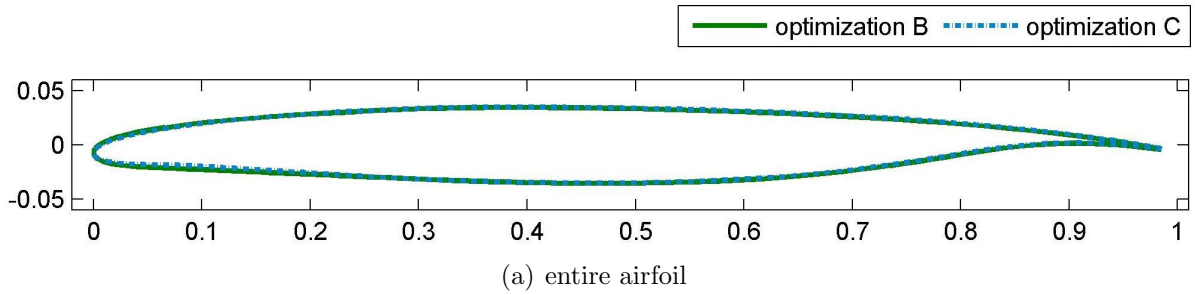

(a) entire airfoil

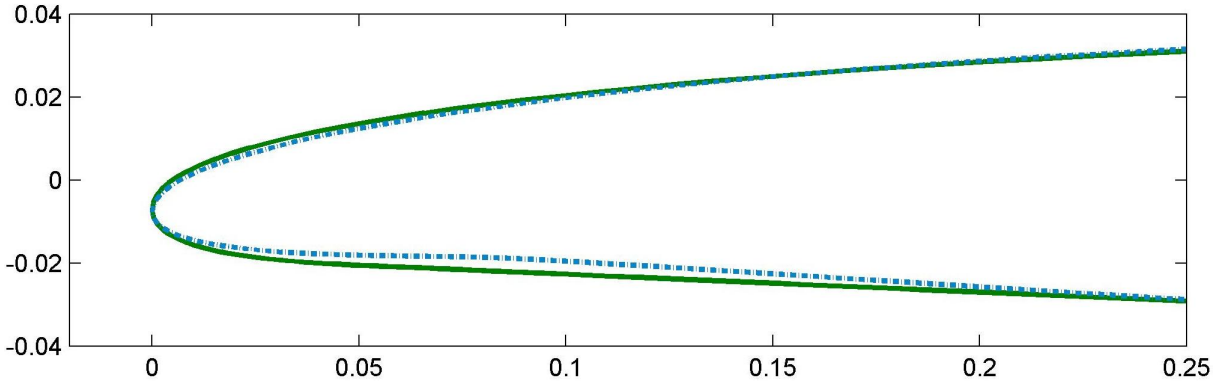

(b) leading edge

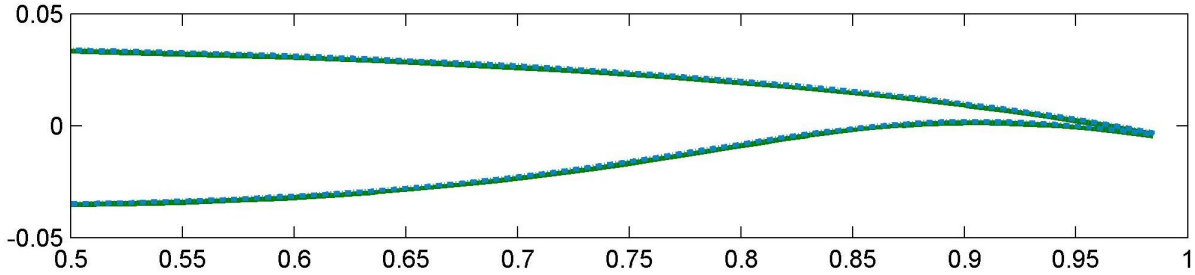

(c) trailing edge

Figure 7-4: Comparison of outer wing airfoil profiles for SAX31B* and SAX31C*

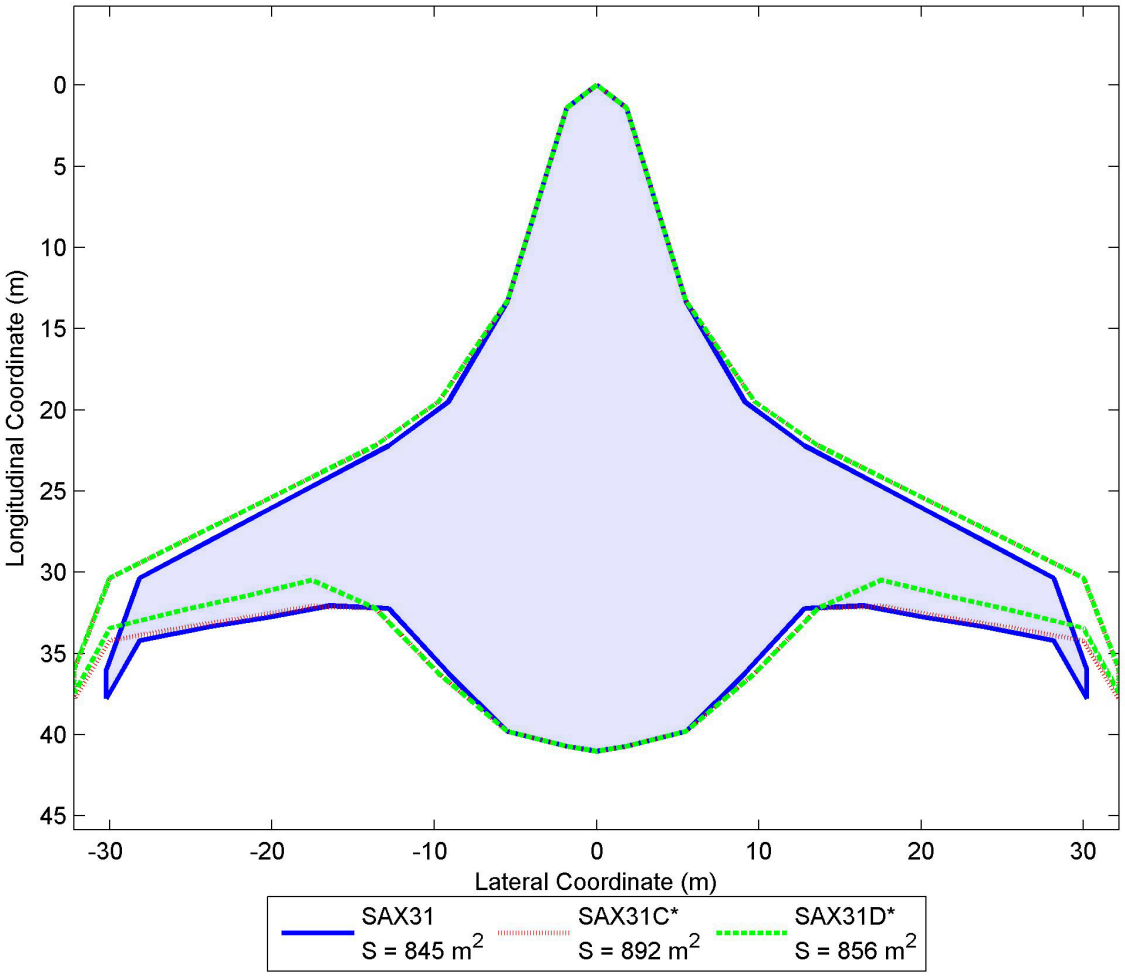

Figure 7-5: Comparison of planforms

planform area than the results of the single-level optimization. The smaller planform of SAX31D* results in a structural weight savings of more than 1,000 lbs with respect to SAX31C*. As in the single-level optimizations, the distributed optimization results in a lower initial climb Mach number, in this case the lower bound, and a large fan diameter. The airfoil profiles, however, do not change significantly from those of $SAX31_0$.

The noise versus flight path angle for SAX31D* was plotted in Figure 7-6 to demonstrate the tradeoff in noise and flight path angle. The distributed optimization does not find the exact optimal angle shown in this figure, but the optimization converges to $\gamma = 5.98°$ which results in a noise value within the fidelity of the noise

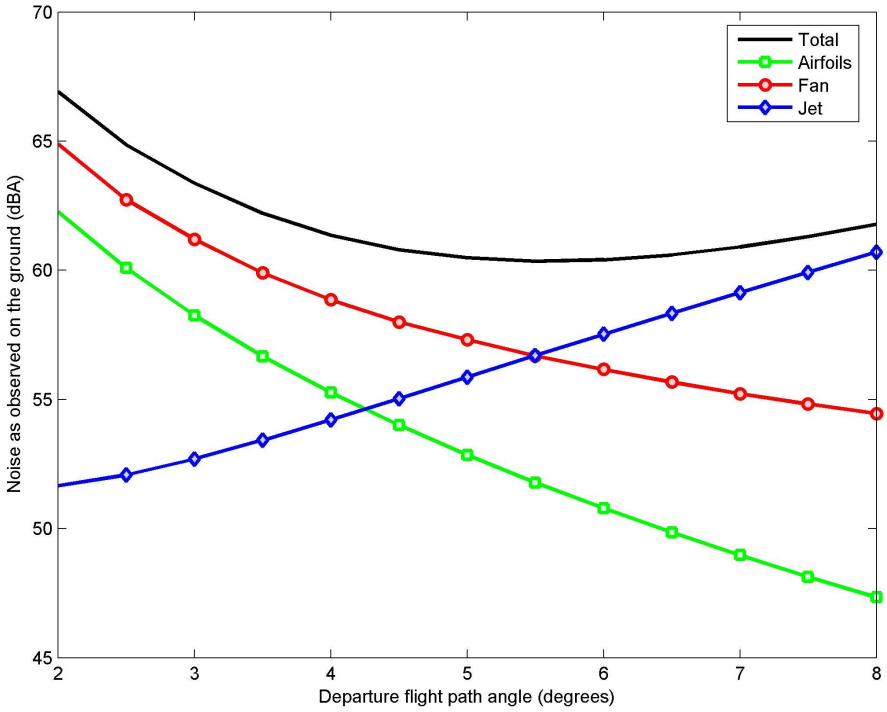

Figure 7-6: Observed noise versus departure flight path angle for SAX31D*

prediction models.

The distributed optimization resulted in a different design than did the single-level optimization. The $SAX31_0$, SAX31A*, SAX31B*, and SAX31C*, all results of the single-level optimization, have very similar thrust-to-weight ratios and nearly identical planform areas. The SAX31D*, however, has a much smaller planform and higher thrust-to-weight ratio. While the single-level optimization tended to increase planform area to gain altitude, the distributed optimization tended to decrease MTOW and increase the thrust available during the initial climb. As a result, the SAX31D* crosses the airport boundary approximately 25 meters higher than the single-level optimization results. To confirm that SAX31D* is at least a local optimum, a single-level optimization was initialized from the SAX31D* design point. This single-level optimization also converged at SAX31D*.

In the distributed optimization framework, the system level optimizer has some direct control over the lift-to-drag ratio via C_{D_i}, whereas the single-level optimizer can only control L/D indirectly through the wingspan, chords, and 24 airfoil profile design

variables. From the single-level optimizations, it is known that the aircraft design and operations design variables are largely responsible for any noise reduction while the airfoil variables can be used to reduce fuel burn. By decomposing the problem in this way, the system optimizer finds the lowest noise design as a function of the planform and operations with a target L/D. The airfoil profile and wing design optimization is then responsible for creating a wing capable of achieving that L/D.

7.5 Design Conclusions

From the optimizations performed on the SAX31 design, three primary conclusions can be drawn. First, the vast majority of noise reduction is a result of the aircraft design and operations rather than airfoil design. Secondly, airfoil profile optimization has little impact on noise reduction, but can have significant impact on fuel burn. For the SAX31 design, airfoil optimization regained 33% of the fuel burn lost in the design-operations optimization for low noise. Third, for this problem the results of a distributed optimization are fundamentally different than those of a single-level optimization.

In the single-level optimization, the design-operations solutions reduce acoustic power and increase the distance from the noise source to the observer in order to minimize noise. To lower the acoustic power generated by the airfoils passing through the air, the optimal designs fly about 12% slower than the baseline case. Airfoil self-noise is proportional to velocity to the fifth power, thus reducing airspeed reduces airfoil noise. Although the thrust required and jet exit velocity for the optimal designs is higher than that of SAX31, the optimal results utilize the upper bound on fan diameter, thus reducing jet exit velocity as much as possible. Exploiting the inverse-square law of geometric attenuation, the optimal designs pass over the noise observation point at a much higher altitude than SAX31. To accomplish this, the wingspan is lengthened to very near the upper bound and the outer wing chords are grown. Together, this results in a larger lifting surface and thus more lift available during climb. The larger airframe requires more thrust to maintain a given climb an-

gle, but the optimization captures the climb angle versus jet noise tradeoff as shown in Figure 7-1.

In the distributed optimization, the design solution has the same noise level as the other minimum noise designs to within the fidelity of the noise prediction models, but is a fundamentally different design with a much lower fuel burn than the single-level optimization results. Using this framework, the result is an aircraft with a low MTOW and high thrust. There is little change to the airfoil profiles, but due to the much higher thrust-to-weight ratio the aircraft crosses the airport boundary at a higher altitude than the other design solutions. As in the single-level optimization, the climb angle versus jet noise tradeoff is captured, the Mach number is low, and the fan diameter is at the upper bound.

7.6 Optimization Risks

Since optimization is known to exploit loopholes in numerical models, it is important to consider the assumptions made in the development of the model used for this work. First, the only noise sources considered in this analysis are the airframe, fan, and jet. It is assumed that noise levels due to other sources, such as the turbine and combustor, are well below those of the sources considered, even at the lowest-noise designs. Secondly, a constant parasite drag coefficient is assumed for all designs, regardless of the planform, engine, or airfoil profiles. Additional friction drag due to larger planforms or engines is not accounted for in the optimization.

Because the model does not perform high-fidelity analysis, there are some constraints that have not been modeled. For example, it was assumed that an engine design is feasible if the fan diameter is within 5% of the Granta-3201 fan. While this is a good rule of thumb with respect to the engine cycle, it does not account for structural constraints on the fan blades themselves. Also, it is assumed that the FAR stall speed requirements can be met up to an angle of attack of 16° on initial climb. In a higher-fidelity analysis, it would be preferable to constrain the sectional lift coefficients at this critical mission point rather than the angle of attack.

The primary risk in the optimization setup is the choice of objective function. The noise value defined as the objective function is the noise as observed at a single point directly under the aircraft. Because no information about noise values elsewhere on the ground is known at the time of optimization, it is possible that the value of the objective function is not the loudest point on the ground. Post-optimization, this possibility was examined for both the spanwise and streamwise case.

Contours of noise levels were plotted for both SAX31 and SAX31C* to get a picture of the noise experienced in the general vicinity of the aircraft as it passes over the airport boundary. In Figures 7-7 through 7-10, the aircraft is located at coordinate (0,0) and is flying towards the right. For each noise source, there are small regions of higher noise slightly outboard of (0,0) in the spanwise direction, $(0,\epsilon)$. Although the optimizer does not have information about these louder regions, by minimizing the noise at the (0,0) point, the noise levels everywhere drop and the optimal design is indeed quieter than the initial design at all points.

In the streamwise direction, there is some concern that the optimization could lower noise by simply rotating the aircraft (changing the angle of attack, thrust vectoring angle, or flight path angle) to move the loudest point forward or aft. Post-optimization, total noise levels along the flight path were plotted in Figure 7-11. Figure 7-11 is a cut along a horizontal line passing through y=0 in Figure 7-10(b). From this plot, it is clear that the loudest point in the streamwise direction along the flight path is indeed directly under the aircraft. There is no guarantee that this is the case for every design analyzed during the optimization, but it is supporting evidence of the validity of the SAX31C* minimum noise design.

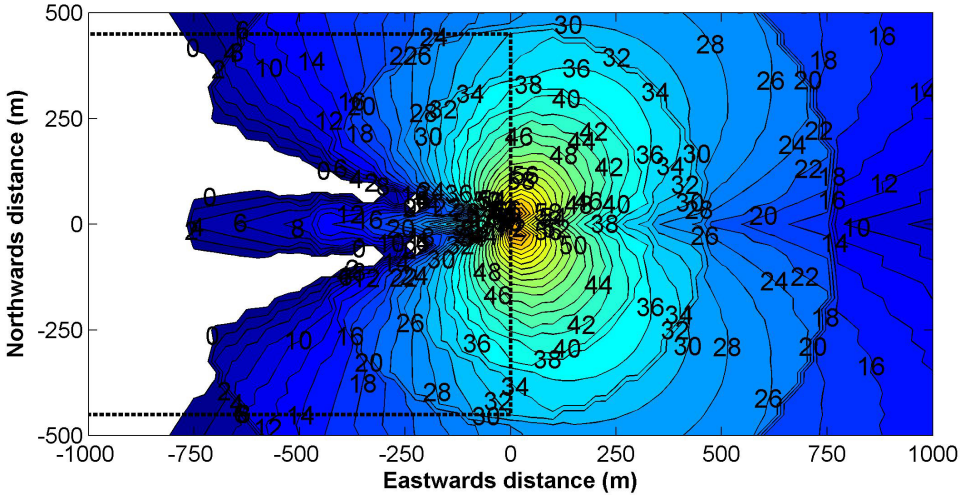

(a) SAX31

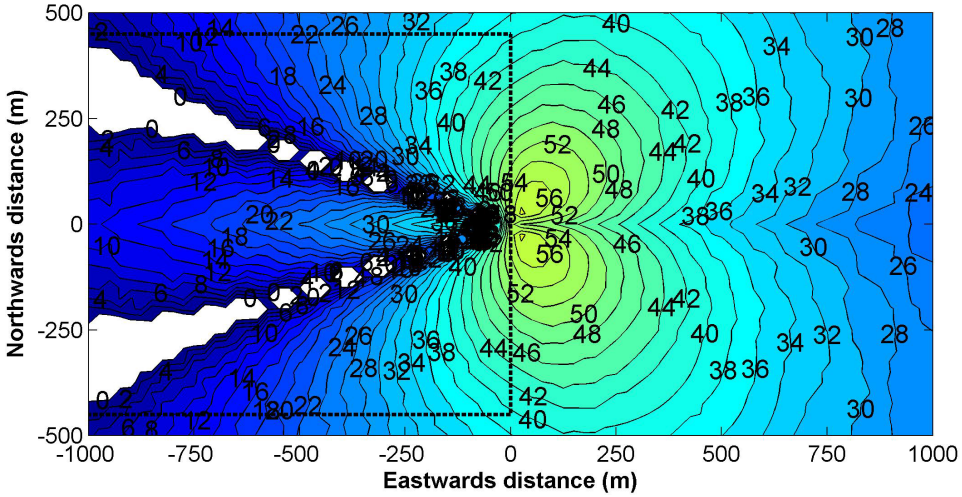

(b) SAX31C*

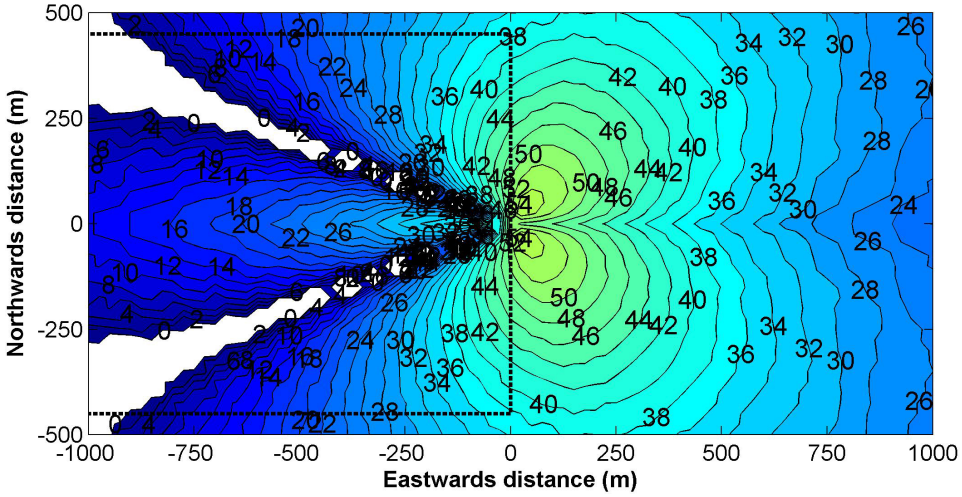

(c) SAX31D*

Figure 7-7: Contours of airfoil self-noise (dBA) as observed on the ground

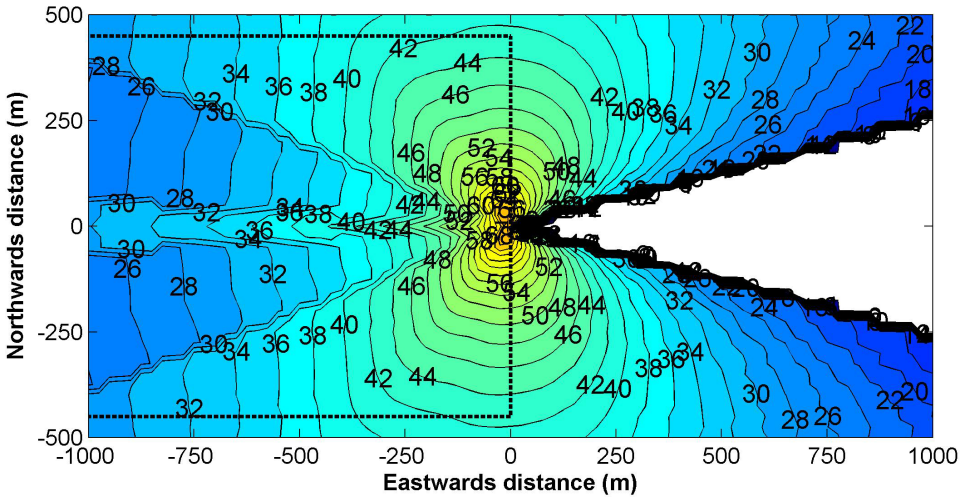

(a) SAX31

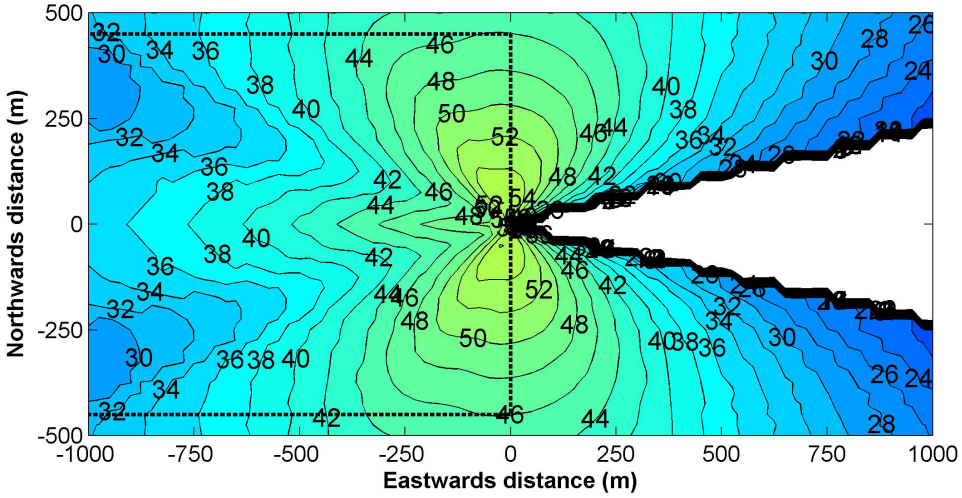

(b) SAX31C*

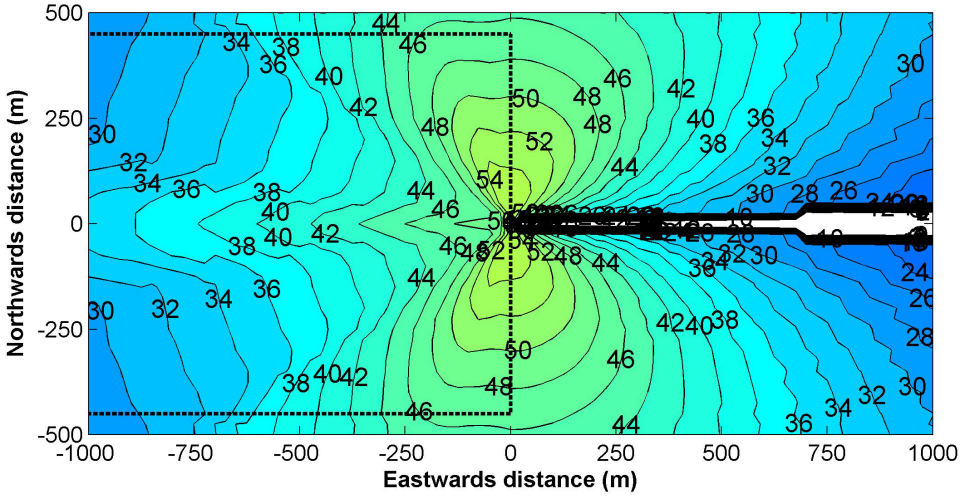

(c) SAX31D*

Figure 7-8: Contours of rearward propagating fan noise (dBA) as observed on the ground

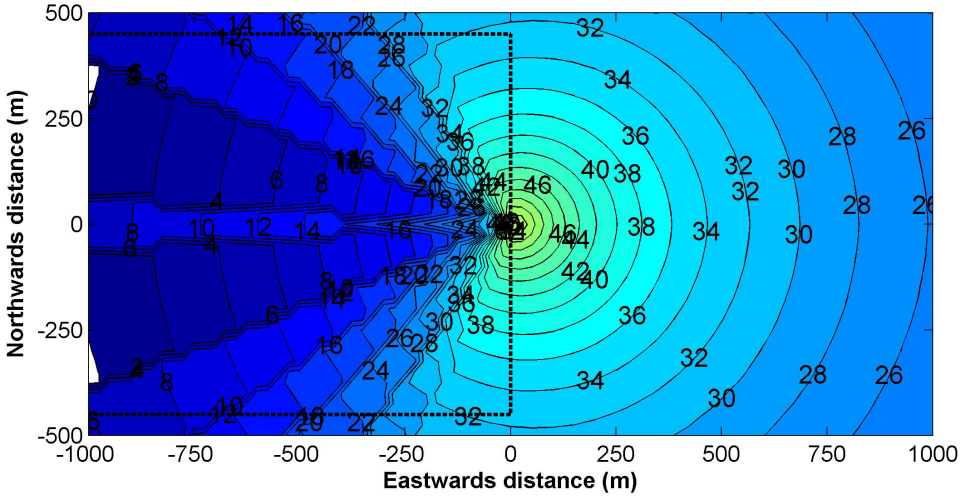

(a) SAX31

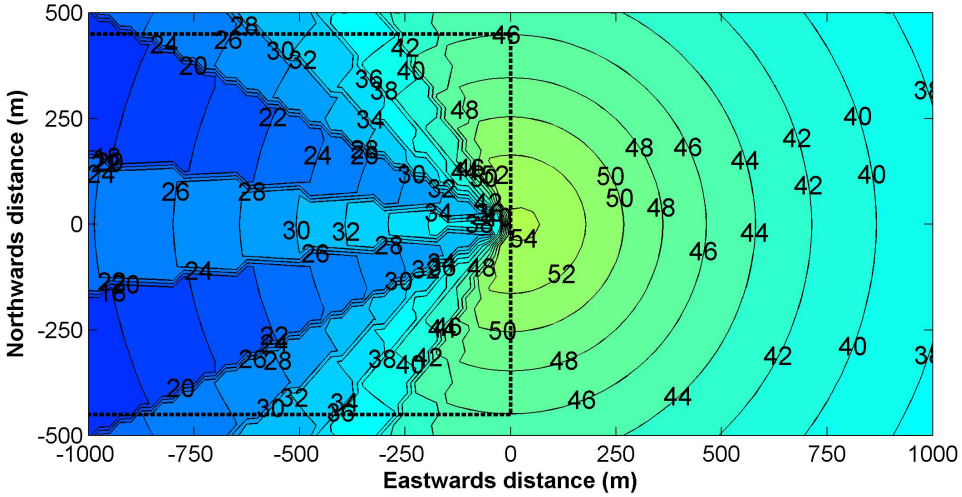

(b) SAX31C*

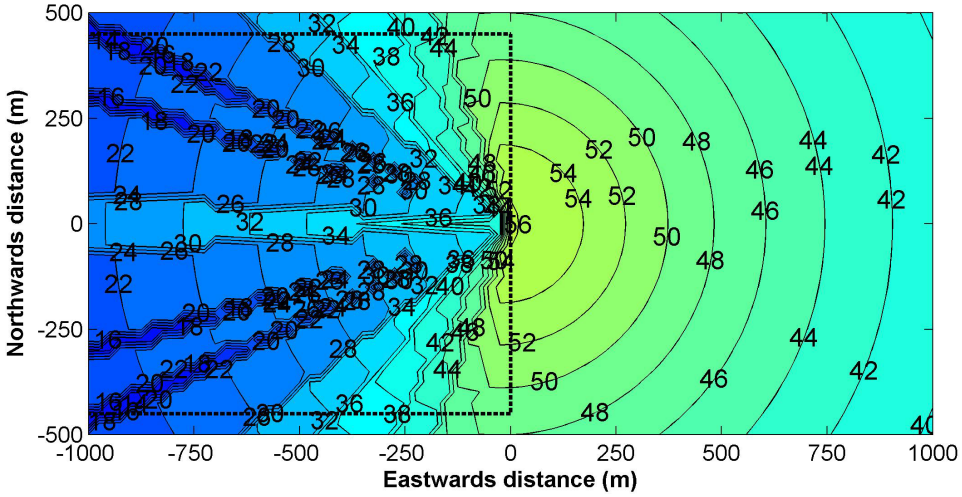

(c) SAX31D*

Figure 7-9: Contours of jet noise (dBA) as observed on the ground

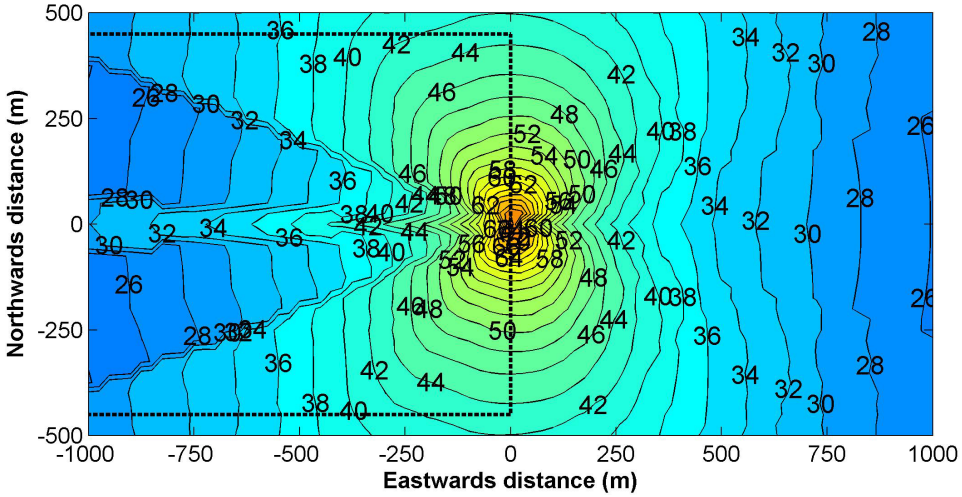

(a) SAX31

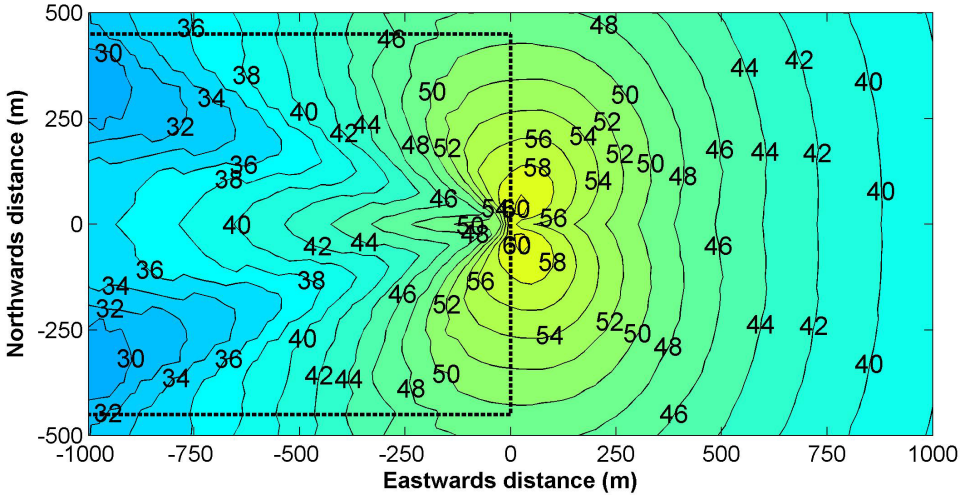

(b) SAX31C*

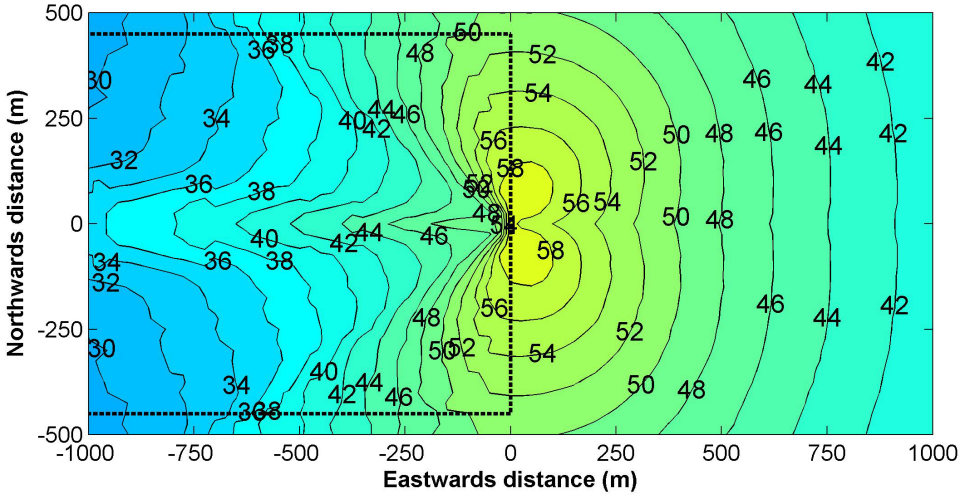

(c) SAX31D*

Figure 7-10: Contours of total aircraft noise (dBA) (airfoil, fan, jet) as observed on the ground

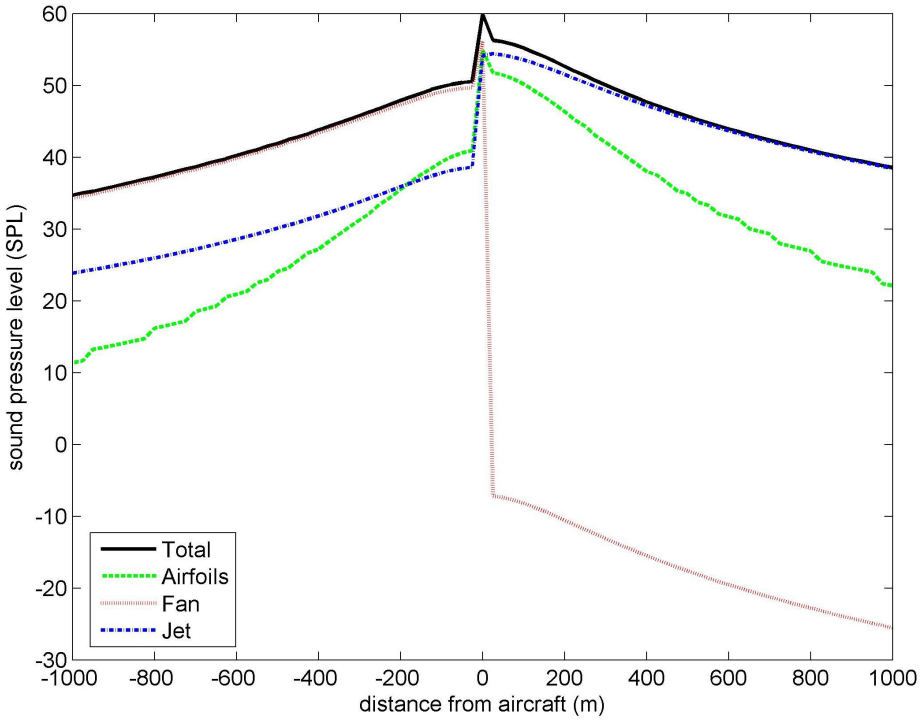

Figure 7-11: Sound pressure levels along the SAX31C* line of flight

Chapter 8

Conclusions

The ultimate goal of this research was to quantify tradeoffs in airframe design, engine design, airfoil design, and aircraft operations to develop the an aircraft-operations system so quiet that the aircraft is imperceptible outside of the airport boundary in a typical urban area. To this end, contributions were made in the areas of modeling, optimization, and unconventional aircraft design. In this chapter, the contributions of this research as well as the limitations and recommendations for future work are summarized.

8.1 Summary

A weight and center of gravity model for an unconventional BWB-like aircraft was developed and analyzed quantitatively via a sensitivity analysis. The sensitivity of both the aircraft weight and center of gravity to various parameters was calculated. It was found that although the structural weight estimate of an unconventional aircraft configuration has a high degree of uncertainty, the maximum takeoff weight is not sensitive to this value. However, the aircraft center of gravity is sensitive to the location of the structural weight.

Two optimization frameworks were built, one single-level and one distributed. In the single-level optimization framework, the entire aircraft design and analysis model is linked directly to a single optimizer. In the distributed optimization framework,

the problem is decomposed into three subspaces: airframe and engine design, wing design, and operations. The airframe and engine design is performed at the system level and the system, along with the operations subspace, is optimized for minimum noise. The wing design subspace is responsible for meeting the requirements set by the system level optimization.

It was found that takeoff noise can be drastically reduced by modifying the airframe planform, engine size, and takeoff flight path. Airfoil profile optimization does not have a significant effect on noise but can be used to improve fuel burn. As a result, unconventional aircraft configurations can be optimized to achieve a low noise design while maintaining competitive fuel burn.

In the single-level optimization, the design-operations solutions reduce acoustic power and increase the distance from the noise source to the observer in order to minimize noise. Acoustic power is reduced by both lowering the departure Mach number and increasing the fan diameter. The altitude at the airport boundary is increased by designing a larger wing. The larger airframe requires more thrust to maintain a given flight path angle, but the optimization captures the climb angle versus jet noise tradeoff.

In the distributed optimization, the design solution has the same noise level as that obtained through the single-level optimization, but is a fundamentally different design with a much lower fuel burn. The distributed optimization framework allowed for the exploration of different regions of the design space, the result of which is an aircraft with a small wing, low MTOW, and high thrust. There is little change to the airfoil profiles, but due to a much higher thrust-to-weight ratio the aircraft crosses the airport boundary at a relatively high altitude. As in the single-level optimization, the climb angle versus jet noise tradeoff is captured, the Mach number is low, and the fan diameter is at the upper bound.

8.2 Limitations and Future Work

The difficulties of developing a high-fidelity design framework for an unconventional aircraft are obvious. There are no empirical data or industry standards on which to base design decisions. Consequently, the model developed here is a combination of simple-physics and empirical relations which are used to scale a reference aircraft design and predict the takeoff noise of the new aircraft. Some constraints, such as fan blade structure and manufacturability, are not modeled in this design scaling. In the noise prediction analysis it is assumed that the noise sources considered here (airframe, fan, jet) dominate the aircraft noise on takeoff. To improve the optimization results, higher fidelity models should be incorporated with the optimization frameworks developed here. In particular, increased fidelity would be useful in generating higher resolution airframe designs, better aerodynamic analysis, prediction of more noise sources, and a more detailed engine cycle analysis.

It has been shown that optimization can reduce the single point noise on takeoff, but no effort has been made here to incorporate other noise metrics or mission points. For certification purposes, noise is quantified using Effective Perceived Noise Level (EPNdB) which accounts not only for frequencies but also for duration. In future studies, an optimization for minimum EPNdB along a flight path rather than single point A-weighted decibels would provide a more practical result. Also, it is important to consider other mission points, namely approach. For instance, the distributed optimization result found here is a low noise aircraft design with competitive fuel burn. This design seems ideal on takeoff, but it may not have sufficient wing area to maintain the slow and steep flight path commonly associated with a quiet approach.

The distributed optimization framework has been shown to produce promising designs that are not found through single-level optimization. This design methodology should be pursued and expanded. Because of the modular nature of the framework, it is a relatively simple matter to, for example, replace the vortex lattice analysis used here with CFD. The higher fidelity aerodynamic analysis would lend a great deal of credibility to the final aircraft design. Similarly, an approach operations module, a

structural analysis module, and a higher-fidelity noise prediction module could all be incorporated into the optimization with minimal effort to produce a more complete low noise aircraft design-operations system with competitive fuel burn.

Bibliography

[1] "Aircraft weight and balance control," Federal Aviation Administration Advisory Circular, June 2005.

[2] N. Antoine and I. Kroo, "Aircraft optimization for minimal environmental impact," AIAA 2002-5667, 2002.

[3] ——, "Optimizing aircraft and operations for minimum noise," AIAA 2002-5868, 2002.

[4] N. Antoine, I. Kroo, K. Willcox, and G. Barter, "A framework for aircraft conceptual design and environmental performance studies," AIAA 2004-4314, 2004.

[5] Boeing Commercial Airplanes, personal communication, non-advocate review, May 2005.

[6] R. Braun, "Collaborative optimization: An architecture for large-scale distributed design," Ph.D. dissertation, Stanford University, May 1996.

[7] B. Caves, L. Jenkinson, and D. Rhodes, "Adapting civil aircraft conceptual design methods to account for broader based constraints," AIAA 97-5595, 1997.

[8] R. Caves and D. Rhodes, "Steeper approaches: A contribution to alleviating airport environmental and physical capacity constraints," AIAA 95-3907, 1995.

[9] C. Chinoy, "Prediction of noise generated by fans and compressors in turbojet and turbofan engines," ESDU International plc, Item 98008, London, UK, 1998.

[10] ——, "Airframe noise prediction," ESDU International plc, Item 90023, London, UK, 2003.

[11] L. Clark and C. Gerhold, "Inlet noise reduction by shielding for the blended-wing-body airplane," AIAA 99-1937, 1999.

[12] J. Clarke and R. Hansman, "Systems analysis of noise abatement procedures enabled by advanced flight guidance technology," AIAA 97-0490, 1997.

[13] D. Crichton, L. Xu, and C. Hall, "Preliminary fan design for a silent aircraft," GT2006-90564, 2006, presented at the ASME Turbo Expo, Barcelona, Spain.

[14] J. Croft, "IFE: Home theatre in the skies," ATW website, October 2005, http://www.atwonline.com/magazine/article.html?articleID=1424, cited February 2006.

[15] A. Diedrich, "The multidisciplinary design and optimization of an unconventional, extremely quiet transport aircraft," Master's thesis, Massachusetts Institute of Technology, 2005.

[16] A. Diedrich, J. Hileman, D. Tan, K. Willcox, and Z. Spakovsky, "Multidisciplinary design and optimization of the silent aircraft," AIAA 2006-1323, 2006.

[17] A. Dowling and J. Ffowcs Williams, *Sound and Sources of Sound*. Ellis Horwood Limited, 1983.

[18] M. Drela and H. Youngren, "Avl," MIT website, September 2004, http://web.mit.edu/drela/Public/web/avl/, cited March 2006.

[19] P. Evans, "Evaluation of the attenuation of sound by a uniform atmosphere," ESDU International plc, Item 78002, London, UK, 2004.

[20] "FICAN position on research into effects of aircraft noise on classroom learning," Federal Interagency Committee on Aviation Noise, Tech. Rep., September 2000.

[21] R. Golub, J. Rawls, and J. Russell, "Evaluation of the advanced subsonic technology program noise reduction benefits," NASA, Langley Research Center, Hampton, VA, Technical Memorandum TM-2005-212144, May 2005.

[22] C. Hall, personal communication, April 2006.

[23] C. Hall and D. Crichton, "Engine and installation configurations for a silent aircraft," ISABE 2005-1164, 2005, presented at the 17th International Symposium on Airbreathing Engines, Munich, Germany.

[24] ——, "Engine design studies for a silent aircraft," GT2006-90559, 2006, presented at the ASME Turbo Expo, Barcelona, Spain.

[25] M. Heidmann, "Interim prediction method for fan and compressor source noise," NASA Technical Memorandum X-71763, 1979.

[26] J. Hileman, Z. Spakovszky, M. Drela, and M. Sargeant, "Aerodynamic and aeroacoustic three-dimensional design for a "silent" aircraft," AIAA 2006-241, January 2006.

[27] "Information on levels of environmental noise requisite to protect public health and welfare with an adequate margin of safety," Environmental Protection Agency Office of Noise Abatement and Control, Tech. Rep. 550/9-74-004, March 1974.

[28] I. Kroo, "Multidisciplinary optimization applications in preliminary design–status and directions," AIAA 97-1408, April 1996.

[29] I. Kroo, S. Altus, R. Braun, P. Gage, and I. Sobieski, "Multidisciplinary optimization methods for aircraft preliminary design," AIAA 94-4325, 1994.

[30] I. Kroo and V. Manning, "Collaborative optimization: Status and directions," AIAA 2000-4721, 2000.

[31] L. Leifsson, W. Mason, J. Schetz, R. Haftka, and B. Grossman, "Multidisciplinary design optimization of low-airframe-noise transport aircraft," AIAA 2006-230, 2006.

[32] R. Liebeck, "Design of the blended wing body subsonic transport," *Journal of Aircraft*, vol. 41, no. 1, pp. 10–25, January-February 2004.

[33] ——, personal communication, January 2006.

[34] R. Liebeck, M. Page, and B. Rawdon, "Blended-wing-body subsonic commercial transport," AIAA 98-0438, January 1998.

[35] M. Lighthill, "On sound generated aerodynamically, Part I: General theory," *Proceedings of the Royal Society of London, Series A, Mathematical and Physical Sciences*, vol. 211, no. 1107, pp. 564–587, March 1952.

[36] G. Lilley, "A quest for quiet commercial passenger transport aircraft for take-off and landing," AIAA 2004-2922, 2004.

[37] D. Lockard and G. Lilley, "The airframe noise reduction challenge," NASA, Langley Research Center, Hampton, VA, Technical Memorandum TM-2004-213013, April 2004.

[38] "Noise impacts of airport developments considered in the national consultation documents," United Kingdom Department for Transportation, Tech. Rep., 2003.

[39] P. Papalambros and D. Wilde, *Principles of Optimal Design: Modeling and Computation*, 2nd ed. Cambridge University Press, 2000.

[40] D. Pilczer, "Noise reduction assessments and preliminary design implications for a functionally-silent aircraft," Master's thesis, Massachusetts Institude of Technology, June 2003.

[41] "Public health and welfare criteria for noise," Environmental Protection Agency Office of Noise Abatement and Control, Tech. Rep. 550/9-73-002, July 1973.

[42] D. Raymer, *Aircraft Design: A Conceptual Approach*, 3rd ed. Reston, VA: American Institute of Aeronautics and Astronautics, 1999.

[43] J. Roskam, *Airplane Design, Part V: Component Weight Estimation*, 2nd ed. Ottawa, Kansas: Roskam Aviation and Engineering Corporation, 1989, pp. 97–112.

[44] F. Sietzen, "New blueprint for NASA aeronautics," *Aerospace America*, pp. 24–28, August 2002.

[45] J. Stone, D. Groesbeck, and C. Zola, "An improved prediction model for noise generated by conventional prole coaxial jets," NASA Report 82712, 1981.

[46] J. Stone and F. Montegani, "An improved prediction method for the noise generated in flight by circular jets," NASA Technical Memorandum 81470, 1980.

[47] D. Tan, "Design trade studies and assessment for advanced quiet aircraft concepts," Master's thesis, Massachusetts Institute of Technology, 2005.

[48] D. Tenney, "NASA's aeronautics vision," NASA Langley Research Center, Hampton, VA, 2004.

[49] H. Visser and R. Wijnen, "Optimization of noise abatement departure trajectories," AIAA 2000-3991, 2000.

[50] S. Wakayama, "Multidisciplinary design optimization of the blended-wing-body," AIAA 98-4938, 1998.

[51] ——, "Blended-wing-body optimization problem setup," AIAA 2000-4740, September 2000.

[52] S. Wakayama and I. Kroo, "The challenge and promise of blended-wing-body optimization," AIAA 98-4736, 1998.

[53] S. Wakayama and R. Liebeck, "Multidisciplinary optimization on an advanced composite wing," AIAA 96-4003, September 1996.